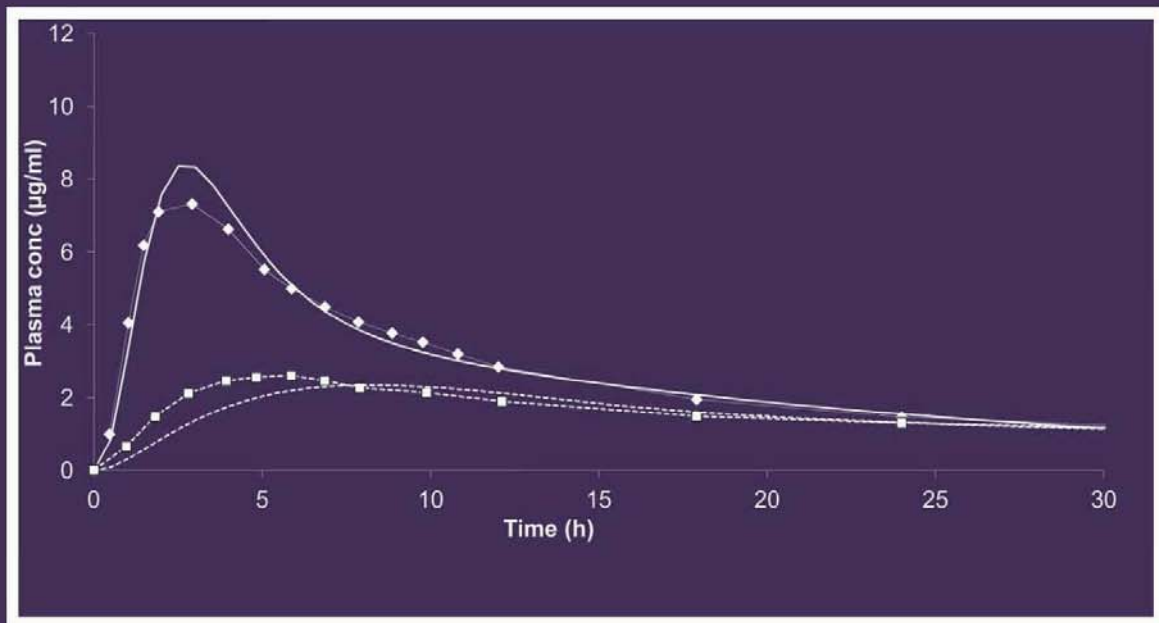


Analytics of dissolution testing of products containing nanosized drugs with a view to predicting plasma profiles









**Analytics of dissolution testing of products containing nanosized drugs
with a view to predicting plasma profiles**

Dissertation

Zur Erlangung des Doktorgrades

der Naturwissenschaften

vorgelegt beim

Fachbereich Biochemie, Chemie und Pharmazie

der Johann Wolfgang Goethe – Universität

in Frankfurt am Main

von

Daniel Jünemann

aus Emsbüren

Frankfurt am Main, 2011

(D30)



Bibliografische Information der Deutschen Nationalbibliothek

Die Deutsche Nationalbibliothek verzeichnet diese Publikation in der Deutschen Nationalbibliografie; detaillierte bibliografische Daten sind im Internet über <http://dnb.d-nb.de> abrufbar.

1. Aufl. - Göttingen : Cuvillier, 2012

Zugl.: Frankfurt am Main, Univ., Diss., 2012

978-3-95404-000-1

Vom Fachbereich Biochemie, Chemie und Pharmazie der
Johann Wolfgang Goethe – Universität als Dissertation angenommen.

Dekan: Prof. Dr. Dieter Steinhilber

Gutachter: Prof. Dr. Jennifer B. Dressman

Prof. Dr. Jörg Kreuter

Datum der Disputation: 13.01.2012

© CUVILLIER VERLAG, Göttingen 2012

Nonnenstieg 8, 37075 Göttingen

Telefon: 0551-54724-0

Telefax: 0551-54724-21

www.cuvillier.de

Alle Rechte vorbehalten. Ohne ausdrückliche Genehmigung des Verlages ist es nicht gestattet, das Buch oder Teile daraus auf fotomechanischem Weg (Fotokopie, Mikrokopie) zu vervielfältigen.

1. Auflage, 2012

Gedruckt auf säurefreiem Papier

978-3-95404-000-1



Danksagung

Die vorliegende Arbeit wurde unter Leitung von Frau Professor Jennifer B. Dressman am Institut für pharmazeutische Technologie der Johann Wolfgang Goethe-Universität in Zusammenarbeit mit Janssen Pharmaceutica erstellt.

Ich möchte meiner Doktormutter, Jennifer B. Dressman für ihre unermüdliche Unterstützung danken. Sie betreute mich fachlich bei dieser Arbeit hervorragend, zudem erlangte ich durch sie ein umfangreiches Wissen auf dem Gebiet der pharmazeutischen Technologie

Ich bedanke mich bei „Ekkie“, Ekarat Jantratid für seine Hilfe. Wir werden dich nie vergessen.

Weiterhin bedanke ich mich bei Sandra Klein ihre Diskussionsbereitschaft im Labor, bei Klaus Langer für seine Hilfe gerade bei analytischen Fragestellungen.

Professor Reppas und Dr. Vertzoni danke ich für die Unterstützung bei der Anwendung der Simulations-Software.

Ein herzlicher Dank an Janssen Pharmaceutica für die finanzielle und wissenschaftliche Unterstützung, insbesondere durch Hugo Bohets und Karl Peeters.

Ein spezielles Dankeschön geht an Murat Kilic, für unsere Freundschaft und die wertvollen wissenschaftlichen Diskussionen während der letzten zehn Jahre.

Ein herzliches Dankeschön geht an meine Freunde und Kollegen des Arbeitskreises und Instituts: Thomas „TomTom“ Zöller, Kathrin Nollenberger, Tine Petereit, Dieter Bischoff, Stefanie Strauch, Kevin Kiehm, Nils Janssen, Corina Becker, Marcel Arndt, Thomas Taupitz, Christian Wagner, Yasushi Shono, Anja Zensi, Stefanie Wohlfart, Sebastian Gaca, Matthias Wacker, Melisande Holzer, Jürgen Kufleitner und Kirsten Thelen. Ebenso bedanke ich mich bei allen weiteren Mitarbeitern des Instituts.

Viele Grüße gehen an Freddy Modrack, Meike Bunz, Janett Eckmann, Anita Schuwald, Christine Schütz, Doris Bichai und Mareike Modrack.

Ein besonderer Dank geht an meine Eltern Magda und Helmut, die mir das Studium erst ermöglicht haben.

Ina, dir danke ich für deine Liebe. Diese Arbeit ist für dich.





Table of contents:

1	Introduction	1
1.1	<i>Oral bioavailability</i>	1
1.2	<i>Factors limiting oral bioavailability</i>	2
1.3	<i>Solubility and drug dissolution</i>	3
1.4	<i>The biopharmaceutics classification system</i>	5
1.5	<i>Formulation of poorly soluble substances</i>	8
1.6	<i>Particle size reduction in pharmaceutical technology</i>	13
1.6.1	<i>Particle size reduction</i>	14
1.6.2	<i>Dry milling methods</i>	16
1.6.3	<i>Wet milling methods</i>	17
1.6.4	<i>Comparison of dry and wet milling techniques</i>	17
1.6.5	<i>Combining micronization with other techniques</i>	18
1.7	<i>Rationale for nanonization of drug particles</i>	19
1.8	<i>Preparation of nanosized drug particles</i>	20
1.8.1	<i>Wet-milling methods (bead mills)</i>	21
1.8.2	<i>High pressure homogenization</i>	23
1.8.3	<i>Commercialized nanosized drugs</i>	24
1.8.4	<i>Increase of bioavailability by nanonization</i>	25
1.8.5	<i>The lack of food effects using nanosized APIs</i>	27
1.8.6	<i>Improvement of bioavailability for drugs with an absorption window</i>	28
1.9	<i>Sample preparation and analysis in dissolution testing</i>	29
1.9.1	<i>HPLC-UV</i>	30
1.9.1.1	<i>The use of syringe filter</i>	30
1.9.1.2	<i>Centrifugal filter devices</i>	31
1.9.1.3	<i>Dialysis methods</i>	31
1.9.1.4	<i>Microdialysis</i>	32
1.9.2	<i>Fiber optics</i>	32
1.9.3	<i>Turbidity measurement</i>	34
1.9.4	<i>ResoScan</i>	35
1.9.5	<i>Asymmetrical flow - field-flow fractionation</i>	35
1.9.6	<i>Ion-selective electrode</i>	37
2	Aims of thesis	39
2.1	<i>Evaluation of the use of an ion-selective electrode system in biorelevant dissolution testing using diphenhydramine HCl as model drug</i>	39



2.2	<i>Evaluation of the ion-selective electrode as potential tool for analysis of supersaturated systems</i>	39
2.3	<i>Evaluation of analytical methods in dissolution testing of nanosized fenofibrate</i>	40
2.4	<i>Establishment of an in vitro - in vivo - correlation for a nanosized drug using an in silico simulation approach</i>	40
3	Materials and Methods	41
3.1	<i>Materials</i>	41
3.1.1	<i>Chemicals</i>	41
3.1.2	<i>Model substance diphenhydramine HCl</i>	43
3.1.3	<i>Model substance fenofibrate</i>	44
3.2	<i>Methods</i>	46
3.2.1	<i>Case example of particle size reduction: fenofibrate</i>	46
3.2.2	<i>Dissolution studies</i>	48
3.2.3	<i>Composition of dissolution media</i>	49
3.2.4	<i>Syringe filters</i>	50
3.2.5	<i>Microdialysis system</i>	51
3.2.6	<i>Centrifugal filter devices</i>	51
3.2.7	<i>High performance liquid chromatography (HPLC-UV) used for assays</i>	52
3.2.8	<i>ResoScan system</i>	53
3.2.9	<i>Analyses of in vitro data</i>	54
3.2.9.1	<i>Model independent f_1- and f_2- factor calculation</i>	54
3.3	<i>Special methods for diphenhydramine HCl</i>	54
3.3.1	<i>Filter adsorption studies for diphenhydramine HCl</i>	54
3.3.2	<i>Dynamic light scattering</i>	55
3.3.3	<i>The ion-selective electrode</i>	55
3.3.4	<i>Calibration of the ion-selective electrode for diphenhydramine HCl</i>	56
3.3.5	<i>Dissolution testing</i>	57
3.3.6	<i>Endpoint calibration via ISE (method A)</i>	57
3.3.7	<i>Endpoint calibration via HPLC-UV (method B)</i>	58
3.3.8	<i>Adaption of Method B for measurement of poorly soluble substances</i>	58
3.3.9	<i>Analysis of significance using ANOVA</i>	58
3.4	<i>Special methods for fenofibrate</i>	59
3.4.1	<i>Filter adsorption studies for fenofibrate</i>	59
3.4.2	<i>Analysis of in vivo pharmacokinetic data</i>	59
3.4.3	<i>Computer simulation of fenofibric acid plasma profiles</i>	60
3.4.3.1	<i>The STELLA[®] model</i>	60



3.4.3.2	Calculation of z-value.....	66
3.4.3.3	Adaption of original model for permeability restrictions	67
3.4.4	Comparison of simulated plasma profiles to in vivo data.....	68
3.4.5	Sensitivity analyses.....	69
4	Results and discussion	70
4.1	Discussion of methods evaluated for in situ measurement of the analyte in the dissolution test	70
4.2	ResoScan.....	71
4.3	Microdialysis.....	72
4.4	Centrifugal filter devices	73
4.1	Ion-selective electrode	75
4.1.1	Filter adsorption studies.....	75
4.1.2	FaSSGF.....	75
4.1.3	FaSSIF	77
4.1.4	FaSSIF-V2.....	82
4.1.5	FeSSGF.....	84
4.1.6	FeSSIF / FeSSIF-V2.....	86
4.1.7	Evaluation of potential use of the ISE for nanosized drugs	88
4.2	Fenofibrate	91
4.2.1	Filter adsorption studies.....	91
4.2.2	Solubility studies.....	94
4.2.3	Dissolution in FaSSIF and FeSSIF using various filter pore sizes	95
4.3	Theoretical increase of dissolution rate by particle size reduction.....	99
4.4	Comparison of dissolution rate in theory and in practice	102
4.5	Evaluation of the STELLA [®] software to generate simulated plasma profiles	103
4.6	Discussion of the conventional approach vs. a new method for rapidly dissolving compounds.....	105
4.7	Calculation of z-values	109
4.8	Simulated plasma profiles of fenofibric acid Model A	110
4.8.1	Sensitivity analyses model A	111
4.8.1.1	Influence of gastric emptying rate.....	111
4.8.1.2	Influence of gastric dissolution rate	114
4.8.1.3	Influence of intestinal dissolution rate.....	116
4.9	Simulated plasma profiles of fenofibric acid model B.....	118
4.9.1	Sensitivity analyses Model B	119
4.9.1.1	Influence of intestinal dissolution in the fasted state.....	120



4.9.1.2	<i>Influence of gastric emptying rate in the fed state.....</i>	<i>121</i>
4.9.1.3	<i>Influence of permeation rate across the intestinal mucosa.....</i>	<i>122</i>
4.9.2	<i>Discussion of STELLA[®] software</i>	<i>123</i>
4.9.2.1	<i>Possible applications using the presented model in STELLA[®]</i>	<i>124</i>
4.9.2.2	<i>Limitations of the STELLA[®] model</i>	<i>125</i>
5	General discussion of thesis	126
6	Outlook	133
6.1	<i>Studies regarding the ISE</i>	<i>133</i>
6.2	<i>Filter adsorption testing.....</i>	<i>133</i>
6.3	<i>Establishment of an in vitro - in vivo - correlation for a nanosized drug.....</i>	<i>134</i>
7	Summary	135
8	Appendix	141
9	References	166
10	Summary (German)	173
11	Curriculum vitae	179



Figures:

<i>Figure 1.1: Current market share of drugs according to the Biopharmaceutic Classification System (derived from [23] and [22])</i>	7
<i>Figure 1.2: Market share of recently developed drugs according to the BCS [22, 23]</i>	8
<i>Figure 1.3: Decision tree in formulation finding for poorly soluble compounds (derived from [24])</i>	9
<i>Figure 1.4: Basic scheme of the Ostwald ripening process: an unequal size distribution under the drug particles induces dissolution of smaller particles. The dissolved drug precipitates on larger particles.</i> ..	21
<i>Figure 1.5: Schematic representation of media milling process(taken from [54])</i>	22
<i>Figure 1.6: Principle of the DissoCube[®] -Technology (taken from [57])</i>	24
<i>Figure 1.7: Illustration of dissolution (blue) limited absorption (green) using micronized API</i>	26
<i>Figure 1.8: Faster dissolution (blue) of nanosized API utilizes maximum absorption rate (green)</i>	26
<i>Figure 1.9: Illustration of an absorption window (green) utilized by conventional drug particles with slow</i>	29
<i>Figure 1.10: Illustration of an adsorption window (green) nearly fully utilized by nanosized drug particles with rapid dissolution rate (blue)</i>	29
<i>Figure 1.11: Principle of fiber optics (source unknown)</i>	33
<i>Figure 1.12: Basic principle of separation using AF4 [79]</i>	36
<i>Figure 1.13: Schematic process of analyte cloud separation using AF4 [79]</i>	37
<i>Figure 3.1: Structure of diphenhydramine (free base)</i>	43
<i>Figure 3.2: Structure of fenofibrate</i>	45
<i>Figure 3.3: The basic principle of suprabioavailable fenofibrate formulation</i>	47
<i>Figure 3.4: WinNonlin[®] model 12</i>	60
<i>Figure 3.5: WinNonlin[®] model 12 in STELLA[®]</i>	61
<i>Figure 3.6: Map of STELLA[®] model A</i>	63
<i>Figure 3.7: Model Map enabling permeability restrictions, Model B</i>	68
<i>Figure 4.1: Dissolution profile of Lipidil Ter[®] (dotted line) and Lipidil 145 ONE[®] (solid line) in FaSSIF using Microcon[®] 100 kDa centrifugal filter devices</i>	73
<i>Figure 4.2: Dissolution profile of Lipidil Ter[®] (dotted line) and Lipidil 145 ONE[®] (solid line) in FeSSIF using Microcon[®] 100 kDa centrifugal filter devices</i>	73
<i>Figure 4.3: Recovery of fenofibrate from Microcon[®] centrifugal filter devices in FaSSIF and FeSSIF</i>	74
<i>Figure 4.4: Recovery of Diphenhydramine HCl after filtration through Minisart[®] RC 25 regenerated cellulose, 0.2 µm</i>	75
<i>Figure 4.5: Dissolution profiles of Nustasium[®] in FaSSGF obtained by manual sampling and subsequent HPLC-UV analysis (solid line) and ISE (dotted line) Method A electrode 1</i>	76
<i>Figure 4.6: Dissolution profiles of Nustasium[®] in FaSSGF obtained by manual sampling and subsequent HPLC-UV analysis (solid line) and ISE (dotted line) Method B electrode 1</i>	76



<i>Figure 4.7: Dissolution profiles of Nustasium[®] in FaSSIF obtained by manual sampling and subsequent HPLC-UV analysis (solid line) and ISE (dotted line) (A) Method A electrode 1 – 3</i>	<i>79</i>
<i>Figure 4.8: Dissolution profiles of Nustasium[®] in FaSSIF obtained by manual sampling and subsequent HPLC-UV analysis (solid line) and ISE (dotted line) (A) Method B electrode 1 – 3.....</i>	<i>80</i>
<i>Figure 4.9: Dissolution profiles of Nustasium[®] in FaSSIF-V2 obtained by manual sampling and subsequent HPLC-UV analysis (solid line) and ISE (dotted line) Method A</i>	<i>83</i>
<i>Figure 4.10: Dissolution profiles of Nustasium[®] in FaSSIF-V2 obtained by manual sampling and subsequent HPLC-UV analysis (solid line) and ISE (dotted line) Method B.....</i>	<i>84</i>
<i>Figure 4.11: Plot of measured concentration against amount of added standard electrode 1-3. The dotted lines above and under the solid lines show the standard deviations</i>	<i>85</i>
<i>Figure 4.12: Picture of freshly prepared FeSSIF-V2 (left vessel) and FeSSIF-V2 after 24 hours at 37°C and 75 rpm (right vessel).....</i>	<i>86</i>
<i>Figure 4.13: Calibration Curve of Diphenhydramine HCl in FeSSIF-V2.....</i>	<i>87</i>
<i>Figure 4.14: Adsorption of fenofibrate to various filter materials from a FaSSGF solution containing fenofibrate.....</i>	<i>91</i>
<i>Figure 4.15: Adsorption of fenofibrate to various filter materials from a clear FaSSIF solution*</i>	<i>91</i>
<i>Figure 4.16: Adsorption of fenofibrate to various filter materials from a clear FaSSIF-V2 solution.....</i>	<i>92</i>
<i>Figure 4.17: Adsorption of fenofibrate to various filter materials from a clear FeSSIF solution</i>	<i>92</i>
<i>Figure 4.18: Adsorption of fenofibrate to various filter materials from a clear FeSSIF-V2 solution.....</i>	<i>92</i>
<i>Figure 4.19: Dissolution profiles of Lipidil 145 ONE[®] in FaSSIF and FeSSIF using various filter pore sizes</i>	<i>95</i>
<i>Figure 4.20: Dissolution profiles of Lipidil Ter[®] in FaSSIF and FeSSIF using various filter pore sizes.....</i>	<i>96</i>
<i>Figure 4.21: Comparison of plasma profiles, Lipidil Ter[®], fasted state</i>	<i>103</i>
<i>Figure 4.22: Comparison of plasma profiles, Lipidil 145 ONE[®], fasted state</i>	<i>104</i>
<i>Figure 4.23: Comparison of plasma profiles, Lipidil Ter[®], fed state</i>	<i>104</i>
<i>Figure 4.24: Comparison of plasma profiles, Lipidil 145 ONE[®], fed state</i>	<i>104</i>
<i>Figure 4.25: z-value in dependency of released drug.....</i>	<i>107</i>
<i>Figure 4.26: In vivo and in silico plasma profiles of fenofibric acid using the conventional z-value approach.....</i>	<i>108</i>
<i>Figure 4.27: Simulated plasma profiles of Lipidil 145 ONE[®] and Lipidil Ter[®] in comparison to in vivo data (fasted state, Model A)</i>	<i>110</i>
<i>Figure 4.28: Simulated plasma profiles of Lipidil 145 ONE[®] and Lipidil Ter[®] in comparison to in vivo data (fed state, Model A).....</i>	<i>110</i>
<i>Figure 4.29: Sensitivity analysis of GER for Lipidil Ter[®] in the fasted state.....</i>	<i>112</i>
<i>Figure 4.30: Sensitivity analysis of GER for Lipidil 145 ONE[®] in the fasted state.....</i>	<i>112</i>
<i>Figure 4.31: Sensitivity analysis of GER for Lipidil Ter[®] in the fed state.....</i>	<i>113</i>
<i>Figure 4.32: Sensitivity analysis of GER for Lipidil 145 ONE[®] in the fed state.....</i>	<i>113</i>
<i>Figure 4.33: Sensitivity analysis of gastric dissolution for Lipidil Ter[®] in the fasted state</i>	<i>114</i>



<i>Figure 4.34: Sensitivity analysis of gastric dissolution for Lipidil 145 ONE[®] in the fasted state</i>	<i>114</i>
<i>Figure 4.35: Sensitivity analysis of gastric dissolution for Lipidil Ter[®] in the fed state</i>	<i>115</i>
<i>Figure 4.36: Sensitivity analysis of gastric dissolution for Lipidil 145 ONE[®] in the fed state</i>	<i>115</i>
<i>Figure 4.37: Sensitivity analysis of intestinal dissolution for Lipidil Ter[®] in the fasted state</i>	<i>116</i>
<i>Figure 4.38: Sensitivity analysis of intestinal dissolution for Lipidil 145 ONE[®] in the fasted state</i>	<i>116</i>
<i>Figure 4.39: Simulated plasma profiles of Lipidil 145 ONE[®] and Lipidil Ter[®] in comparison to in vivo data (fasted state, Model B)</i>	<i>118</i>
<i>Figure 4.40: Simulated plasma profiles of Lipidil 145 ONE[®] and Lipidil Ter[®] in comparison to in vivo data (fed state, Model B)</i>	<i>118</i>
<i>Figure 4.41: Sensitivity analysis of intestinal dissolution for Lipidil Ter[®] in the fasted state (model B)</i>	<i>120</i>
<i>Figure 4.42: Sensitivity analysis of intestinal dissolution for Lipidil 145 ONE[®] in fasted state (model B)</i>	<i>120</i>
<i>Figure 4.43: Sensitivity analysis of GER for Lipidil Ter[®] in the fed state (model B)</i>	<i>121</i>
<i>Figure 4.44: Sensitivity analysis of GER for Lipidil 145 ONE[®] in the fed state (Model B)</i>	<i>121</i>
<i>Figure 4.45: Sensitivity analysis of permeation rate for Lipidil 145 ONE[®] in the fasted state</i>	<i>122</i>
<i>Figure 4.46: Correlation of z-values against c_{max}</i>	<i>125</i>
<i>Figure 8.1: Equation Set STELLA[®] for Lipidil 145 ONE[®], fasted state, Model A</i>	<i>153</i>
<i>Figure 8.2: Equation Set STELLA[®] for Lipidil 145 ONE[®], fasted state, Model B</i>	<i>154</i>
<i>Figure 8.3: Equation Set STELLA[®] for Lipidil Ter[®], fasted state, Model A</i>	<i>155</i>
<i>Figure 8.4: Equation Set STELLA[®] for Lipidil Ter[®], fasted state, Model B</i>	<i>156</i>
<i>Figure 8.5: Equation Set STELLA[®] for Lipidil 145 ONE[®], fed state, Model A</i>	<i>157</i>
<i>Figure 8.6: Equation Set STELLA[®] for Lipidil 145 ONE[®], fed state, Model B</i>	<i>158</i>
<i>Figure 8.7: Equation Set STELLA[®] for Ter[®], fed state, Model A</i>	<i>159</i>
<i>Figure 8.8: Equation Set STELLA[®] for Ter[®], fed state, Model B</i>	<i>160</i>
<i>Figure 8.9: Example of 25-step calibration potential / time</i>	<i>165</i>



Tables:

<i>Table 1.1: Probabilities for IVIVC as suggested by Amidon [13, 21]</i>	6
<i>Table 1.2: The LFCS as proposed by Pouton [37]</i>	11
<i>Table 1.3: Dry milling operations [48]</i>	16
<i>Table 1.4: Wet milling operations [48]</i>	17
<i>Table 1.5: List of commercialized nanosized drugs (modified from [55])</i>	25
<i>Table 3.1: Chemicals used in this study</i>	41
<i>Table 3.2: Dissolution study parameters for diphenhydramine and fenofibrate</i>	48
<i>Table 3.3: Composition of dissolution media</i>	49
<i>Table 3.4: Syringe filters used in this study.</i>	50
<i>Table 3.5: Model parameter used in the STELLA[®] models</i>	64
<i>Table 4.1: f_1-/ f_2-values for each medium / each electrode in comparison to manual sampling and subsequent HPLC-UV analysis</i>	77
<i>Table 4.2: Comparison of the ISE to manual sampling and subsequent HPLC-UV analysis and ISE within the same vessel during dissolution test with Method A</i>	81
<i>Table 4.3: Comparison of the ISE to manual sampling and subsequent HPLC-UV analysis and ISE within the same vessel during dissolution test with Method B</i>	82
<i>Table 4.4: f_1-/f_2-values for each medium / each electrode in comparison to manual sampling and subsequent HPLC-UV analysis with the adapted Method B, using t_{25} instead of t_{45}.</i>	90
<i>Table 4.5: Apparent solubility (24h) of fenofibrate in various media at 37 °C in $\mu\text{g/ml}$ (mean \pm SD)</i>	94
<i>Table 4.6: Comparison of dissolution profiles using the f_2-value (0.1μm pore size as reference)</i>	96
<i>Table 4.7: Calculation of change of diffusion boundary layer using various models (for particle sizes decreased in d from 5μm to 0.4μm)</i>	101
<i>Table 4.8: MDTs (min) for Lipidil Ter[®] and Lipidil 145 ONE[®] in various media</i>	102
<i>Table 4.9: Dependence of z on X_s</i>	106
<i>Table 4.10: Point estimate ratios of predicted and in vivo plasma profiles</i>	108
<i>Table 4.11: z-values of Lipidil 145 ONE[®]</i>	109
<i>Table 4.12: z-values of Lipidil Ter[®]</i>	109
<i>Table 4.13: Point estimate ratios of in silico / in vivo data Model A</i>	111
<i>Table 4.14: Point estimate ratios of in silico / in vivo data Model B</i>	118
<i>Table 5.1: Sample withdrawal scheme using Anopore filter of 0.02 μm, $n = 3$, * is for sampling point</i>	130
<i>Table 8.1: Dissolution of Lipidil 145 ONE[®] in FaSSiF, Centrifugal filter device 100 kDa</i>	141
<i>Table 8.2: Dissolution of Lipidil Ter[®] in FaSSiF, Centrifugal filter device 100 kDa</i>	141
<i>Table 8.3: Dissolution of Lipidil 145 ONE[®] in FeSSiF, Centrifugal filter device 100 kDa</i>	141
<i>Table 8.4: Dissolution of Lipidil Ter[®] in FeSSiF, Centrifugal filter device 100 kDa</i>	142



<i>Table 8.5: Comparison of filter adsorption of Lipidil Ter® in FaSSIF, 0.2µm RC compared to centrifugal filter device 100 kDa.....</i>	<i>142</i>
<i>Table 8.6: Comparison of filter adsorption of Lipidil Ter® in FeSSIF, 0.2µm RC compared to centrifugal filter device 100 kDa.....</i>	<i>142</i>
<i>Table 8.7: Filteradsorption from clear FaSSGF - solution with various filter.....</i>	<i>143</i>
<i>Table 8.8: Filteradsorption from clear FaSSIF - solution with various filters.....</i>	<i>143</i>
<i>Table 8.9: Filteradsorption from clear FaSSIF-V2 – solution with various filters</i>	<i>143</i>
<i>Table 8.10: Filteradsorption from clear FeSSIF – solution with various filters</i>	<i>143</i>
<i>Table 8.11: Filteradsorption from clear FeSSIF-V2 – solution with various filters.....</i>	<i>143</i>
<i>Table 8.12: Dissolution of Lipidil 145 ONE® in FaSSIF, 0.02 µm Anopore</i>	<i>144</i>
<i>Table 8.13: Dissolution of Lipidil 145 ONE® in FaSSIF, 0.1 µm Anopore</i>	<i>144</i>
<i>Table 8.14: Dissolution of Lipidil 145 ONE® in FaSSIF, 0.2 µm RC</i>	<i>144</i>
<i>Table 8.15: Dissolution of Lipidil 145 ONE® in FaSSIF, 0.45 µm RC</i>	<i>145</i>
<i>Table 8.16: Dissolution of Lipidil Ter® in FaSSIF, 0.02 µm Anopore</i>	<i>145</i>
<i>Table 8.17: Dissolution of Lipidil Ter® in FaSSIF, 0.1 µm Anopore</i>	<i>145</i>
<i>Table 8.18: Dissolution of Lipidil Ter® in FaSSIF, 0.2 µm RC.....</i>	<i>146</i>
<i>Table 8.19: Dissolution of Lipidil Ter® in FaSSIF, 0.45 µm Anopore</i>	<i>146</i>
<i>Table 8.20: Dissolution of Lipidil 145 ONE® in FeSSIF, 0.02 µm Anopore</i>	<i>146</i>
<i>Table 8.21: Dissolution of Lipidil 145 ONE® in FeSSIF, 0.1 µm Anopore</i>	<i>146</i>
<i>Table 8.22: Dissolution of Lipidil 145 ONE® in FeSSIF, 0.2 µm RC</i>	<i>147</i>
<i>Table 8.23: Dissolution of Lipidil 145 ONE® in FeSSIF, 0.45 µm RC</i>	<i>147</i>
<i>Table 8.24: Dissolution of Lipidil Ter® in FeSSIF, 0.02 µm Anopore</i>	<i>147</i>
<i>Table 8.25: Dissolution of Lipidil Ter® in FeSSIF, 0.1 µm Anopore</i>	<i>147</i>
<i>Table 8.26: Dissolution of Lipidil Ter® in FeSSIF, 0.2 µm RC.....</i>	<i>148</i>
<i>Table 8.27: Dissolution of Lipidil Ter® in FeSSIF, 0.45 µm PTFE</i>	<i>148</i>
<i>Table 8.28: Dissolution of Lipidil 145 ONE® in FaSSIF – V2, 0.1 µm Anopore</i>	<i>148</i>
<i>Table 8.29: Dissolution of Lipidil 145 ONE® in FaSSIF – V2, 0.2 µm RC.....</i>	<i>148</i>
<i>Table 8.30: Dissolution of Lipidil Ter® in FaSSIF – V2, 0.1 µm Anopore.....</i>	<i>149</i>
<i>Table 8.31: Dissolution of Lipidil Ter® in FaSSIF – V2, 0.2 µm RC.....</i>	<i>149</i>
<i>Table 8.32: Dissolution of Lipidil 145 ONE® in FeSSIF – V2, 0.1 µm Anopore</i>	<i>149</i>
<i>Table 8.33: Dissolution of Lipidil 145 ONE® in FeSSIF – V2, 0.2 µm RC.....</i>	<i>150</i>
<i>Table 8.34: Dissolution of Lipidil Ter® in FeSSIF – V2, 0.1µm Anopore</i>	<i>150</i>
<i>Table 8.35: Dissolution of Lipidil Ter® in FeSSIF – V2, 0.2 µm RC.....</i>	<i>150</i>
<i>Table 8.36: Initial Dissolution of Lipidil 145 ONE® in FaSSGF, 0.1 µm Anopore</i>	<i>151</i>
<i>Table 8.37: Initial Dissolution of Lipidil Ter® in FaSSGF, 0.2 µm RC.....</i>	<i>151</i>
<i>Table 8.38: Initial Dissolution of Lipidil 145 ONE® in FaSSIF - V2, 0.1 µm Anopore</i>	<i>151</i>



<i>Table 8.39: Initial Dissolution of Lipidil Ter® in FaSSIF - V2 0.2 µm RC</i>	<i>152</i>
<i>Table 8.40: Initial Dissolution of Lipidil 145 ONE® in FeSSIF - V2, 0.1 µm Anopore</i>	<i>152</i>
<i>Table 8.41: Initial Dissolution of Lipidil Ter® in FeSSIF - V2, 0.2 µm RC</i>	<i>152</i>
<i>Table 8.42: Filteradsorption of Diphenhydramine (DPH) to 0.2 µm RC filter in various media</i>	<i>161</i>
<i>Table 8.43: Dissolution of DPH in FaSSGF, HPLC method</i>	<i>161</i>
<i>Table 8.44: Dissolution of DPH in FaSSGF, ISE method A</i>	<i>161</i>
<i>Table 8.45: Dissolution of DPH in FaSSGF, ISE method B</i>	<i>161</i>
<i>Table 8.46: Dissolution of DPH in FaSSIF-V2, HPLC method</i>	<i>162</i>
<i>Table 8.47: Dissolution of DPH in FaSSIF-V2, ISE Electrode 1, method A</i>	<i>162</i>
<i>Table 8.48: Dissolution of DPH in FaSSIF-V2, ISE Electrode 1, method B</i>	<i>162</i>
<i>Table 8.49: Dissolution of DPH in FaSSIF-V2, ISE Electrode 2, method A</i>	<i>162</i>
<i>Table 8.50: Dissolution of DPH in FaSSIF-V2, ISE Electrode 2, method B</i>	<i>163</i>
<i>Table 8.51: Dissolution of DPH in FaSSIF, HPLC method</i>	<i>163</i>
<i>Table 8.52: Dissolution of DPH in FaSSIF, ISE Electrode 1, method A</i>	<i>163</i>
<i>Table 8.53: Dissolution of DPH in FaSSIF, ISE Electrode 1, method B</i>	<i>163</i>
<i>Table 8.54: Dissolution of DPH in FaSSIF, ISE Electrode 2, method A</i>	<i>164</i>
<i>Table 8.55: Dissolution of DPH in FaSSIF, ISE Electrode 2, method B</i>	<i>164</i>
<i>Table 8.56: Dissolution of DPH in FaSSIF, ISE Electrode 3, method A</i>	<i>164</i>
<i>Table 8.57: Dissolution of DPH in FaSSIF, ISE Electrode 3, method B</i>	<i>164</i>



1 Introduction

1.1 Oral bioavailability

The term “bioavailability” was coined in the late sixties. It describes the rate and the extent to which the fraction absorbed reaches the general circulation [1]. The primary parameter used to describe the bioavailability is the Area Under the Curve (AUC), reflecting the extent of absorption by an integration of the area underneath a plasma profile of a drug. The AUC after an intravenous (i.v.) injection corresponds to the maximum extent of drug since no absorption step is involved (100%). c_{\max} is a further important parameter that provides information about the rate of absorption. In the i.v. case, the maximum plasma concentration is reached directly after injection at t_0 .

The absolute bioavailability describes the rate and the extent of absorption from a formulation, e.g. a tablet, in comparison to i.v. data.

The relative bioavailability compares two formulations with each other, using one of them as reference. This is often evaluated in formulation development with an eye to improving the initial formulation e.g. to reach a different AUC and/or c_{\max} profile. The development of generic drugs is also guided by the relative bioavailability, with the 90% confidence intervals around the point estimates of AUC and c_{\max} in the plasma profiles needing to fall within the acceptance criteria based on the innovator product.



1.2 Factors limiting oral bioavailability

In 1961, it was realized that low solubility correlates with low bioavailability [2]. In 1971, up to sevenfold differences in plasma levels from different digoxin-formulations were observed [3]. This prompted the question as to whether dissolution rates are responsible for these differences [4, 5]. In 1975, Jounela et al. [6] were able to correlate the particle size and subsequently the dissolution rates of digoxin with its bioavailability. So the aforementioned question could be answered with an unequivocal “yes”.

These findings within the period from 1961 to 1975 can be considered as the origin of pharmacokinetically driven formulation development.

Incomplete drug absorption from an orally administered dosage form is usually due to one or more of four mechanisms [7]:

- 1.) The API is not delivered from its formulation in an appropriate time frame, to facilitate complete dissolution, resulting in elimination from the GI-tract before absorption is complete (dissolution-limited absorption).
- 2.) The drug degrades in the physiological GI fluids or non-absorbable complexes are formed.
- 3.) The drug is not transported efficiently across the GI-membrane (permeation-limited absorption).
- 4.) The drug is metabolized and/or eliminated before it enters the systemic circulation.



The mechanisms 2.), 3.) and 4.) are difficult to address in formulation development. While degradation e.g. by gastric fluids can easily be resolved by coating processes using gastric fluid resistant polymers, permeation across the mucosa is still an issue that formulations scientists have to face. Despite some reports in literature enhancing permeation by the use of chitosan [8, 9], permeation issues are still not successfully worked out or fail due to lack of safety data about the excipient used to improve permeability [10]. Metabolism can sometimes be used for improvement of drug performance, but mostly these effects are caused by pharmacokinetic instead of galenical issues. An example for such effects is the boosting of anti-HIV-drug pharmacokinetics using subtherapeutic doses of Ritonavir. This drug inhibits CYP-enzymes. By a concomitant dosing of Lopinavir and Ritonavir, the degradation of Lopinavir by the CYP-enzymes is hindered and the duration of therapeutic plasma concentration of Lopinavir is prolonged [11].

But the major hurdle that can be addressed in formulation development is low aqueous solubility and subsequent slow dissolution, leading to insufficient bioavailability, as mentioned in point 1.) above.

1.3 Solubility and drug dissolution

As mentioned above it is obvious that an increase of dissolution rate can lead to an improved bioavailability. Several options are available to do so:

One of the classical approaches to increase the rate of dissolution is through decreasing particle size. Arthur Noyes and Willis Whitney identified the underlying



basis for the correlation between particle size and dissolution rate in 1897. In the original publication its mathematical expression is:

$$\frac{dx}{dt} = C(S - x)$$

Eq. 1.1

where S represents the solubility of the substance, or the concentration of its saturated solution; x is the amount of dissolved drug at time t , and C is a constant [12].

In 1904, the equation was modified by Nernst-Brunner and became what is nowadays one of the most important equations in pharmaceutical science.

$$DR = \frac{A_{Drug} \cdot D_{Drug}}{\delta} \cdot (C_S - C_t)$$

Eq. 1.2

where DR is the dissolution rate, A_{Drug} is the drug surface area, D_{Drug} is the diffusion coefficient of the drug, δ is the diffusion layer thickness, C_S is the saturation solubility of the drug and C_t is the concentration of the dissolved drug at time t .

After the “digoxin-incident” [3, 5], the focus in dissolution testing for drug dissolution for poorly soluble substances shifted to establishing *in vitro* – *in vivo* – correlations (IVIVC). Since the gastrointestinal (GI) environment is a varying milieu with a pH-range from 1 - 7.4. and varying amount of electrolytes and bile salts, it is logical to adjust the composition of the dissolution media and the hydrodynamics of the test conditions to the human physiology [7]. In the ideal case, the *in vivo* performance is predicted by the



dissolution test using IVIVC. Oversimplification of the test conditions, for example by using compendial media which take only the pH-value of the GI tract into account, often leads to implausible predictions of *in vivo* behaviour [13]. Biorelevant media including FaSSIF and FeSSIF were introduced in 1998 [14]. Since these media better correspond to the *in vivo* situation [7], a better prediction of *in vivo* behavior of the drug formulation could be established, including the prediction of food effects. The media have been recently revised by Jantratid et al. [15], altering the media composition of FaSSIF and FeSSIF and introducing media for the gastric dissolution (FaSSGF, FeSSGF, “snapshot media”). The use of these media enables the prediction of food effects in combination with physiologically based pharmacokinetic modeling to generate *in silico* plasma profiles [16, 17].

1.4 The biopharmaceutics classification system

Dissolution testing can also be employed to facilitate drug product approval by allowing waiver of *in vivo* bioequivalence studies [18-20].

The interplay of solubility and absorption was acknowledged in 1995 in the Biopharmaceutics Classification System (BCS): Amidon et al. proposed a scheme, based on solubility and permeability, according to which a biowaiver can be granted [21]. Applicability of IVIVC to formulation development can also be determined according to this scheme:



Table 1.1: Probabilities for IVIVC as suggested by Amidon [13, 21]

Class	Solubility	Permeability	IVIVC Expectation
I	High	High	IVIVC if dissolution rate is slower than gastric emptying rate (e.g. controlled release dosage forms)
II	Low	High	IVIVC if dissolution rate is similar to the in vivo dissolution rate, unless dose is very high
III	High	Low	Permeability is rate determining, limited or no IVIVC
IV	Low	Low	Limited or no IVIVC expected

Active pharmaceutical ingredients (API) belonging to the BCS classes I and III are not likely to cause problems in terms of dissolution-limited bioavailability. The drugs of these classes are highly soluble, so dissolution is not an issue for the formulation. In case of BCS class III, poor bioavailability cannot be corrected easily by formulation since it is usually due to poor uptake at the gut wall. Taking a look at the current market share of drugs, more than 60% of the drugs belong to BCS class I or III (compare Figure 1.1 derived from [22]).

The formulation of poorly soluble substances has become more and more an issue in pharmaceutical industry over the past decades. The oral route is generally preferred. But since the early 90's, APIs are often identified by high throughput screening and combinatorial chemistry. These approaches often lead to substances that possess physicochemical characteristics unfavorable for oral absorption. A major hurdle is their



low aqueous solubility and subsequent slow dissolution, resulting in insufficient bioavailability according to the Nernst-Brunner equation (compare Eq. 1.2). For the formulation scientist it is essential to resolve dissolution-limited absorption by the right choice of dissolution rate enhancing techniques, which will be described in detail in later sections.

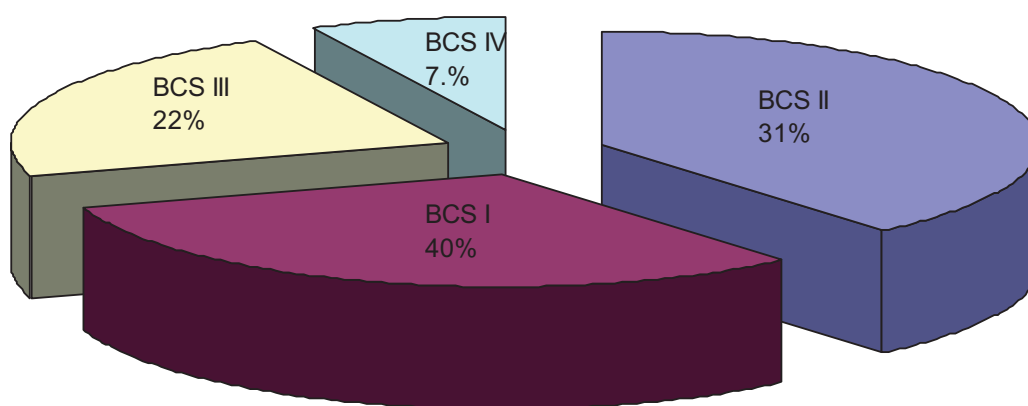


Figure 1.1: Current market share of drugs according to the Biopharmaceutics Classification System (derived from [23] and [22])

Figure 1.1 indicates that nearly 50% of marketed drugs exhibit low aqueous solubility. However, if only APIs approved in the last decade are taken into account, the market share shows a tendency towards more BCS Class II and IV compounds:

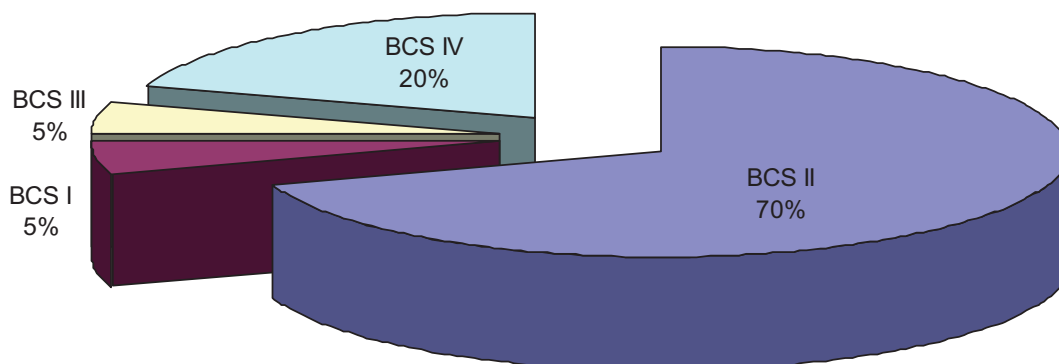


Figure 1.2: Market share of recently developed drugs according to the BCS [22, 23]

Figure 1.2 shows that solubility improvement is necessary for up to 90% of recently developed drugs and clearly illustrates the need for new formulation approaches to increase bioavailability.

The possibilities to formulate BCS class II and IV substances for oral administration will be described in the next section.

1.5 Formulation of poorly soluble substances

The flow process chart in Figure 1.3 gives an overview of how to find a suitable formulation for a poorly soluble API [24].

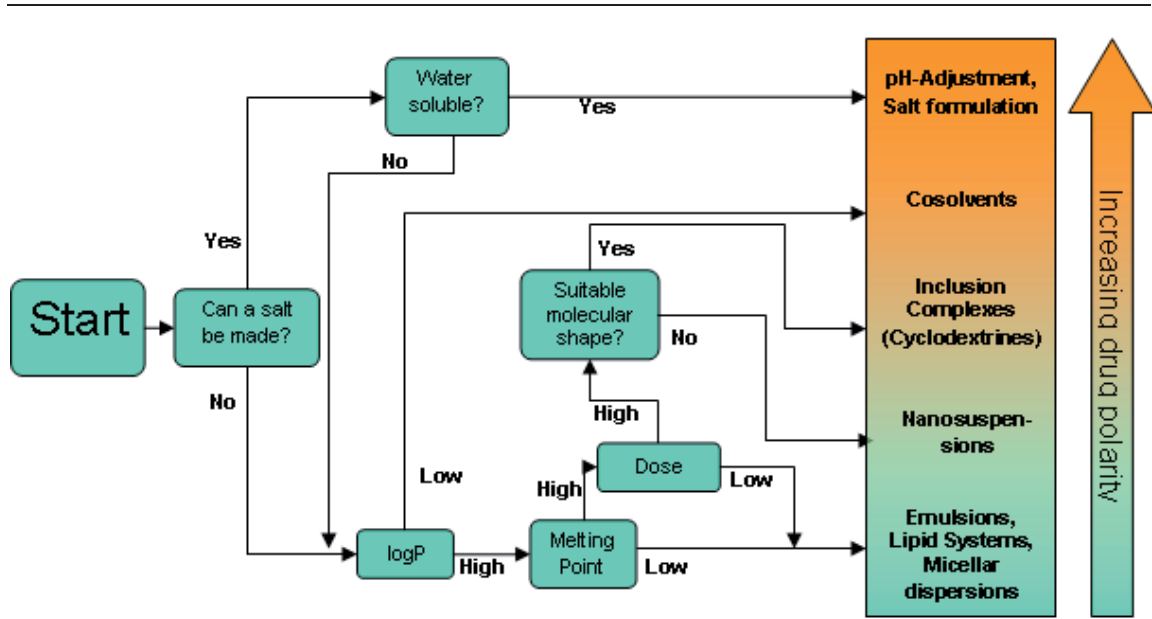


Figure 1.3: Decision tree in formulation finding for poorly soluble compounds (derived from [24])

Formation of a water-soluble salt from a water-insoluble compound is the method of choice to increase bioavailability, since salt formation is an easy and well-described technique [25-27]. There is a broad variety of counterions for anions as well as for cations, although most frequent used counterions are sodium and hydrochloride [28]. In addition to solubility improvement and hence dissolution rate enhancement, salt formation can positively influence hygroscopicity, chemical stability, crystal form and mechanical properties [29].

The use of cosolvents can be applied to poorly soluble compounds for injection, but for orally administered drugs as solid dosage forms, this is obviously not the method of choice.



Cyclodextrins are able to increase the saturation solubility of a compound by its complexation. In this way, supersaturated systems are created. According to Eq. 1.2 the dissolution rate, and subsequently the bioavailability, for drugs of BCS class II and IV is increased, especially when cyclodextrins are also able to function as a permeability enhancer [30, 31]. Nevertheless, cyclodextrins are not the answer to every challenge in oral drug formulation. For a variety of reasons, including toxicological considerations, formulation bulk and production cost, the use of as small amounts of cyclodextrins as possible in pharmaceutical formulations is preferred [32]. Since cyclodextrins often bind to the drug in a certain molecular ratio (usually 1:1 or 2:1), they are less suitable for highly dosed drugs. Nevertheless, cyclodextrins and their derivatives are used for orally administered pharmaceutical products, and there is even a sublingual tablet Prostarmon E[®] (Ono Pharmaceutical Co, Japan), which contains β -cyclodextrin to solubilise prostaglandine E [33]. Especially for low dosed APIs, derivatives of cyclodextrins with improved physicochemical characteristics appear to be suitable for enhancement of drug solubility [34].

The enhancement of bioavailability by the use of lipid-based systems has been recognized for many years [35]. These formulations are able to keep the poorly soluble compound in solution and thus maintain a concentration of dissolved drug as the driving force for absorption [36]. Pouton has proposed the lipid formulation classification system (LFCS) [37]:



Table 1.2: The LFCS as proposed by Pouton [37]

LFCS type	Characteristics	Advantages	Disadvantages
Type I	Non-dispersing, requires digestion	GRAS status; simple; excellent capsule Compatibility	Formulation has poor solvent capacity unless drug is highly lipophilic
Type II	SEDDS without water-soluble Components	Unlikely to lose solvent capacity on Dispersion	Turbid o/w dispersion (particle size 0.25–2 µm)
Type IIIa	SEDDS/SMEDDS with water-soluble Components	Clear or almost clear dispersion; drug absorption without digestion	Possible loss of solvent capacity on dispersion; less easily digested
Type IIIb	SMEDDS with water-soluble components and low oil content	Clear dispersion; drug absorption without digestion	Likely loss of solvent capacity on Dispersion
Type IV	Oil-free formulation based on surfactants and cosolvents	Good solvent capacity for many drugs; disperses to micellar solution	Loss of solvent capacity on dispersion; may not be digestible

Nowadays lipophilic drug delivery systems are used for about 2% of oral formulations. An example for such patented systems is the Lidose[®] platform technology by S.M.B. Laboratoires [38]. This technology utilizes a mixture of API and lipophilic excipients in a hard gelatine capsule, either semi-solid or solid. The mixture melts at body temperature, forming a stable suspension or solution, which in turn leads to increased absorption of drug and subsequently more reliable blood plasma profiles. This patent was commercialized using fenofibrate (Fenogal[®]). The dosage form shows bioequivalence to the micronized, suprabioavailable formulation Tricor[®] or Lipidil Ter[®],



products marketed by Abbott and Solvay, respectively (compare section 3.2.1). The challenge in using lipid formulation approaches is the potentially metastable state of the formulation in the GI tract: with a change of environment, e. g. by dilution in the stomach depending on its content, the system might not be able to hold the API in solution and precipitation can occur before the drug enters the small intestine, the main site of absorption. But even when the formulation reaches the intestine intact, the digestion of lipid components of the formulation might cause a rapid disassembly of the formulation, resulting in precipitation of the API (if in solution) or a change of crystalline state (if in suspension).

The crystalline state of the drug can influence solubility and dissolution behaviour significantly. Depending on thermodynamics, form A of a drug might be more stable than form B, resulting in a longer shelf life of the dosage form. But often the more stable form possesses disadvantageous characteristics regarding drug solubility and dissolution. An amorphous state is more favorable in this respect, since no crystal lattice energy has to be overcome to dissolve the drug. But amorphous states are metastable by definition, and a transition of the desired amorphous form into an unfavorable crystalline form can occur [37, 39, 40].

The possibility of an unwanted phase transition remains a challenge for formulations containing amorphous API. An example is the conversion in a liquid formulation of ritonavir from form I to the less soluble form II in the soft capsule. This results in supersaturation and subsequent precipitation of drug within the capsules [41].



Nowadays there are often approaches to utilize the benefits from amorphous formulations. By dispersing the API into polymers, forming solid dispersions, the amorphous state can be preserved at least temporarily. Of course, phase conversion can happen here as well, depending on the drug. A well described technique to form amorphous dispersions in solid states is the melt extrusion of polymers. The API, amorphous dispersed or dissolved in the polymer melt, is immobilized in a matrix by dropping the temperature below the glass transition temperature. Even if recrystallisation occurs within a hydrophilic polymer, often only very small crystals are formed due to the inability of the lipophilic drug to mix with the polymer [42]. Consequently, the performance of the dosage forms may not be drastically affected by such a transformation. Not only the bioavailability but also the applicability and subsequently the compliance of the patient can be improved by melt extrusion (e.g. there is no need for refrigeration of the melt extrusion product Kaletra[®] in contrast with the predecessor liquid formulation). Drawbacks include the high input of energy in form of temperature and shear forces, which may lead to a high degree of degradation for thermolabile drugs [37, 42].

1.6 Particle size reduction in pharmaceutical technology

By optimizing the particle size within a drug powder, the following aims can be achieved:



-
- (i) The application can be made easier, e.g. pulverization of a drug can lead to shorter extraction times.
 - (ii) The accuracy of dosing can be improved. This is certainly not the case for very high dosages, but in cases of very potent drugs a narrow particle size distribution is a prerequisite for accurate dosing.
 - (iii) Flowability is often related to particle size. By matching the right particle size and its distribution, tableting and dispergibility of a powder, e.g. in ointments can be improved
 - (iv) According to the Nernst-Brunner equation the reduction of particle size leads to an increase surface area and subsequently to an enhanced dissolution rate. In consequence, a larger amount of dissolved drug is provided for absorption and bioavailability can be increased. Several studies prove the success of this formulation approach [6, 43-45].

1.6.1 Particle size reduction

From the very first attempts to manufacture pharmaceutical preparations hundreds of years ago, pharmacists reduced the particle size of powders and drugs using a mortar and a pestle. By using this easy but effective technique, it was possible to grind plant components into powders with a subsequent release of essential oils that have a healing effect. The mortar and pestle are still in use in pharmacies, e.g. for the preparation of extemporaneous prescriptions. Nowadays, these simple tools are more common in the kitchen at home for grinding of spices and for preparation of food.



Here the mortar and pestle demonstrates superiority to many modern tools for particle size reduction: They can be used for grinding both dry substances like peppercorns as well for wet milling operations as the preparation of a delicious pesto [46].

Nevertheless, particle size reduction has become its own science that divides the mechanism of particle size reduction into (i) pressure and friction, as is the case for the mortar and pestle method, (ii) collision and (iii) hammer and (iv) shear forces.

The reduction ratio can be easily expressed as

$$Z = \frac{d_0}{d_1}$$

Eq. 1.3

Where Z is the reduction ratio, d_0 is the initial particle size and d_1 the particle size after the milling process. The reduction ratio is dependent on (i) the type of technical operation, (ii) the operating conditions and (iii) the physicochemical characteristics of the milled substance. Solid substances contain predetermined fission points in each particle, caused by imperfections of the crystal lattice. As particle size is decreased, these imperfections become fewer and the energy needed for further reduction increases. The maximum energy that can be applied is determined by the choice of equipment and the operating conditions [47].



1.6.2 Dry milling methods

An overview of tools used for dry milling is provided in Table 1.3 [48].

Table 1.3: Dry milling operations [48]

Tool	Working principle	Degree of fineness	Principle of particle size reduction
Roller crusher	Rollers running against each other, smooth or spiny	1 – 2 mm	Pressure, friction
Cutting mill	Rotating kniferoll, stationary cutting edge	1 – 5 mm	Chopping
Hammer mill	Rotating hammer (rotor), stationary jaw (stator)	0,3 – 2 mm	Collision, hammer
Ball mill	Cylindric, rotating vessel containing spherical grinding elements	ca. 20 μm	Collision, hammer, pressure
Pin disc mill	Rotating pair of discs with interleaved pins	20 – 200 μm	Collision, hammer
Mortar mill	Mortar with stationary, versatile pestle	n.a.	Pressure, friction
Jet mill	No moving parts, powder-loaded jet-stream	1-30 μm	Hammer, friction

Using a dry milling technique, climate control within the production rooms is very important. Hygroscopic substances may bind more water in a humid atmosphere, making them more resistant to milling. In addition, it has to be guaranteed that no explosive dusts are generated.

For poorly soluble substances the need for climate control of production rooms can be circumvented by applying a wet milling technique. These are described in the next section:



1.6.3 Wet milling methods

An overview of tools used for wet milling is provided in Table 1.4 [48]:

Table 1.4: Wet milling operations [48]

Tool	Working principle	Degree of fineness	Principle of particle size reduction
Rasper	Fan pushes grinding material through a piercing cylinder	1 – 5 mm	Pressure, chopping
Three-roll mill	Rollers rolling against each other, adjustable	50 – 200 μm	Pressure, friction
Agitator ball mill	Fast-rotating discs with abrasion-resistant milling beads or sand in a cylindric vessel	1 – 30 μm	Friction, shear forces
Colloid mill	Fast-rotating wet-mill with rotor-stator-arrangement	1 – 30 μm	Friction, shear forces, (chopping)

1.6.4 Comparison of dry and wet milling techniques

To come back to the mortar and pestle, it is obvious that not many mills are capable of dealing with both dry and wet materials. The mortar takes a special place here, as since antiquity it has been used to mill both dry and wet material. Nevertheless, by comparing particle size reduction possible, only the jet-mill is capable of delivering micronized material using a dry milling approach, while among the wet milling techniques several are capable of micronization. Coming back to the energy required, jet-milling is not the method of choice if a wet-milling technique can provide the same outcome for a given API. Referring to section 1.6.1, the input of energy is one of the



key factors in particle size reduction, so the wet milling techniques are often preferred. For the jet-mill, two gas streams are needed, which are capable of generating explosive dusts. This is not the case with the wet-milling methods, so they are advantageous in terms of safety and efficiency.

To sum up, both dry and wet milling techniques are capable of delivering micronized material and in turn improving the oral bioavailability.

Unfortunately, recently developed drugs tend to be practically insoluble in aqueous media so that even micronization often does not result in a sufficiently fast dissolution rate. In these cases, there is the possibility of combining micronization with other techniques.

1.6.5 Combining micronization with other techniques

In case micronization alone does not improve the rate of dissolution sufficiently, this technique can be combined with others in order to achieve the desired product attributes.

Coprocessing of solubilising agents like PVP or SLS into the formulation might improve the dissolution rate. To achieve an ideal contact between the solubilizer and the API the solubilizer should be brought to the same size. This can be done practically by cogrinding the drug with its solubilizer. There are some examples in the literature which have utilized this technique successfully [49, 50].



Guichard et al. developed Lipidil-Ter[®] by spraying micronized fenofibrate onto a water-soluble core in order to improve the dissolution rate of fenofibrate [51]. Vogt et al. described an improvement of dissolution rate of fenofibrate by cogrinding the drug with PVP, SLS or Lactose. Results were advantageous over the commercial formulation of Lipidil Ter[®] [52, 53].

1.7 Rationale for nanonization of drug particles

For very poorly soluble substances, micronization is an attractive way to enhance the dissolution rate, but often meets with only modest success. The API still tends to be eliminated from the GI tract before it is fully dissolved, limiting its absorption into the circulation. This is often dependent on the prandial state, since solubility of the drug is affected by the surrounding GI liquids, resulting in a food effect, e.g. a higher bioavailability in the fed state. In consequence a high intra- and interindividual variability of plasma profiles and lack of dose proportionality of the bioavailability is observed.

Despite its more favorable pharmacokinetics compared to the non-micronized formulation, this is also the case for the suprabioavailable fenofibrate formulation described in section 3.2.1. So the dissolution rate of formulations developed using such approaches is still dependent on the surrounding medium due to solubility.

By contrast, the nanonization of a drug is an approach to enhance the surface area of a drug so enormously that dissolution behaviour of the drug is virtually independent of the solubility in the surrounding medium.



1.8 Preparation of nanosized drug particles

The preparation of nanocrystalline drug suspensions is more difficult than micronization since several challenges come into play when particle size falls below the micrometer range. Conventional milling methods such as hammer- or jet-mill cannot fulfill the goal of nanonization due to their construction principles and resulting physical limitations.

Therefore, there is a need for a suitable preparation method to mill the API into the nanometer range and provide a reproducible particle size. Once the particle sizes decrease below one micron, agglomeration or even particle growth by Ostwald ripening may occur. The choice of a suitable stabilizer, e.g. polysorbates or povidones, is crucial to stability. Both the stabilizer and its ratio to drug have to be evaluated empirically. The drug to stabilizer ratio usually ranges from 20:1 to 2:1. [54]. A too low ratio will result in agglomeration of particles, while when a too high ratio is present in the nanodispersion it will already dissolve small quantities of the drug. This will lead to increased Ostwald ripening due to the imbalance between particle sizes, resulting in redistribution of mass among particles based on their curvature. To prevent this effect, it is also important that the production processes result in a narrow particle size distribution (Figure 1.4.).

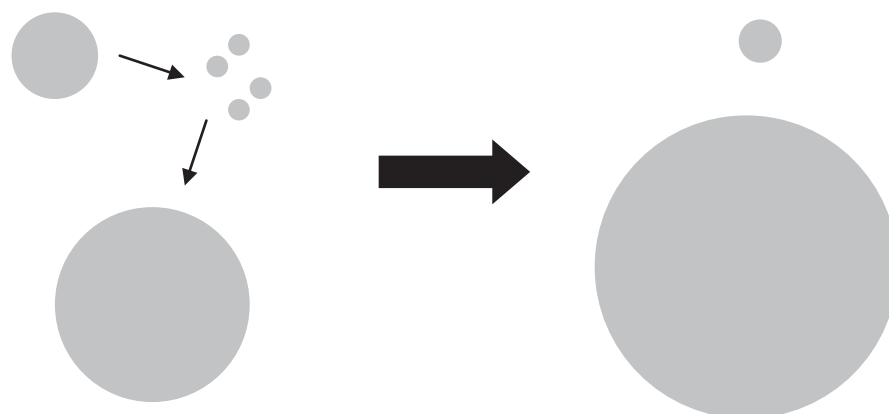


Figure 1.4: Basic scheme of the Ostwald ripening process: an unequal size distribution under the drug particles induces dissolution of smaller particles. The dissolved drug precipitates on larger particles.

In principle, there are two main methods to produce stable nanosuspensions of poorly soluble APIs:

- Wet milling methods (Bead mills)
- High pressure homogenization

1.8.1 Wet-milling methods (bead mills)

Wet-milling using bead mills are one of the most effective ways to decrease the particle size of an API. With this technique, large drug crystals are suspended in a milling medium. The milling medium consists of a fluid containing the milling beads and the the API, which must be insoluble in the milling medium. The milling beads need to show more physical robustness than the drug to be nanomilled and must of course be stable against high shear forces in general. A crude slurry consisting of drug, water and stabilizer is fed into the milling chamber. In the milling chamber, the drug



crystals are subject to high energy input provided by the milling medium. The process can be run either in a batch mode or in recirculation. The typical residence time to mill the API down to about 200 nm in mean diameter is 30 to 60 minutes in batch-mode [54]. Nevertheless, the time-frame needed is drug specific and in other cases it can take hours or even days to achieve the desired size of drug crystal [55, 56].

The choice of beads used for milling is contingent on their ability to resist abrasion during the milling process, which would lead to product contamination [57]. Beads made from glass or zirconium are likely to withstand the milling process, but even with these beads potential product contamination by abrasive bead fragments has to be considered carefully.

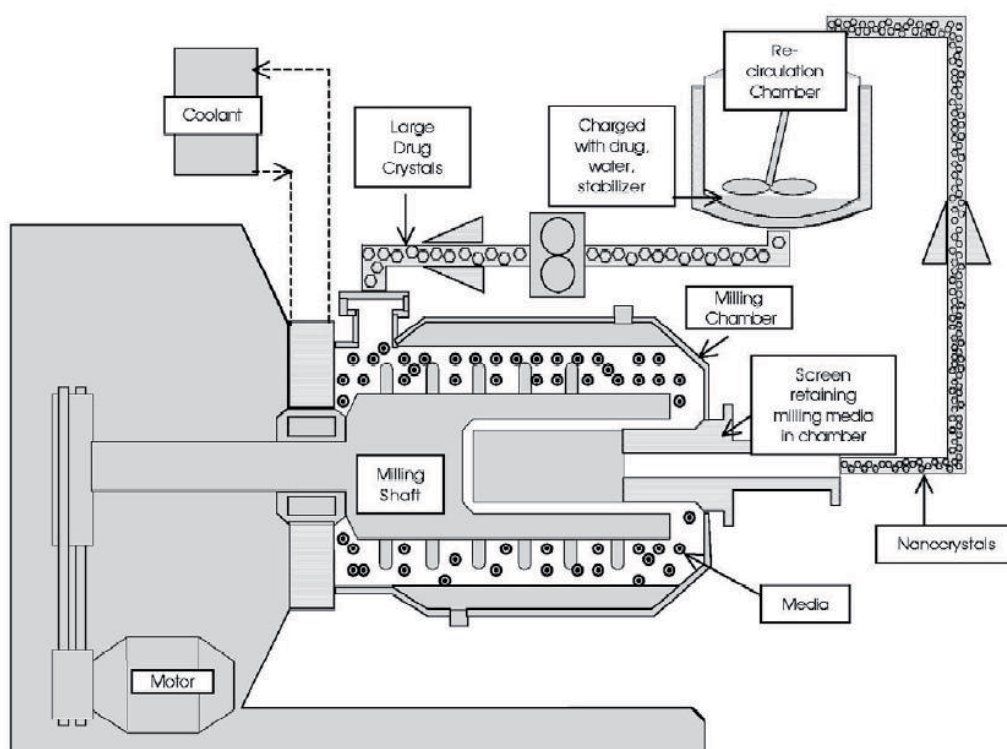


Figure 1.5: Schematic representation of media milling process(taken from [54])



1.8.2 High pressure homogenization

After the wet milling method, high pressure homogenization is the second most frequently applied disintegration method to obtain nanosized drugs. An example is the IDD-P technology from Skye Pharma. This technology creates high shear forces, cavitation and/or impaction to reduce the particle size to less than a micron [58]. In contrast to the wet-milling process, no milling beads are required here, obviating the risk of contamination by eroded beads or machinery parts.

The IDD platform can be further divided into (i) homogenization by microfluidisation and (ii) homogenization by the use of a piston-gap:

Microfluidisation is a jet stream principle, in which the suspended drug particles flow into a homogenization chamber. In this chamber, the direction of flow is changed several times, leading to high impact collisions that reduce the particle size further and further. The principle is well-known from the jet mill and can be considered as its fluid analog [57]. This technology requires long production cycles and is unfavorable for large scale production.

Homogenization using a piston-gap is more common. The drug suspension flows through a channel of about 3 cm in diameter. This flow channel diameter is diminished to a gap of about 25 μm , resulting in high pressure. This results in a sudden change of hydrodynamic pressure and as consequence, the fluid cavitates. After this gap, the diameter expands again to 3 cm. The gas bubbles that were formed in the gap implode.



The released energy gets transferred into the drug particles, which break and reduce in size. This technique is also known as the DissoCube[®] technology [57].

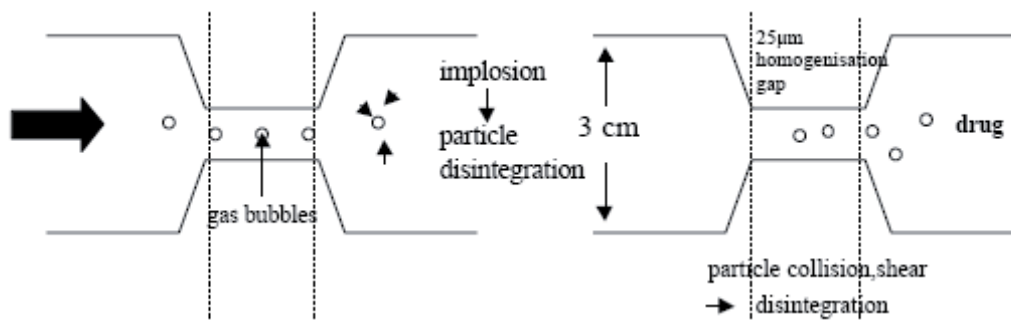


Figure 1.6: Principle of the DissoCube[®] -Technology (taken from [57])

1.8.3 Commercialized nanosized drugs

Table 1.5 lists the commercialized products currently available that use a nanoparticle technology (modified from [55]). Due to the fact that there are several other products in the pipeline of several companies, an expansion of this list is expected within the next years.



Table 1.5: List of commercialized nanosized drugs (modified from [55])

Product	Drug compound	Indication	Company	Nanoparticle technology
Rapamune [®]	Sirolimus	Immunosuppressant	Wyeth	Elan Drug Delivery Nanocrystals [®]
Emend [®]	Aprepitant	Antiemetic	Merck	Elan Drug Delivery Nanocrystals [®]
Tricor [®] (Lipidil 145 ONE [®])	Fenofibrate	Treatment of Hypercholesteria	Abbott (Solvay)	Elan Drug Delivery Nanocrystals [®]
Megace ES [®]	Megestrol acetate	Appetite stimulant	Par Pharmaceuticals	Elan Drug Delivery Nanocrystals [®]
Triglide [®]	Fenofibrate	Treatment of Hypercholesteria	First Horizon Pharmaceuticals	SkyePharma IDD [®] -P technology
Invega Sustenna [®]	Paliperidone palmitate	Treatment of Schizophrenia	Janssen	Elan Drug Delivery Nanocrystals [®]

1.8.4 Increase of bioavailability by nanonization

By employing Nanocrystals[®] for fenofibrate (Tricor[®], Lipidil 145 ONE[®]), the dissolution rate is enhanced by the further increase of surface area in comparison to the micronized formulation (compare Eq. 1-2).

These nanocrystalline formulations exhibit even better bioavailability than the micronized version, so that the dose could be lowered from 160 mg to 145 mg of fenofibrate and still maintain bioequivalence to the 200 mg conventional capsule. With the nanosized formulation it is possible to administer fenofibrate independently of meal intake, since no food effect is observed [59]. Additionally, formulations with



reduced particle size have been demonstrated to provide a more efficient and better tolerated treatment of hypercholesterolemia and hypertriglyceridemia. Due to rapid dissolution of nanosized API it is possible to fully utilize the absorption mechanism in the GI tract, so a sufficient amount of dissolved drug for absorption is provided. The underlying basis for the dissolution limited bioavailability and its improvement by nanonization is illustrated in Figure 1.7 and Figure 1.8.

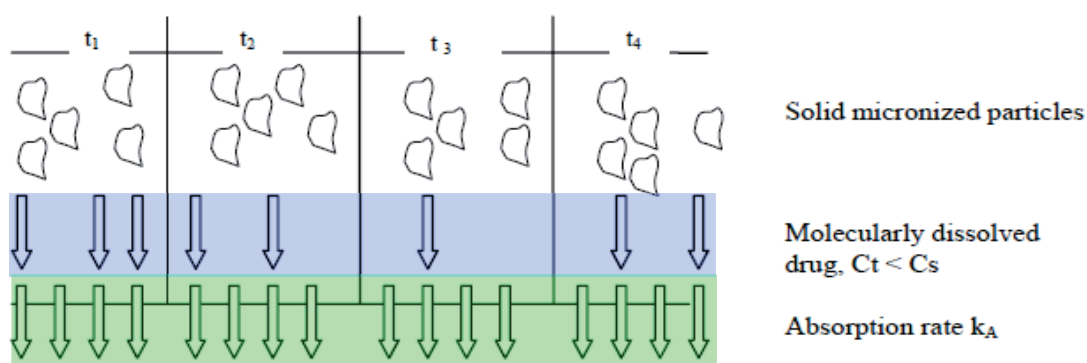


Figure 1.7: Illustration of dissolution (blue) limited absorption (green) using micronized API

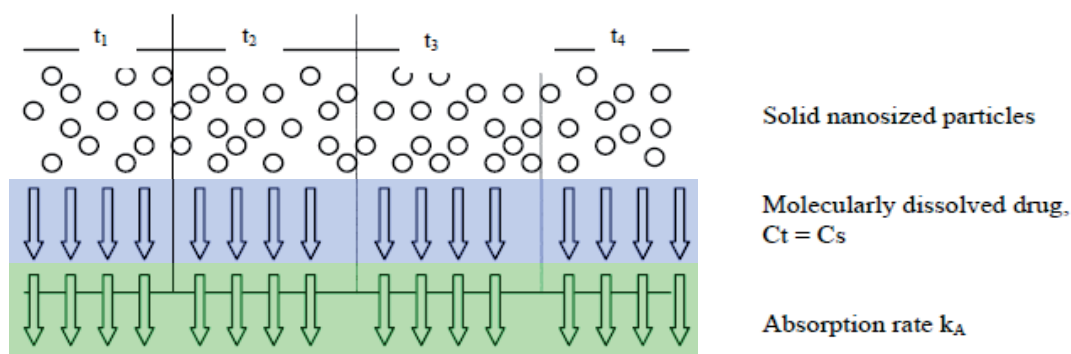


Figure 1.8: Faster dissolution (blue) of nanosized API utilizes maximum absorption rate (green)



1.8.5 The lack of food effects using nanosized APIs

In case of fenofibrate, the variability of the bioavailability can at least partly be affected to the prandial status of the patients: Fenofibrate exhibits a strong positive food effect. Given without food, the bioavailability is low, resulting in plasma levels of fenofibric acid being subtherapeutical. As consequence, intake is recommended with a meal [60].

A common explanation for the increased postprandial bioavailability of poorly soluble drugs is the improved rate of dissolution and solubilization due to the increased levels of bile salts such as sodium taurocholate and the presence of lipid digestion products, e.g. glycerol monooleate, within the intestinal lumen [61]. The higher solubility of the drug in these fluids increases the dissolution rate and subsequently the oral bioavailability.

By nanonization of the drug, the food effect can be attenuated or even eliminated. Due to the rapid dissolution in the fasted and in the fed state the drug can be delivered from its formulation to the intestinal membranes within a sufficient time frame. Additionally, the increase in surface area compensates for the differences in the rate of dissolution in the fasted and fed state.



1.8.6 Improvement of bioavailability for drugs with an absorption window

The dissolution in an appropriate time-frame is essential for drugs with an absorption window in the upper intestinal. The process is illustrated in Figure 1.9 and Figure 1.10:

In the first case the absorption window cannot be fully utilized. When the absorption window is reached, only a small quantity of drug has already dissolved. In consequence, a fraction of the drug is not available for absorption and is eliminated with the feces.

When nanosized API is employed, the absorption window can be utilized much better, resulting in a better bioavailability of the drug.

The ineffective use of an absorption window might also be related to a food effect, since both can be related to poor solubility of the drug.

The marketed product Emend[®] containing aprepitant has such an absorption window and exhibits a food effect. Nanonization of the drug enables the patient to take Emend[®] without a meal, which improves the treatment of nausea caused by cytotoxic agents [62].

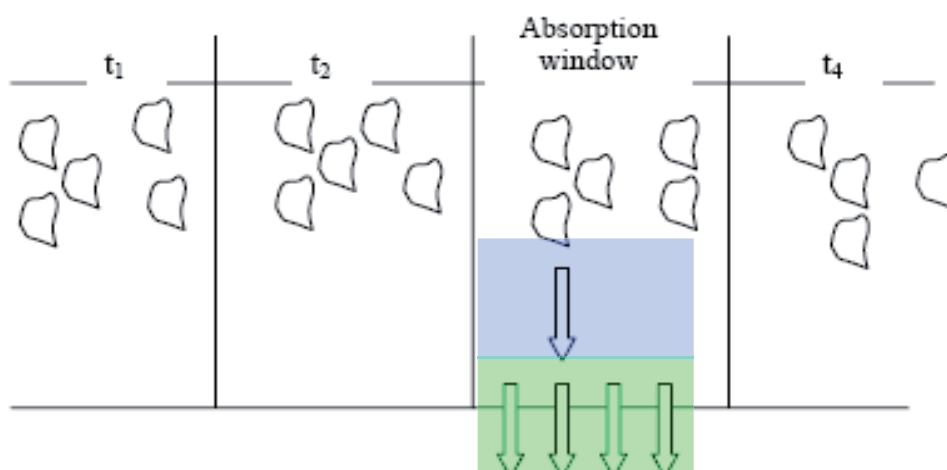


Figure 1.9: Illustration of an absorption window (green) utilized by conventional drug particles with slow dissolution rate (blue)

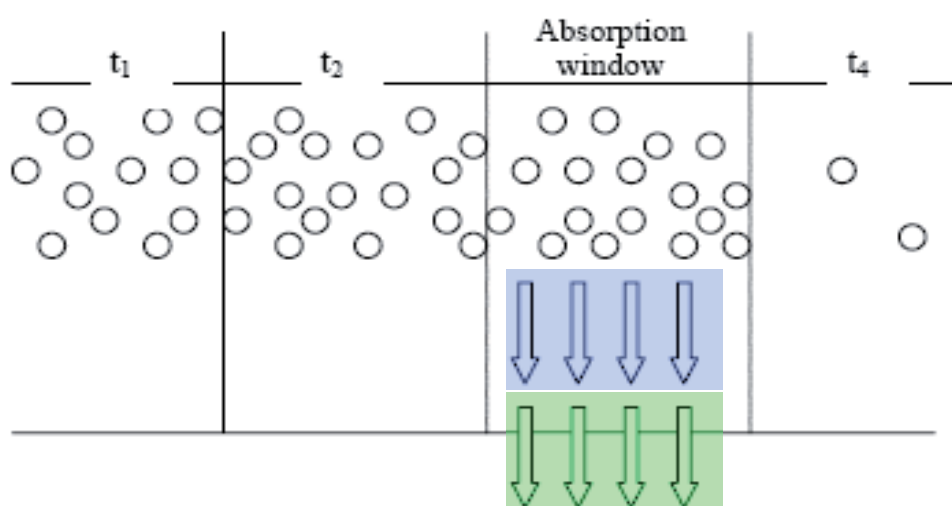


Figure 1.10: Illustration of an adsorption window (green) nearly fully utilized by nanosized drug particles with rapid dissolution rate (blue)

1.9 Sample preparation and analysis in dissolution testing

Dissolution testing aims to predict the amount of dissolved drug in the GI tract, since only dissolved drug is available to be taken up through the mucosa. Consequently, sample preparation in dissolution testing always comprises the need to separate solid drug particles from already dissolved drug particles with (i) a suitable sample



preparation or (ii) an analytical technique which does not require the need for sample preparation since only dissolved drug is detected.

1.9.1 HPLC-UV

Sample analysis by HPLC-UV is the standard method in dissolution testing. It combines simplicity with high accuracy. The basic necessity is the separation of solid drug particles from dissolved drug within the sample. This can be conducted in different ways:

1.9.1.1 The use of syringe filter

The use of syringe filter is simple but efficient. After sample drawing with a glass syringe, filters with a pore size of 0.45 μm are used. The filter membrane consists of hydrophilic or inert materials to avoid adsorption of a lipophilic drug to the membrane. Typical materials are polytetrafluoroethylen (PTFE), regenerated cellulose (RC) or polyvinylidene difluoride (PVDF). Adsorption to the membrane can be decreased by a presaturation of the membrane, e.g. by discarding the first 2 ml of the dissolution test sample [23]. In case of very small drug particle sizes, e.g. less in diameter than the nominal filter pore size, it is likely that solid drug particles will be found in the filtrate.



1.9.1.2 Centrifugal filter devices

For suspensions with very small particles, centrifugal filter devices can be used to separate solid material from dissolved drug, e.g. the Microcon[®] series by Millipore. The pore size of these filters ranges from 3 kDa to 100 kDa. The filter devices are filled with the sample and spun in a centrifuge afterwards. This is a technique commonly used to concentrate protein samples or to analyze the sustained release from nanoparticles. The subsequent analysis of the filtrate can be conducted via HPLC-UV.

1.9.1.3 Dialysis methods

Dialysis is a common method to measure concentration gradients of two liquids divided by a dialysis membrane (side-by-side dialysis). The subsequent analysis can be conducted via HPLC-UV. The disadvantage is the long equilibrium time needed by the API to diffuse through the dialysis membrane. Hence this technique is more common for long-term release dosage forms like implants, stents or injectable long-life nanoparticles [63]. Nevertheless, there are reports of dialysis methods like the dialysis bag for dissolution testing of instant release dosage forms [64]. A remaining question with the use of dialysis is whether one measures the rate of mass diffusion through the dialysis membrane instead of the release from the dosage form, especially for very fast dissolving compounds.



1.9.1.4 Microdialysis

Microdialysis is a technique commonly used in pharmacokinetic studies. [65] The small probe can easily be implanted into the tissue to analyze the concentration of drug in situ at the place of action. To visualize the process, one can draw an analogy between the microdialysis probe and a blood capillary. A microdialysis probe is usually constructed as a concentric tube where the perfusion fluid enters through an inner tube, flows to its end, exits the tube, and flows back between the inner tube and the outer dialysis membrane. The rate of recovery is dependent on (i) the molecular weight cut-off of the dialysis membrane (MWCO), (ii) the flow rate and the choice of perfusate and (iii) the gradient of concentration between the perfusate and the outer phase, in this case the dissolution medium [65].

Again, the subsequent analysis can be conducted using an HPLC-UV system. This technique has already been described for dissolution testing and appears to be a promising technique for dissolution in simple dissolution media such as water [66-69]

1.9.2 Fiber optics

The use of fiber optics does not require sample preparation, the dissolution process can be monitored online [70]. It is a spectroscopic method that uses the specific UV-absorption of a drug.

The UV cell can be located into the hollow shaft of the stirrer in dissolution testing to avoid hydrodynamic disturbances caused by a probe [71]. The basic principle of this technique is shown in Figure 1.11.

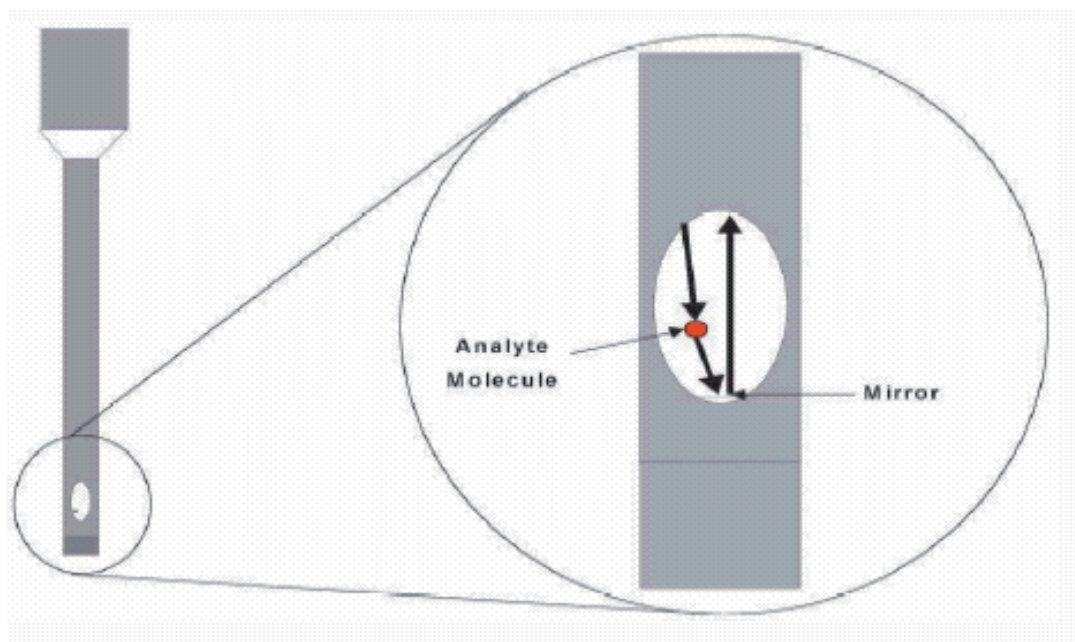


Figure 1.11: Principle of fiber optics (source unknown)

With this method the need for sample preparation is obviated, resulting in a save of time and organic solvents. In addition, more complete dissolution profiles are generated: The dissolution profile consists not of few sampling time points as with the use of e.g. syringe filters but rather generates a continuous profile with measurements every few seconds.

On-line monitoring in biorelevant media is often associated with challenges since fiber optics and flow-through UV methods are sensitive to light scattering effects. Wavelength-independent interference of UV-absorption in simple buffers can easily be corrected by baseline offset to the entire UV-range. But micellar solutions, including all biorelevant media, show Tyndall scattering. The correction of this wavelength-



dependent scattering requires complicated mathematical approaches such as multivariate analysis or second-derivative algorithms [72, 73].

In case of a very turbid medium, the fiber optics technology can barely be employed. These turbidities can be caused by a medium itself, as is the case in FeSSGF, which contains 50% milk. The formulation of drug can also cause turbidity, e.g. melt extrudates or nanosized drugs result in strong turbidity, excluding the use of fiber optics [73, 74].

Such turbidity, which is problematic to analysis in this case, can be turned to advantageous using a different technique as follows:

1.9.3 Turbidity measurement

In case of dissolution studies using the pure nanosized API, dissolution can be measured via the change of turbidity of the dissolution medium. The API is insoluble in the medium and forms a nanosuspension. The value of turbidity forms the baseline of the medium before dissolution of drug. When the medium conditions change, e.g. by addition of a surfactant, the API dissolves and the turbidity decreases [75].

Despite the practicality of this approach, it cannot be used in dissolution testing of finished dosage forms. The ingredients of the formulation contribute to the turbidity and are at least partly soluble. So the turbidity cannot be directly correlated to the amount of dissolved drug.



1.9.4 ResoScan

The ResoScan system is an analytical system using the Ultrasonic Resonator Technology (URT). This technique enables to detect changes of the sound velocity in a liquid sample by the creation of a standing field of acoustic waves between two parallel transducers. The velocity of ultrasound is dependent on the solute concentration, the solute structure, charge and sample homogeneity. Assuming a constant environment in the dissolution medium, the only changing parameter is the concentration of dissolved drug. Solids have only marginal influence on the propagation of waves as long as they are not compressible by ultrasound (i.e. unlike liposomes). To measure the speed of the sound waves, the temperature must be held constant. Using a reference buffer, e.g. the pure dissolution medium compared to a sample buffer, it is possible to establish a calibration curve to measure the concentration of a sample [76].

This technique offers some advantages to the user: The ResoScan system requires a minimum of sample volume (ca. 200 µl). The need for sample preparation, the most important issue in dissolution testing, is obviated.

1.9.5 Asymmetrical flow - field-flow fractionation

The asymmetrical flow-field-flow fractionation (AF4) is a new variation of the conventional flow-field-flow systems. These techniques are commonly used for particle size analysis. The underlying basics for this technique can be explained briefly as follows [77-79]:



The AF4-system consists of a narrow ribbon-like channel. Inside this channel a laminar flow of the mobile phase is consistent. The parabolic flow profile causes a concentration of larger particles at the wall of the channel while smaller particles remain in the middle of the flow, where the velocity of fluids is highest. In principle, smaller and larger particles are separated by the flow distribution, but in the proximity of the wall, back diffusion towards the middle of the flow takes place, resulting in turbulences of the flowing particles and a diffuse separation. Therefore, an additional force is needed to (i) establish a steady state equilibrium with the mean layer I, (ii) to elute different sized analytes at varying velocities depending on their mean layer distance from the channel wall. In case of AF4, this additional force is generated by a cross-flow of mobile phase through a semi permeable membrane. Using this separation field, the parabolic flow profile of eluent amplifies the differences between the analyte clouds.

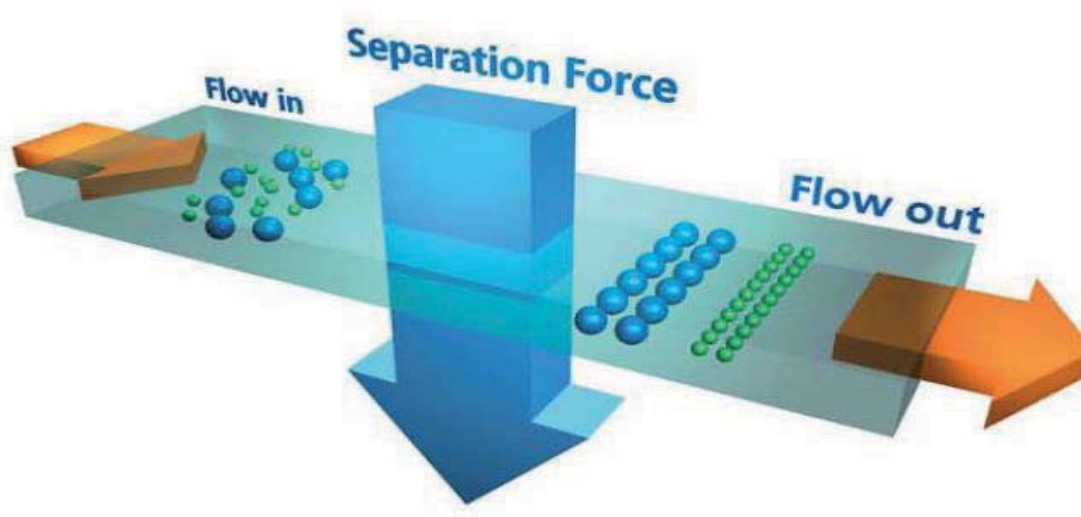


Figure 1.12: Basic principle of separation using AF4 [79]

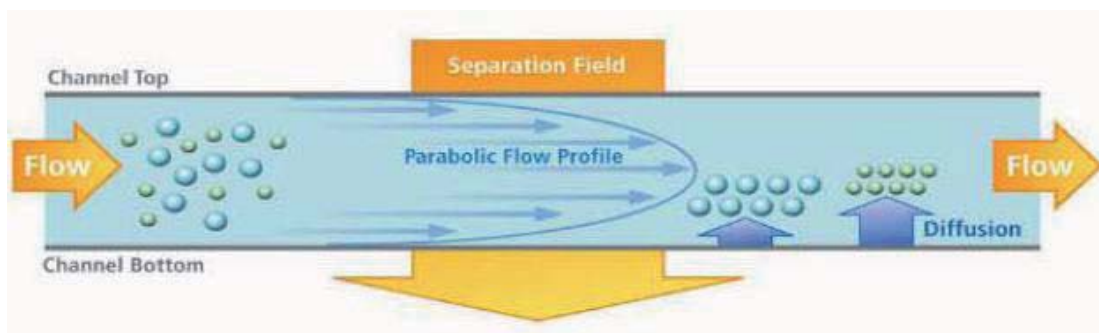


Figure 1.13: Schematic process of analyte cloud separation using AF4 [79]

The idea of using AF4 in dissolution testing was to separate even the smallest particles from the dissolved amount of drug by this technique. A subsequent analysis of the particle free fraction could be conducted to directly measure the dissolved drug. A dissolution test using this technique would not only provide information on the dissolved drug but also about the particle size distribution of the drug after the tablet has disintegrated into the dissolution medium.

1.9.6 Ion-selective electrode

In 2007, Bohets et al. introduced a potentiometric, Ion-Selective Electrode sensor system (ISE) to monitor the process of dissolution on-line. The ISE is sensitive for a given charged model drug (i.e. each ISE is conditioned for its target drug analyte), but insensitive to uncharged molecules and undissolved material [80]. In consequence, this technique does not require any additional sample preparation that might influence the accuracy of analysis.

Peeters et al. have shown that these potentiometric sensors are suitable for dissolution testing of various drugs (loperamide, cinnarizine, domperidone) in simple



buffer media. Moreover, ISE can be used to obtain accurate results in turbid media [81].

The ISE appears to be a very suitable to the needs of dissolution testing, as long as the target analyte is charged. One issue might be the calibration of the ISE if the method used by Bohets and Peeters is used: The ISE can only be calibrated up to the saturation solubility of the drug in its medium. This implies that metastable, supersaturated systems cannot be reliably analyzed by this system as concentrations outside the calibration range would be generated. In addition, the use of concentrated stock solutions for calibration is not suitable for very poorly soluble drugs. The use of the ISE for such drugs will be addressed in the aims of this thesis.



2 Aims of thesis

The foregoing description results in several questions, which were to be addressed in this study.

2.1 Evaluation of the use of an ion-selective electrode system in biorelevant dissolution testing using diphenhydramine HCl as model drug

It was to be evaluated whether the ISE is capable to measure the dissolution of drugs in biorelevant media, since these are particularly useful for characterizing the dissolution behavior of poorly soluble drugs

As a model drug diphenhydramine HCl was chosen. The dissolution of this drug in conventional (buffer) media has been well characterized. Amongst other drugs [80, 81], the ISE manufacturer has reported that it had been successfully analyzed by the ISE in simple buffer media (data for diphenhydramine not shown).

2.2 Evaluation of the ion-selective electrode as potential tool for analysis of supersaturated systems

An alternative way of endpoint calibration, broadening the application range for the ISE to potentially encompass even supersaturated systems of poorly soluble substances was to be developed. This was achieved by adding a single sample draw which was analyzed via HPLC-UV.



2.3 Evaluation of analytical methods in dissolution testing of nanosized fenofibrate

Several methods were evaluated for measurement of dissolution of nanosized drugs. Fenofibrate was chosen as model drug, which is available in a nanosized formulation (Lipidil 145 ONE[®]).

If it was not possible due to lack of equipment or if the method was considered to be not suitable only by design, no experiments were conducted. In these cases, the methods were evaluated on a theoretical basis.

2.4 Establishment of an *in vitro* - *in vivo* - correlation for a nanosized drug using an *in silico* simulation approach

Once a suitable analytical method for the nanosized fenofibrate was found, it was possible to establish an *in vitro* - *in vivo* - correlation by combining the dissolution data with disposition kinetics in a computer-based simulation model using STELLA[®]-Software. Comparison of simulations with *in vivo* - data was carried out to determine (i) the results from dissolution data are commensurate with *in vivo* data and (ii) bioavailability of nanosized fenofibrate is affected by dissolution.



3 Materials and Methods

3.1 Materials

3.1.1 Chemicals

The following chemicals were used in this study:

Table 3.1: Chemicals used in this study

Chemical	Registered Trade Name / Specification	Manufacturer	Lot
Acetonitrile	Analytical grade	Sigma-Aldrich	
Deionized water	MilliQ, freshly prepared		
Diphenhydramine tablets	Nustasium [®]	Labima, Brussels, Belgium	07H30
Diphenhydramine HCl		Sigma-Aldrich Chemie GmbH, Steinheim, Germany	
Egg phosphatidylcholine	Lipoid E PC [®] , 97.9% pure	Lipoid GmbH, Ludwigshafen, Germany	108015-1-042
Fenofibrate	Ph. Eur.	Sigma-Aldrich Chemie GmbH, Steinheim, Germany	016K1644
Glacial acid	Analytical grade	Merck KGaA, Darmstadt, Germany	
Glycerylmonololeate	99.5% monoglyceride	Danisco Specialities, Brabrand, Denmark	173403-2202/107
Hydrochloric acid (31-33%)	Analytical grade	Hedinger, Stuttgart, Germany	



Long-life milk	3,5% fat	Milfina, Germany	
Maleic acid	99% pure	Sigma-Aldrich Chemie GmbH, Steinheim, Germany	056K5473
Methanole	Analytical grade	Merck KGaA, Darmstadt, Germany	
Micronized fenofibrate tablets	Lipidil – Ter®	Solvay Arzneimittel, Hannover, Germany	87247
Nanosized fenofibrate tablets	Lipidil 145 ONE®	Solvay Arzneimittel, Hannover, Germany	85900
Ortho-phosphoric acid (85%)	Analytical grade	Fluka Chemie AG, Buchs, Switzerland	
Pepsin	Ph. Eur., 0.51 U/mg	Fluka Chemie AG, Buchs, Switzerland	1241256
Potassium dihydrophosphate	Analytical grade	Merck KGaA, Darmstadt, Germany	
Sodium chloride	Analytical grade	Merck KGaA, Darmstadt, Germany	
Sodium hydroxide	Analytical grade	Merck KGaA, Darmstadt, Germany	
Sodium oleate	82.7% pure	Riedel-de Haën, Seelze, Germany	51110
Sodium taurocholate	> 97% pure	Prodotti Chimici e Alimentari SpA, Basaluzzo, Italy	2007100274



3.1.2 Model substance diphenhydramine HCl

Diphenhydramine HCl (DPH) (IUPAC-Name 2-(diphenylmethoxy)-*N,N*-dimethylethanamine) is a white to nearly white fine crystalline powder. Its molecular weight is 255.35 g/mol referred to the free base. It has a calculated logP of 3.3. The melting point is at 168-171°C. Diphenhydramine HCl shows an aqueous solubility of 3.06 mg / ml. The structure is given in Figure 3.1.

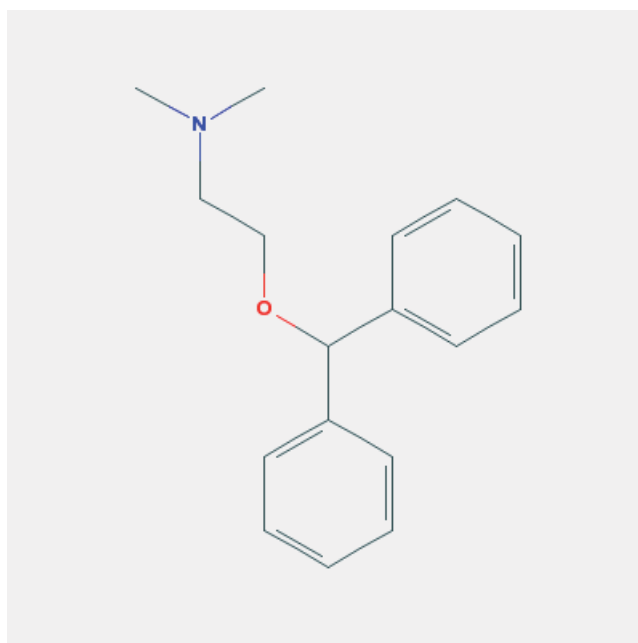


Figure 3.1: Structure of diphenhydramine (free base)

Diphenhydramine is an antihistamine of the first generation (colamine-type) for treatment of allergic reactions. Its pharmacokinetic effects result from blockage of both peripheral and central H₁-receptors. It inhibits the effects of histamine competitively, reducing allergic reactions but also, due to lack of selectivity, causes sedation. With the development of antihistamines of the 2nd generation, which only



affect peripheral H₁-receptors due to their higher hydrophilicity, diphenhydramine lost its meaning for antiallergic treatment but is still used to treat nausea and insomnia, both of which require uptake into the central nervous system [81].

Diphenhydramine HCl was chosen as a model drug because (i) it is a ionizable drug with a high logP, (ii) at the dose used in commercially available formulations (Nustasium[®] 50 mg, Labima, Belgium) it is soluble in dissolution media and (iii) the collaboration partner (Janssen Pharmaceutica Belgium) was experienced in conditioning the ISE to diphenhydramine HCl. Using this model drug, conditioning of the ion selective electrode to the drug could be validated, enabling conclusions to be reached about how the medium affects the performance of the electrode.

3.1.3 Model substance fenofibrate

Fenofibrate (IUPAC-Name propan-2-yl-2-(4-(4-chlorobenzoyl)phenoxy)-2-methylpropanoate) is a white to nearly white fine crystalline powder with a melting point at 80°C [82].

Figure 3.2 shows the structure formula of fenofibrate.

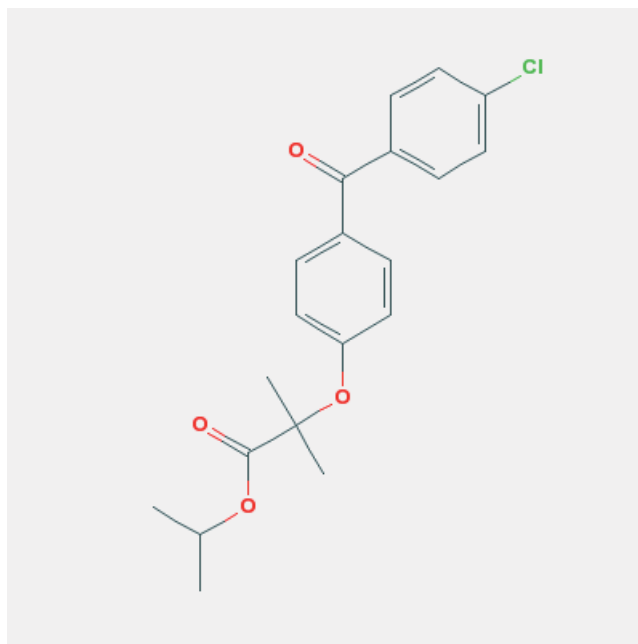


Figure 3.2: Structure of fenofibrate

Fenofibrate is practically insoluble in water. Since it is a neutral compound, the solubility is not influenced by the pH-value. The high lipophilicity ($\log P = 5.24$) points to a good permeability through gastrointestinal membranes. Consequently, fenofibrate is reported to be a BCS class II drug [83]. Fenofibrate or, more precisely its active metabolite fenofibric acid, is a lipid lowering agent used for treatment of hypertriglyceridemia and hypercholesterolemia. The pharmacological effects lead to a reduction in total cholesterol, LDL-C, apo B, total triglycerides and triglyceride-rich lipoproteins. These effects are related to the activation of the peroxisome proliferator activated receptor α (PPAR α), resulting in increased lipolysis, clearance of triglyceride-rich particles from plasma and synthesis of HDL particles via synthesis of AI and AII [84, 85].



Fenofibrate was chosen as a model drug because it is commercially available as the pure substance and additionally available as both a micronized and a nanosized formulation from the same company in a comparable tablet matrix (Lipidil Ter[®] with micronized, Lipidil 145 ONE[®] with nanosized API, Solvay, Germany). These two formulations contain the same excipients, so any variations in the results can be directly linked to the size of the active drug substance.

3.2 Methods

3.2.1 Case example of particle size reduction: fenofibrate

Fenofibrate, a lipid lowering agent, has been assigned to BCS Class II and exhibits a positive food effect [84]. Its oral formulation has been improved over time. An early formulation consisted of a capsule containing coarse fenofibrate in a dose of 200 mg (Lipanthyl[®]). This formulation exhibited high interindividual variability in the plasma profiles, as well as a pronounced food effect, and was recommended to be administered with meals. The absorption of fenofibrate from the GI-tract was about 60%, recovered as active fenofibric acid in the blood. The incomplete absorption can be explained by the very poor solubility and subsequently inadequate dissolution of fenofibrate in the fasted state.

In 1993 “suprabioavailable” tablets (Lipidil Ter[®]) were introduced. This formulation combines micronization of fenofibrate with a spray-coating process [51] resulting in a particle size of 5-15 μm , which is then sprayed onto a water-soluble core (polyvinylpyrrolidone, PVP). Micronization leads to a higher dissolution rate and this

“suprabioavailable” tablet containing 160 mg fenofibrate was demonstrated to be bioequivalent to the 200 mg coarse powder capsule. The technology of this formulation is illustrated in Figure 3.3: As soon as the tablet is exposed to an aqueous medium, disintegration of the tablet and dissolution of the core proceed concomitantly. A microsuspension of fenofibrate remains, which exhibits less intra- and interindividual variability in bioavailability. However, the product still has to be administered with a meal to achieve the desired therapeutic results.

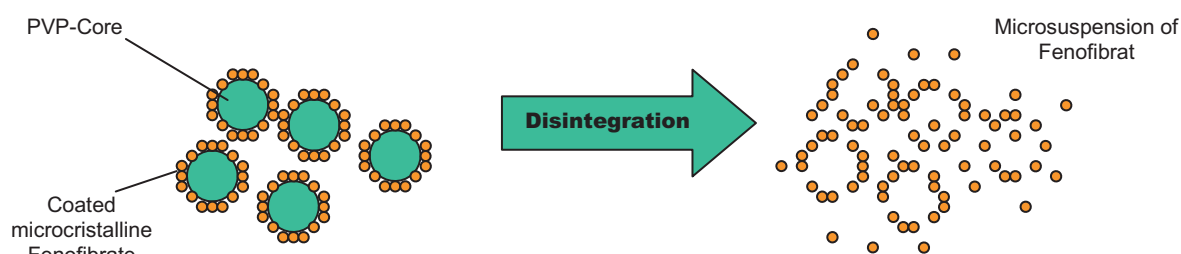


Figure 3.3: The basic principle of suprabioavailable fenofibrate formulation



3.2.2 Dissolution studies

For the model drugs, diphenhydramine and fenofibrate, the dissolution studies were conducted in biorelevant media. Dissolution test parameters can be found in Table 3.2.

Table 3.2: Dissolution study parameters for diphenhydramine and fenofibrate

	Diphenhydramine HCl	Fenofibrate
Dissolution tester	Erweka R6 (Erweka, Heusenstamm, Germany)	Erweka DT 6 (Erweka, Heusenstamm, Germany)
Dissolution method	USP II (paddle)	USP II (paddle)
Medium	Biorelevant (see section 3.2.3)	Biorelevant (see section 3.2.3)
Volume of medium	500 ml	500 ml
Revolutions per minute	75	75
Temperature	37°C	37°C
Sampling time [min]	5, 10, 15, 20, 25, 35, 45	5, 10, 15, 30, 45
Sampling volume	5 ml	5 ml
Filter	RC (0.22 µm)	Various (See section 3.2.4)
Analytics	HPLC-UV, ISE (see sections 3.2.7 and 3.3.3)	HPLC-UV (see section 3.2.7)



3.2.3 Composition of dissolution media

The biorelevant dissolution media were prepared as described by Galia et al. and Jantratid et al. [14, 15], except that KCl was substituted on an osmotically equivalent basis with NaCl. The compositions of the dissolution media are listed in Table 3.3.

Table 3.3: Composition of dissolution media

Medium	Composition	
FaSSGF (pH 1.6)	Sodium taurocholate (μM)	80
	Lecithin (μM)	20
	Pepsin (mg/ml)	0.1
	Sodium chloride (mM)	34.2
	Hydrochloric acid q.s.	ad pH 1.6
	Deionized water q.s.	ad 1 liter
FaSSIF (pH 6.5)	Sodium taurocholate (mM)	3
	Lecithin (mM)	0.75
	Sodium chloride (mM)	103.4
	Potassium dihydrogenphosphate (mM)	26.9
	Sodium hydroxide q.s.	ad pH 6.5
	Deionized water q.s.	ad 1 liter
FaSSIF-V2 (pH 6.5)	Sodium taurocholate (mM)	3
	Lecithin (mM)	0.2
	Sodium chloride (mM)	68.82
	Maleic acid (mM)	19.12
	Sodium hydroxide	34.8
	Deionized water q.s.	ad 1 liter
FeSSGF (pH 5.0)	Sodium chloride (mM)	237.02
	Acetic acid (mM)	17.12
	Sodium acetate (mM)	29.75
	Deionized water /milk 1:1 q.s.	ad 1 liter



FeSSIF (pH 5.0)	Sodium taurocholate (mM)	15
	Lecithin (mM)	3.75
	Sodium chloride (mM)	204.1
	Acetic acid (mM)	144
	Sodium hydroxide q.s.	ad pH 5.0
	Deionized water q.s.	ad 1liter
FeSSIF-V2 (pH 5.8)	Sodium taurocholate (mM)	10
	Lecithin (mM)	2
	Glyceryl monooleate (mM)	5
	Sodium oleate (mM)	0.8
	Maleic acid (mM)	55.02
	Sodium hydroxide (mM)	81.65
	Sodium chloride (mM)	125.5
	Deionized water q.s.	ad 1liter

3.2.4 Syringe filters

The syringe filters used in these studies are listed in Table 3.4.

Table 3.4: Syringe filters used in this study.

Filter	Company	Lot	Material	Pore Size (µm)
Anotop 25 Plus	Whatman, Maidstone, England	07006F	Aluminum Oxide	0.02
Anotop 25 Plus	Whatman, Maidstone, England	07005C	Aluminum Oxide	0.1
Minisart RC 25	Sartorius, Göttingen, Germany	17764	Regenerated Cellulose	0.2
Rezist 30	Whatman, Dassel, Germany	7029474	Polytetrafluoroethylene	0.45
GD/X	Whatman, Florham Park, USA	V378	Glass microfiber GF/D	2.7



3.2.5 Microdialysis system

The microdialysis system consisted of a probe (CMA/12 + guide cannula 14/04 PC, membrane length of 4 mm), containing a dialysis membrane with a molecular weight cut off (MWCO) of 20 kDa (Serial 8309564, Lot# T14114 material: polyacrylsulfonether). A constant flow syringe pump was used to maintain a flow rate of 10µl/min (CMA 400 syringe pump). Dissolution media (biorelevant media) were used as the perfusion medium.

During the dissolution test, samples of 50 µl were collected in 5 minutes fractions in HPLC - microvials, prefilled with 50 µl methanol to ensure an immediate and appropriate dilution.

3.2.6 Centrifugal filter devices

Microcon 100 kDa MWCO (Millipore, RC) filters were used for dissolution testing of fenofibrate. Filter adsorption studies were carried out in each of the dissolution media. To prepare dissolution samples for analysis, 400 µl of the sample were placed into the filtration device and centrifuged for 3.5 minutes at 14.000 rca. 100 µl of the filtrate were diluted with 700 µl of methanol. Analysis of fenofibrate content was done via HPLC-UV.



3.2.7 High performance liquid chromatography (HPLC-UV) used for assays

Fenofibrate:

Samples from the dissolution tests were analyzed by HPLC. The HPLC system consisted of a LaChrom L-7110 pump, a LaChrom L-7400 UV-Vis-Detector, a LaChrom L-7200 autosampler and the EZ-Chrom Elite Data System Software (Merck Hitachi, Darmstadt, Germany). The analysis was performed on a LiChroCART RP-18 5 μ m, 125 \times 4 mm column. The mobile phase consisted of 80% acetonitrile and 20% MilliQ-water. The pH value was adjusted with orthophosphoric acid to 2.5. The flow rate was set at 0.85 ml/min resulting in elution of fenofibrate at approximately 4.5 min. The concentration of drug was determined using a UV detector set at 254 nm.

Diphenhydramine HCl:

Samples from dissolution test were analyzed by HPLC-UV. The HPLC-UV-System consisted of a LaChrom L-7100 pump, a LaChrom L-4250 UV-Vis-Detector, a LaChrom L-200 autosampler and the EZ-Chrome Elite Data System Software (Merck Hitachi, Darmstadt, Germany). The analysis was performed on a LichroChrosphere RP-8 5 μ m, 250-4 mm column. The mobile phase consisted of 55% acetonitrile and 45% aqueous KH_2PO_4 -solution (30 mM). The pH value was adjusted with phosphoric acid to pH 2.5. The flow rate was set at 1.5 ml / min resulting in elution of diphenhydramine approximately at 3.5 min. The amount of released drug was determined using a UV detector at the wavelength of 235 nm. System suitability was ensured by running standards between the dissolution samples. HPLC-UV-data were only evaluated when the standard deviation of the embedded standards was less than 2%.



Sample treatment and calculation of dissolved drug (both fenofibrate and diphenhydramine): The dissolution samples were diluted 1:1 (500 µl of mobile Phase + 500 µl of dissolution sample). The concentration of the drug was calculated using the slope and intercept of the calibration curve and was multiplied by a factor that was calculated as follows:

$(500 \text{ (volume of dissolution medium)} * 2 \text{ (dilution factor)}) * 100 / \text{(Amount of drug in tablet)}$.

For diphenhydramine HCl, the dissolved profiles were corrected for mass loss of the drawn sample to allow comparison of the results with the ISE.

3.2.8 ResoScan system

The ResoScan system used for this study was provided by TF Instruments GmbH (Heidelberg, Germany).

Prior to dissolution testing with a subsequent analysis of drug content by the ResoScan System, a calibration curve was prepared. First, a stock solution of fenofibrate at about the saturation solubility was prepared in the biorelevant medium. This solution was further diluted to obtain a calibration curve (dilutions 1:1, 1:2, 1:3, and 1:5).

200 µl of sample were given into resonator cavity of the system. Then the temperature was equilibrated to 37°C. When the temperature was constant, the ultrasonic sound waves were passed through the sample to obtain a correlation between the time the waves need to interfuse the medium and the concentration of fenofibrate. Only when



a linear correlation between dissolved drug and the resonance of sound was established, were dissolution tests conducted.

3.2.9 Analyses of *in vitro* data

3.2.9.1 Model independent f_1 - and f_2 - factor calculation

f_1 and f_2 factors were used to compare dissolution profiles generated by HPLC-UV and ISE. To allow for better comparison and to include the dissolution at higher percentage release, five time points were always included (i.e. t_5 - t_{25} for diphenhydramine tablets), even if the last time point exceeded 85% dissolution relative to the label strength [86, 87].

3.3 Special methods for diphenhydramine HCl

3.3.1 Filter adsorption studies for diphenhydramine HCl

The performance of the ISE was compared to classical methods for sample analysis i.e. sample withdrawal, filtration and analysis. Thus it was necessary to evaluate filter adsorption of diphenhydramine HCl onto regenerated cellulose filters (Minisart[®] RC 25, 0.2 μm , lot # 17764, Sartorius, Germany). Each medium was filtered at a concentration of about 100 $\mu\text{g}/\text{ml}$ diphenhydramine HCl. The samples were analyzed by HPLC-UV and compared to the results for unfiltered samples ($n=3$) [23].



3.3.2 Dynamic light scattering

To monitor a possible change of micellar formation in FeSSIF-V2 dynamic light scattering measurements were conducted using a Malvern Zetasizer[®] 3000 HSA (Malvern Instruments Ltd., Malvern, UK) at 25°C with a Ne-He-Laser at 633nm, and at a measurement angle of 90°. The samples were placed into single-use PCS-Cells (10 x 10 x 48 mm) (Sarstedt, Nürnberg, Germany).

3.3.3 The ion-selective electrode

The ion-selective electrodes were provided by Janssen Pharmaceutica and have been described previously by Bohets [80]. The most common application of ISEs is pH-measurement using a glass electrode. Differences in the electrochemical potential of solution are measured, enhanced via an electrometer and expressed as pH-value. Bohets et al. modified this principle for the measurement of drugs in solution. Similar to a measurement of pH value, the electrochemical potential alters when an ionizable drug dissolves into the surrounding medium. The ISE is, unlike the pH-electrode, not specific to any particular ion, but rather can be conditioned to an ionizable drug having a logP higher than 4.5. The change of potential is measured via a specially constructed data station. The signal received is converted to a concentration value using a transformation of the Nikolski-Eisenmann equation.

Conditioning of the electrodes to the drug takes up to 48 hours. The conditioning procedure leads to a dedicated potentiometric system for online-measurement of dissolution, specific for the conditioning drug.



For measurement both an ion-selective electrode and a reference electrode (e.g. a standard glass electrode) are needed.

3.3.4 Calibration of the ion-selective electrode for diphenhydramine HCl

Prior to dissolution testing, the electrodes were conditioned at 37°C in the dissolution medium at a DPH concentration of about 110 µg / ml for ≥ 48 hours. This DPH concentration is equivalent to 110% dissolution of Nustasium[®] tablets. The conditioning procedure resulted in low drift and fast response of the ISE to DPH. Calibration curves were constructed by stepwise addition of a standard solution into a vessel containing 500 ml of the test medium. 2 ml aliquots were added in 5 steps, with each 2 ml containing approximately 11 mg of DPH. As in the conditioning step, the final concentration was approximately 110% of the concentration expected at the end of the dissolution of Nustasium[®] tablets. The ISE was used for dissolution testing if the following criteria were fulfilled: a) the correlation coefficient (R^2) of the linear fit of the calibration data exceeded 0.9995, b) the mean slope of this calibration curve did not exceed the value of 63 mV which has been reported orally by the ISE manufacturer to be the maximum tolerable value (compare with the theoretical maximum according to the Nikolski-Eisenmann equation which is 61.5mV at 37°C) [80, 81], c) the sensor response obtained from the stepwise addition of the standards was fast and stable; $t_{90} < 60$ s and d) the drift in signal was less than 0.3 mV for the 2nd to 5th addition.



3.3.5 Dissolution testing

Dissolution tests were carried out at 37°C with a USP type II (paddle) dissolution tester Erweka R6[®] (Erweka, Heusenstamm, Germany), according to section 3.2.2. In some experiments 2 or 3 ISE were placed in a single dissolution vessel to evaluate reproducibility among electrodes. In other experiments, ISE was compared to manual sample removal and subsequent HPLC analysis. Manual samples were taken at 5, 10, 15, 20, 25, 35 and 45 minutes without volume replacement. The filtered samples were diluted appropriately with mobile phase.

3.3.6 Endpoint calibration via ISE (method A)

The conversion of the measured potential to percentage dissolution was carried out according to the procedure described in Bohets et al [80], using an in-house “Potential to Concentration” software. An endpoint calibration to correct for drift of the ISE system was conducted.

When using the ISE as an analytical stand-alone system, the electrodes were placed into a solution containing a known concentration of DPH, typically the calibration solution, after completion of the dissolution run. This was done to confirm that the ISE was still within calibration and to correct for any drift after initial calibration.



3.3.7 Endpoint calibration via HPLC-UV (method B)

With this method, a manual sample was drawn at one time-point (corresponding approximately to the completion of drug release, e.g. t_{45} for Nustasium[®] tablets) and the concentration of DPH was determined by HPLC-UV. The dissolution profile was calculated on the basis of this value.

3.3.8 Adaption of Method B for measurement of poorly soluble substances

The calibration procedure of the ISE is usually based on dilution of a concentrated stock solution. This procedure is obviously not suitable for application to very poorly soluble substances. To overcome this difficulty, the ISE Method B was adapted using a single sample analysis by HPLC-UV. This sample should be drawn just before c_{\max} is reached (i.e. at t_{25} for Nustasium[®] tablets containing diphenhydramine).

3.3.9 Analysis of significance using ANOVA

To compare the dissolution profiles of diphenhydramine tablets (Nustasium[®], Labima, Belgium) in biorelevant media from the ISE dissolution endpoints at t_{45} , ANOVA at a significance level of $\alpha = 0.05$ was applied using Origin[®] 6.0 (Microcal, Northhampton, MA, USA). All other calculations were conducted in Excel[®] 2003 (Microsoft, Redmond, WA, USA).



3.4 Special methods for fenofibrate:

3.4.1 Filter adsorption studies for fenofibrate

Filter adsorption studies were conducted for the filters listed in Table 3.4 (not for 2.7 μm glass microfiber). An excess of fenofibrate was added to the biorelevant media and the suspension was filtered through a 0.45 μm PTFE-filter to obtain a clear solution. Afterwards, aliquots of the solution were filtered using the various filters. The samples were analyzed by HPLC-UV and compared to the peak for the clear solution (n=3) [23].

3.4.2 Analysis of in vivo pharmacokinetic data

An oral two-compartment analysis (WinNonlin[®] model 12) was applied for evaluation of pharmacokinetic parameters using WinNonlin[®] Professional Edition version 4.1 software (Pharsight Corporation, Mountain View, CA, USA). The plasma drug concentration - time profiles were taken from the literature [51, 59]. Since there were no intravenous data for fenofibrate available, the pharmacokinetic parameters k_{10} , k_{12} , k_{21} and V_d were calculated from the plasma profiles after oral administration of fenofibrate (micronized and nanosized fenofibrate, in the fasted and fed states).

3.4.3 Computer simulation of fenofibric acid plasma profiles

3.4.3.1 The STELLA[®] model

In 2001, Nicolaides et al. [17] introduced a method to combine pharmacokinetic data of poorly soluble substances with *in vitro* results obtained from dissolution experiments using the STELLA[®] software (isee systems, NH, USA) to generate *in silico* plasma profiles. The STELLA[®] model is based on the WinNonlin[®] model 12, an oral two-compartment model:

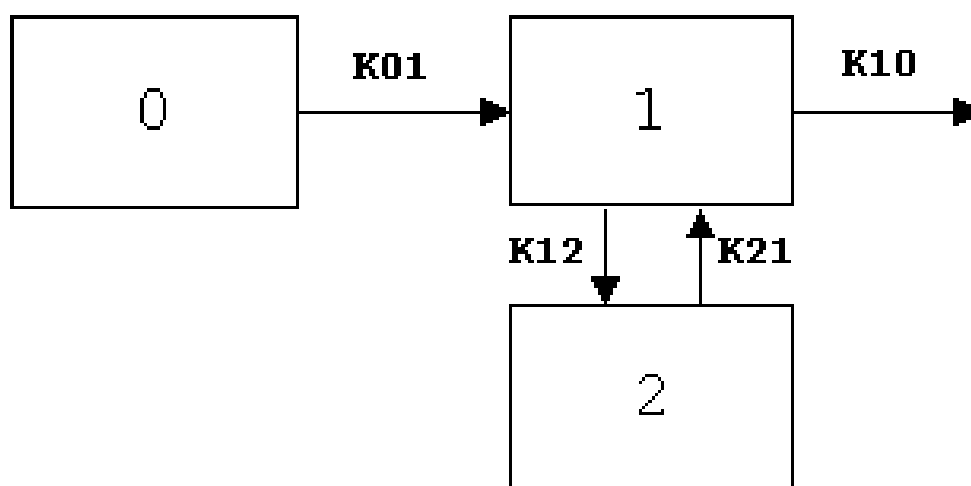


Figure 3.4: WinNonlin[®] model 12

When an *in vivo* plasma profile is available, it is possible to calculate the pharmacokinetic parameters k_{01} , k_{12} , k_{21} , V/F and k_{10} via WinNonlin[®]. These parameters enable STELLA[®] to recalculate the plasma profiles:

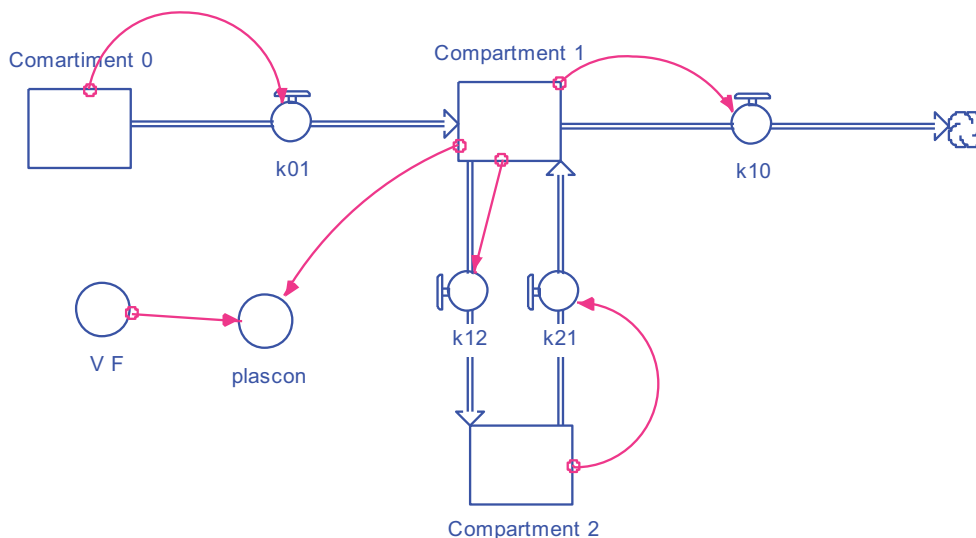


Figure 3.5: WinNonlin[®] model 12 in STELLA[®]

The pharmacokinetic parameter k_{01} generated by WinNonlin[®] is dependent on:

- Volume of fluid given with dose
- Dissolution of API in the stomach
- Gastric emptying rate of liquid (food) components
- Gastric emptying rate of solid (food) components
- Dissolution of API in the intestine
- Rate of permeation across the intestinal mucosa

To combine the STELLA[®] model with experimental dissolution data in order to perform an *in vitro* – *in silico* – *in vivo* – correlation, the model has to be adapted: Instead of the hybrid k_{01} parameter generated by WinNonlin[®] the individual parameters for the upper GI tract and the dissolution results were used as follows:



-
- The volume of fluid is given by the reference data that was taken from literature [17, 88]. The same is valid for amount of calories in meals administrated.
 - It is assumed that absorption via the stomach is negligible; therefore sink conditions for gastric dissolution were not assumed. Experimental data obtained with the *in vitro* dissolution test are used directly in the model.
 - Gastric emptying rate (GER) of solids is given by reference [17]. A time factor is used to preclude generation of a negative volume in the stomach.
 - GER of liquids is given by reference [17]. A time factor is used to preclude generation of a negative volume of liquid in the stomach.
 - The intestine is the main site of absorption. For a BCS-class II drug, sink conditions for intestinal dissolution are assumed. The initial dissolution rates from the *in vitro* dissolution test are used in the model.
 - Instant absorption is assumed for a BCS-class II compound (i.e. no permeability restrictions to uptake).



This leads to the following model map:

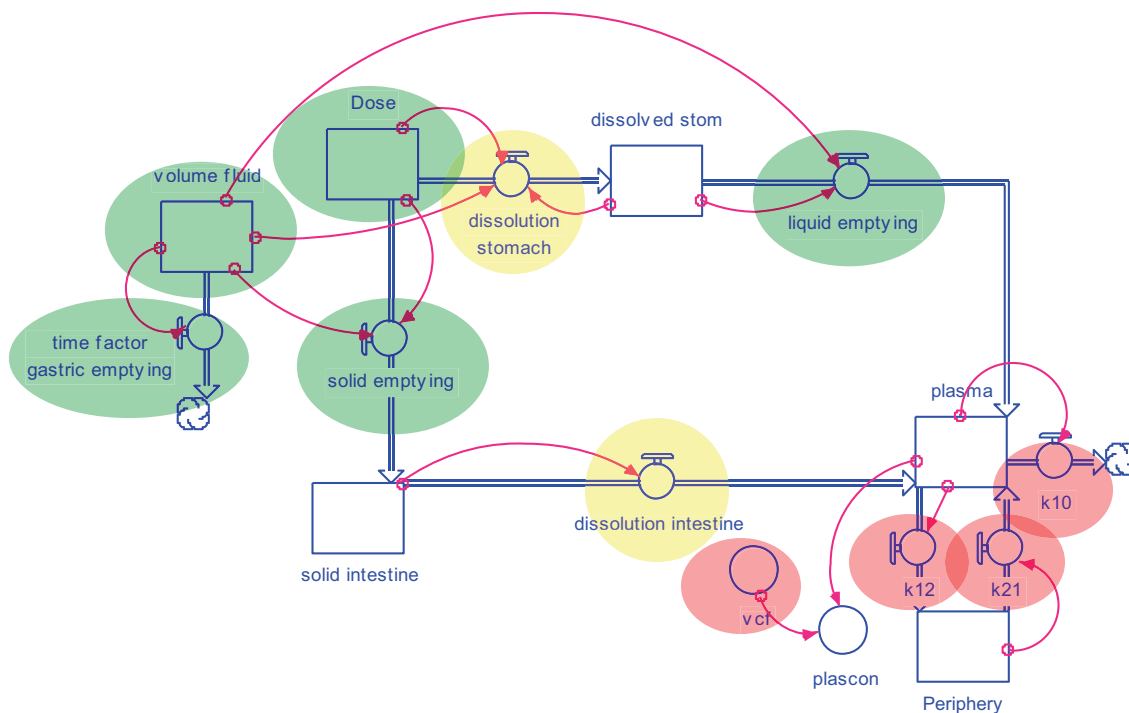


Figure 3.6: Map of STELLA[®] model A

- Green: Input parameter taken from references.
- Red: Input parameter taken from *in vivo* data, generated by WinNonlin[®].
- Yellow: Input parameter obtained by dissolution experiments.
- White: No input parameter required, calculations conducted by STELLA[®].



A list of parameters used is given in Table 3.5

Table 3.5: Model parameter used in the STELLA[®] models

Time factor gastric emptying	Time after which the stomach is empty and no more liquids can be transferred to the intestines.
Volume fluid	Volume of coadministered fluid
Dose	Dose of drug, in the case of fenofibrate this was calculated as fenofibric acid
Time factor gastric emptying	Time after which the stomach is empty and no more liquids can be transferred to the intestines
Dose	Dose of drug, in the case of fenofibrate this was calculated as fenofibric acid
Dissolution stomach	Dissolution of drug in gastric liquids as a function of the Noyes-Whitney equation under non-sink conditions
Dissolved stom	The amount of dissolved drug in the stomach
Liquid emptying	Rate of gastric emptying for liquid compounds, set to 2.8^{-1} in the fasted state and to 4 kcal/min in the fed state
Solid emptying	Rate of gastric emptying for solid compounds, set to 2.8^{-1} in the fasted state and to 4 kcal/min in the fed state
Solid intestine	The amount of drug that enters the intestine as solid
Dissolution intestine	Dissolution of drug in intestinal liquids as a function of the Noyes-Whitney equation
Plasma	Amount of dissolved drug absorbed into the plasma compartment (first compartment in post-absorptive pK model)



Plascon	Absorbed drug divided by the volume of distribution
Vcf	Volume of distribution, taking the bioavailability F into account
Periphery	Second compartment in post-absorptive pK model
k12	Rate constant from Plasma to periphery
k21	Rate constant from Periphery to plasma
k10	Rate constant for excretion to plasma

The input parameters obtained from dissolution experiments are based on the Noyes-Whitney theory for dissolution, as given by the following equation [17]:

$$\frac{dW_t}{dt} = \frac{D\Gamma N^{1/3}}{V\delta\rho^{2/3}} W^{2/3} (X_s - W_t) = zW^{2/3} (C_s - C_t)$$

Eq. 3.1

Where D is the diffusion coefficient of the drug, Γ is the shape factor, N is the number of particles, V is the volume of dissolution medium, δ is the diffusion layer thickness and ρ is the density of drug. W_t is the amount of drug dissolved at time t , W is the amount of drug remaining to be dissolved; X_s is the mass of drug, which saturates the dissolution medium. C_s is the saturation solubility in the dissolution medium, while C_t is the concentration of drug at time t . [16, 17]. The term $\frac{D\Gamma N^{1/3}}{\delta\rho^{2/3}}$ is a constant equal to

z . The z -value is derived from *in vitro* dissolution experiments.



3.4.3.2 Calculation of z-value

The z-value was calculated via Excel®. The calculation is based on the following formula [88]:

$$\frac{\ln \left(\frac{(X_s - X_0)^{\frac{2}{3}} - (X_s - X_0)^{\frac{1}{3}} X_0^{\frac{1}{3}} + X_0^{\frac{2}{3}}}{(X_s - X_0)^{\frac{2}{3}} - (X_s - X_0)^{\frac{1}{3}} X_0^{\frac{1}{3}} + X_0^{\frac{2}{3}}} \right) - 2\sqrt{3} \text{ArcTan} \left[\frac{2X_0^{\frac{1}{3}} - (X_s - X_0)^{\frac{1}{3}}}{\sqrt{3}(X_s - X_0)^{\frac{1}{3}}} \right]}{2(X_s - X_0)^{\frac{2}{3}}} = (z/V) * t$$

Eq. 3.2

For the calculation of z it is necessary that at least three values are taken from dissolution testing before a plateau in the profile is reached, e.g. due to saturation of the medium or completion of the dissolution of the drug.

A second way to calculate z was evaluated: The initial dissolution rate was calculated from the results from dissolution test (linear regression of lnC against t) and the time to dissolve to 10, 15 and 20% of saturation solubility in each medium was calculated. These values were chosen because sink conditions were assumed ($C_t \leq 20\%$). The results obtained with this method are compared to those of the standard method.



3.4.3.3 Adaption of original model for permeability restrictions

In Model B (Figure 3.7) the possibility of a permeability limitation is introduced through an absorption step (absorption, blue). The rate of uptake, which is governed by this absorption step, can be adjusted according to a permeability coefficient (which varies between 0 and 1) and / or the duration of the time-interval implemented for the absorption step. The maximum rate of uptake in this model occurs when the permeability coefficient is 1 and the time-interval of the absorption step is very small ($\rightarrow 0$). The main difference to model A is that in Model A the concentration in the intestinal lumen immediately generates appearance of drug in the plasma, whereas with the additional absorption step in Model B there is a time- and permeability-induced lag between generation of dissolved drug in the intestinal compartment and appearance in the plasma. Since fenofibrate is described as rapidly absorbed [88], a permeability coefficient of 1 was used for the simulations. The time-interval chosen, DT , was 1/10 [h], which resulted in a slight delay of fenofibrate appearance in the plasma compartment within the model. The plasma concentration is of course also highly affected by the pharmacokinetic parameters k_{12} , k_{21} and k_{10} . Thus this model results in various plasma profiles according to both generation of drug in the plasma compartment and its subsequent distribution and elimination.

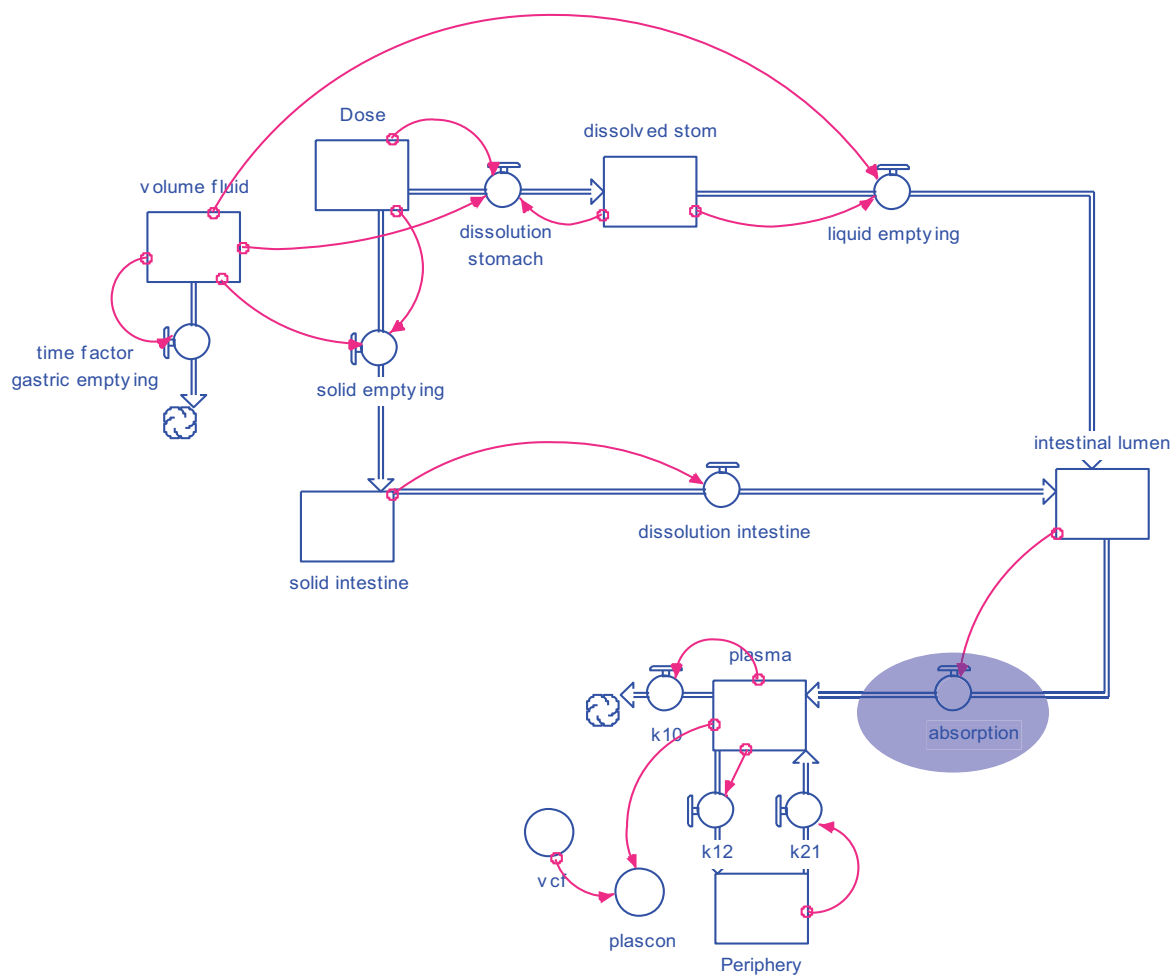


Figure 3.7: Model Map enabling permeability restrictions, Model B

3.4.4 Comparison of simulated plasma profiles to *in vivo* data

The simulated plasma profiles were compared to the *in vivo* data in terms of bioequivalence using the point estimate ratios of AUC and C_{max} . Bioequivalence is established when the confidence intervals around the point estimates for the simulated plasma profile are in the range of 0.8-1.25 of those for the *in vivo* profile [51, 59, 84]. Additionally, the point estimate ratio of t_{max} is presented.



3.4.5 Sensitivity analyses

The sensitivity of the applied models was tested by varying the following parameter from a fifth to five times the initial value:

For Model A sensitivity to the following parameters was tested:

- Gastric emptying rate (fasted state)
- Gastric dissolution ($z_{gastric}$) (fasted and fed state)
- Intestinal dissolution ($z_{intestinal}$) (fasted and fed state)
- Gastric emptying rate in the fed state (by varying GER from 1 kcal / min to 5 kcal / min).

For Model B the following parameter were tested:

- Intestinal dissolution ($z_{intestinal}$) (fasted and fed state)
- Gastric emptying rate in the fed state by varying GER from 1 kcal/min to 5 kcal / min.
- Permeation rate through intestinal mucosa by varying the permeation coefficient from 0.5 to 1.



4 Results and discussion

4.1 Discussion of methods evaluated for in situ measurement of the analyte in the dissolution test

Of the methods presented in section 1.9, most were excluded from further consideration. The dialysis methods, with the exception of microdialysis, were considered to be too slow for the analysis of very fast dissolving formulations in dissolution testing.

In preliminary experiments with both Lipidil 145 ONE[®] and Lipidil Ter[®] it was seen that, independent of the choice of dissolution medium, the formulations form a very turbid suspension. Since not even the paddles of the USP II apparatus could clearly be seen in those suspensions, the use of fiber optics for *in situ* analysis was deemed unsuitable. As a consequence, analysis with fiber optics was not further investigated in this study.

The measurement of turbidity and its correlation to the drug content is surely an interesting idea as long as only pure drug powder is examined, but in case of a tablet formulation with lots of excipients this method is not applicable: The resulting turbidity is not only caused by undissolved drug particles but also the soluble and non-soluble excipients contribute to turbidity. Overlapping effects must be considered, e.g. due to different dissolution rates of excipients and active substance. If a reference placebo were available, this method might be suitable, but this was not the case in the current study.



The asymmetrical flow field-flow-system is an interesting system for analysis of disintegration and dissolution of tablets. Unfortunately such a system was not available for this study. This analytical system might have been able to resolve the question as to with which size the nanoparticles get released from the formulation. For example, Solvay had reported that the fenofibrate nanocrystals are processed to a size of about 150 nm. Afterwards a granulation is conducted and then pressed into tablets. However, it is not clear that the particle size remains so low in the finished product. One could imagine that the rate of particle size decrease could be correlated to the dissolution of the drug for a nanocrystalline system, but this would have to be explored in future studies.

4.2 ResoScan

Using the highest concentration of standard solution, the equilibration of temperature was slow (> 5 minutes). After equilibration, this method of analysis was not able to detect fenofibrate in FaSSIF using ultrasonic sounds. No differences to the control (pure FaSSIF medium) could be found. Analysis using the ResoScan system was abandoned since (i) no improvement of analysis at lower drug concentrations was expected, and (ii) the time needed for temperature equilibration was too long to analyze a system containing undissolved nanoparticles.

For these reasons, the ResoScan system appears to be not suitable for analysis of dissolution testing for instant release formulations.



4.3 Microdialysis

Using the biorelevant medium FaSSIF, it was found that despite the constant flow of the syringe pump, no perfusate could be obtained in the outlet of the system. At the time, all parts of the system were connected directly to the syringe pump. It was found that the probe was clogged. As more perfusate flowed into the clogged probe, the connections between the pump and the probe slipped off because of the pressure increase. All in all, it was found that (i) micelles clog the probe, and (ii) the surfactants in FaSSIF act as a lubricant on the connections between the parts of the system, leading them to slip apart when the pressure rises. Consequently, the microdialysis system used in this experiment is not suitable for dissolution testing in biorelevant media.

Further experiments with other biorelevant media were not conducted since all contain surfactants.



4.4 Centrifugal filter devices

The results of dissolution testing in FaSSIF and FeSSIF using the centrifugal filter devices are shown in Figure 4.1 and Figure 4.2.

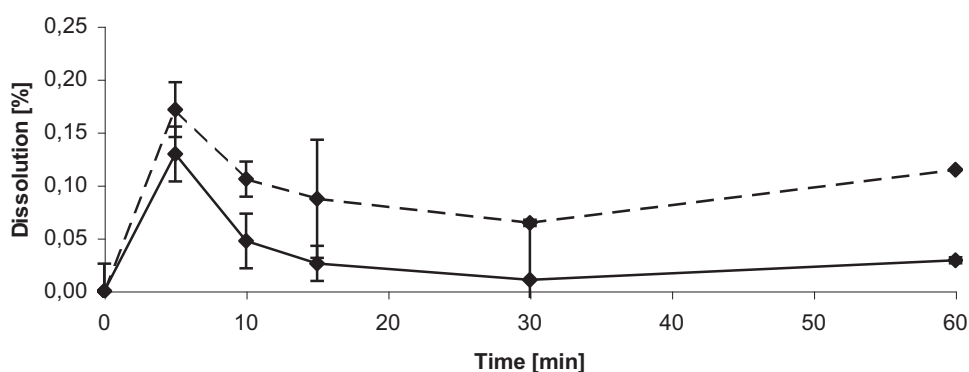


Figure 4.1: Dissolution profile of Lipidil Ter® (dotted line) and Lipidil 145 ONE® (solid line) in FaSSIF using Microcon® 100 kDa centrifugal filter devices

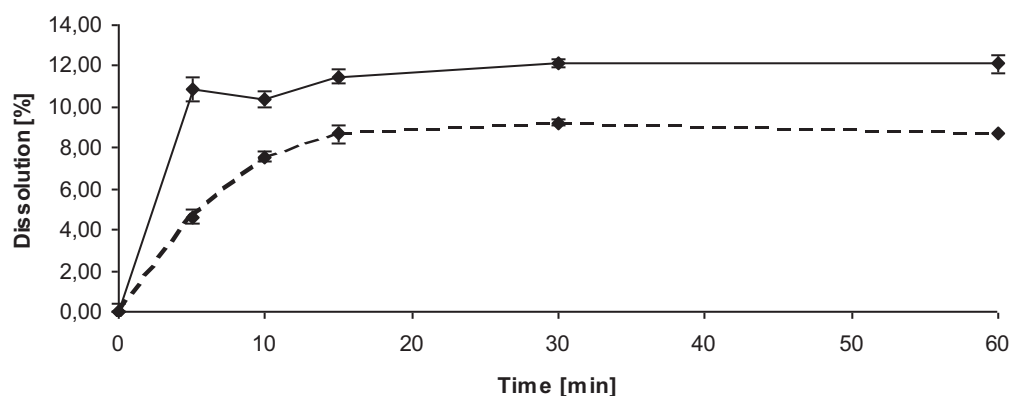


Figure 4.2: Dissolution profile of Lipidil Ter® (dotted line) and Lipidil 145 ONE® (solid line) in FeSSIF using Microcon® 100 kDa centrifugal filter devices

It is noticeable that dissolution in FaSSIF appears to be much lower than the saturation solubility in that medium (about 4.7%). On the basis of the adsorption studies, this observation can obviously be explained by adsorption of fenofibrate to the Microcon® filter (Figure 4.3):

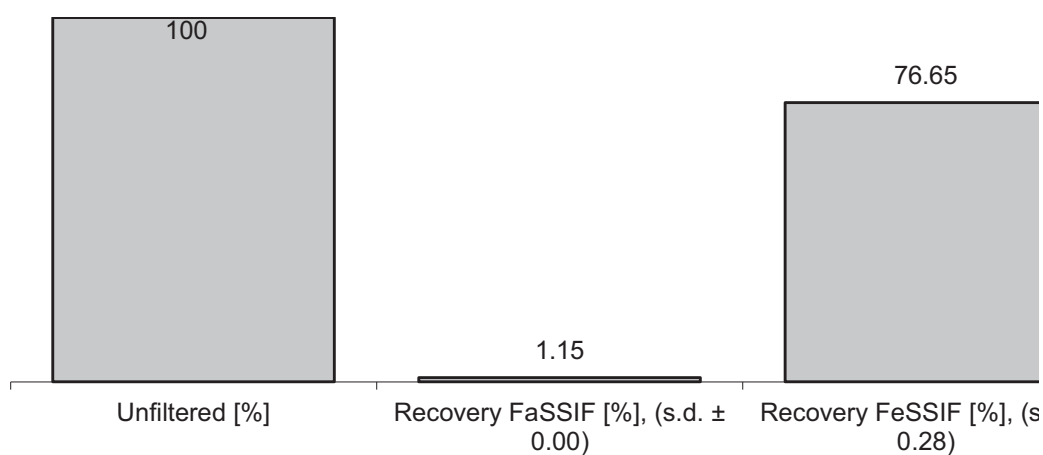


Figure 4.3: Recovery of fenofibrate from Microcon[®] centrifugal filter devices in FaSSIF and FeSSIF

In FeSSIF the adsorption is less critical, but still high (more than 23 %). The difference in adsorption between FaSSIF and FeSSIF can be explained by the higher amount of surfactants in FeSSIF, providing better wettability and subsequently a higher recovery. Nevertheless, dissolution profiles obtained by Microcon[®] centrifugal filtration devices do not reflect the true amounts dissolved due to adsorption and cannot be considered reliable.



4.1 Ion-selective electrode

4.1.1 Filter adsorption studies

To test the suitability of the ISE, the results from dissolution experiments were compared to a standard method using manual sampling, filtration and subsequent HPLC-UV analysis. To ensure the reliability of the standard methods, the syringe filter (RC, 0.22 μm) used for the study were tested for adsorption of diphenhydramine. The recoveries of diphenhydramine HCl after filtration are shown in Figure 4.4. For every medium filter adsorption was low, indicating suitability for sample preparation.

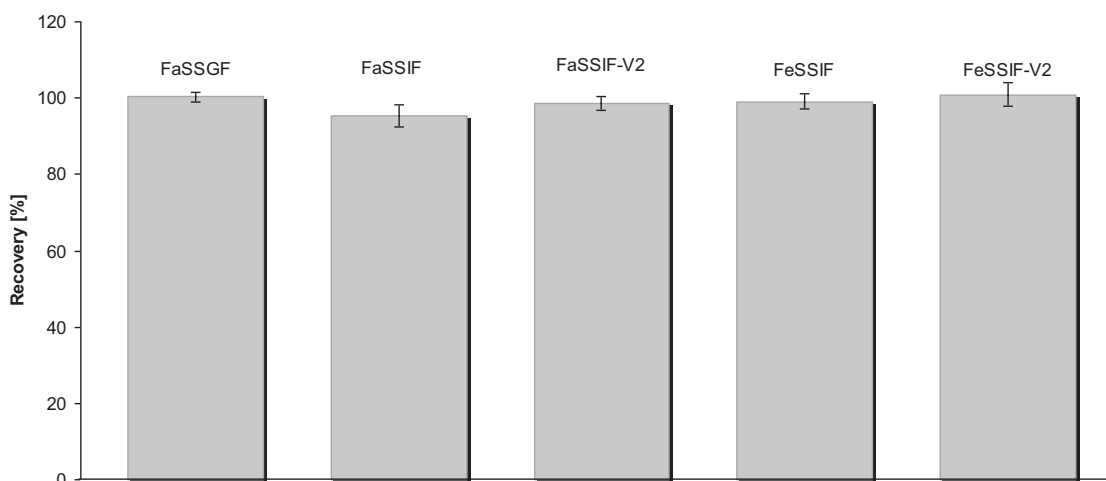


Figure 4.4: Recovery of Diphenhydramine HCl after filtration through Minisart[®] RC 25 regenerated cellulose, 0.2 μm

4.1.2 FaSSGF

After conditioning the electrodes to FaSSGF, the calibration curve was found to yield an R^2 of 0.99994 or better, with a slope of 59.83 ± 0.99 . The quality of the conditioning was considered therefore to be sufficient for dissolution measurements [81].

The results from the dissolution tests are shown in Figure 4.5. The f_1 - and the f_2 -factors indicate that the dissolution results obtained with the ISE (Method A) can be



considered similar to manual sampling with HPLC-UV analysis (Table 4.1) [87]. A combination of ISE and HPLC-UV, as done with Method B, leads to a slight improvement in agreement of the ISE results with those obtained by manual sampling with HPLC-UV analysis and fulfils the goal of obtaining a full dissolution profile with a single sample draw.

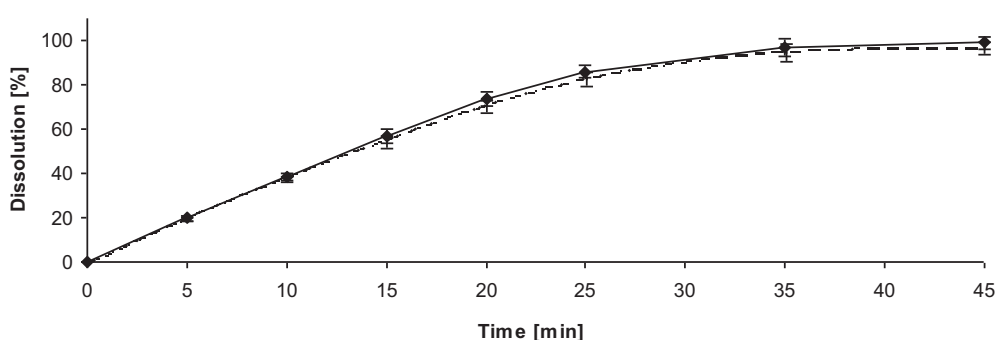


Figure 4.5: Dissolution profiles of Nustasium® in FaSSGF obtained by manual sampling and subsequent HPLC-UV analysis (solid line) and ISE (dotted line) Method A electrode 1

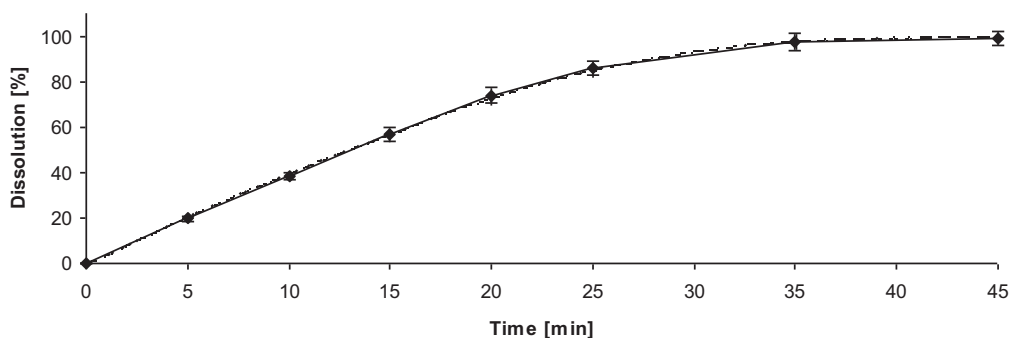


Figure 4.6: Dissolution profiles of Nustasium® in FaSSGF obtained by manual sampling and subsequent HPLC-UV analysis (solid line) and ISE (dotted line) Method B electrode 1



Table 4.1: f_1 -/ f_2 -values for each medium / each electrode in comparison to manual sampling and subsequent HPLC-UV analysis

Medium	Method A		Method B	
	f_1	f_2	f_1	f_2
FaSSGF	4.24	64.57	1.63	86.50
FaSSIF-V2 Electrode 1	3.31	73.72	1.85	94.09
FaSSIF-V2 Electrode 2	3.67	68.86	1.71	99.77
FaSSIF Electrode 1	1.51	86.10	2.65	69.27
FaSSIF Electrode 2	1.80	97.04	2.46	70.75
FaSSIF Electrode 3	5.59	54.01	8.08	45.53

4.1.3 FaSSIF

Three electrodes were used simultaneously for dissolution in FaSSIF to assess reproducibility in the manufacture of the ISE and of the conditioning procedure. The calculated R^2 values of the calibration curves were 0.99990, 0.99994 and 0.99991, respectively, with a mean slope of 62.85 ± 0.52 and therefore met the performance criteria for use in dissolution testing (compare section 3.3.4). The dissolution profiles are shown in Figure 4.7 and Figure 4.8. Methods A and B produced similar results to manual sampling and subsequent HPLC-UV analysis for all three ISEs, showing an f_1 -



factor less than 15. For ISE 1 and 2 the f_2 -value was higher than 50, while for Electrode 3 the value was over 50 for method A but slightly under for Method B. When comparing a single dissolution test profile obtained by manual sampling and HPLC-UV analysis with the corresponding results from the three individual electrodes, it can be seen that the performance of the ISE is very close to HPLC-UV with low standard deviations among the electrodes (compare Table 4.2 and Table 4.3):

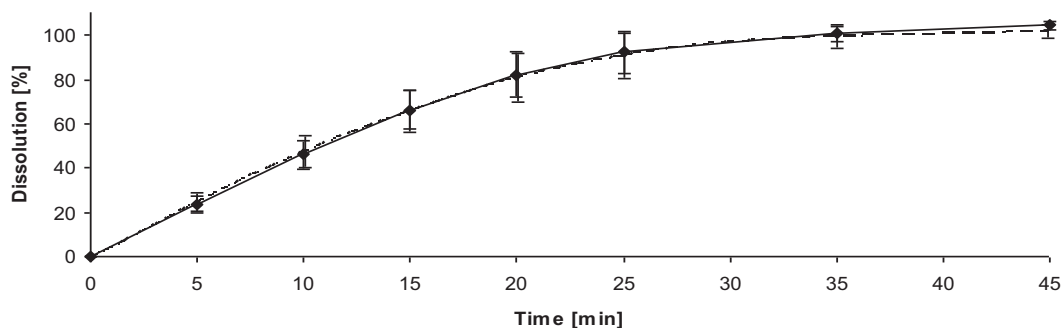
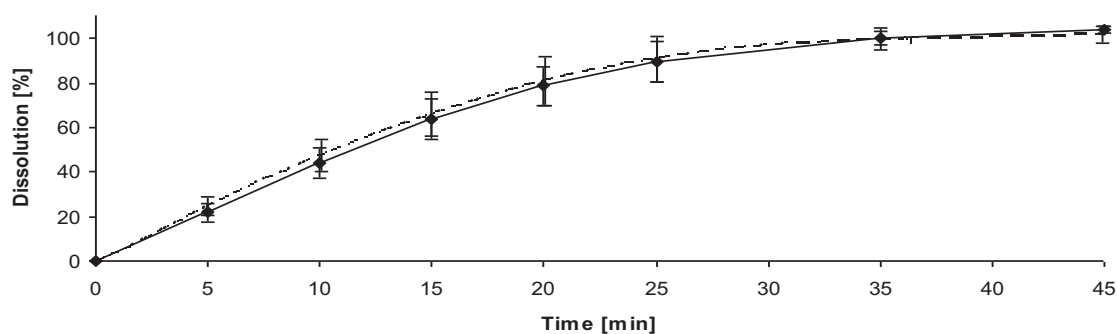
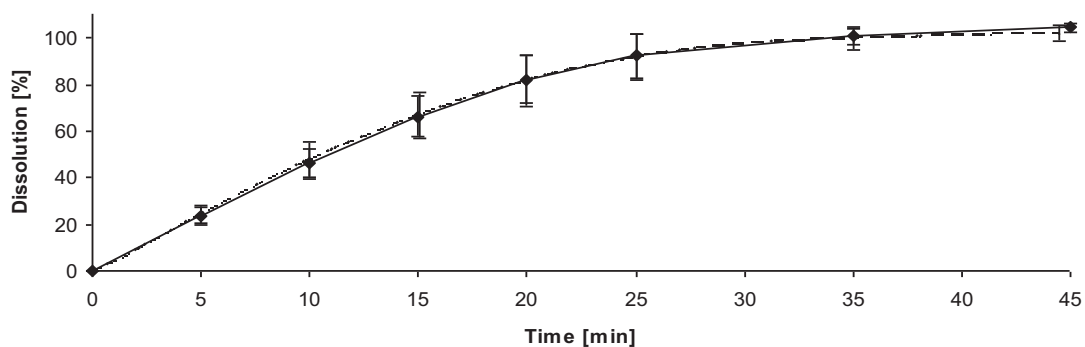


Figure 4.7: Dissolution profiles of Nustasium[®] in FaSSiF obtained by manual sampling and subsequent HPLC-UV analysis (solid line) and ISE (dotted line) (A) Method A electrode 1 – 3

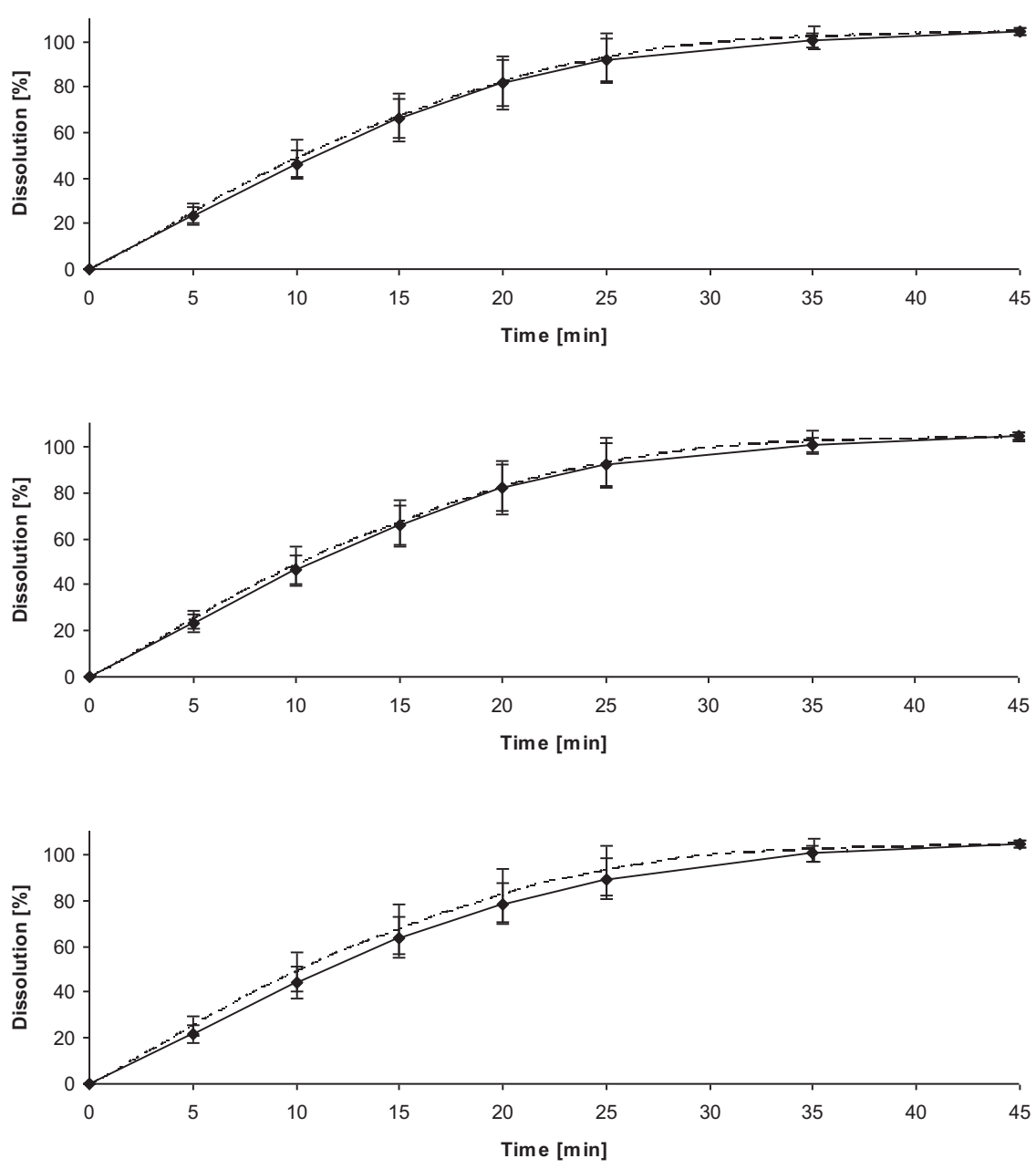


Figure 4.8: Dissolution profiles of Nustasium® in FaSSIF obtained by manual sampling and subsequent HPLC-UV analysis (solid line) and ISE (dotted line) (A) Method B electrode 1 – 3



Table 4.2: Comparison of the ISE to manual sampling and subsequent HPLC-UV analysis and ISE within the same vessel during dissolution test with Method A

Time	HPLC-UV	Electrode 1	Electrode 2	Electrode 3	SD electrodes
5	17.91	18.55	18.63	18.71	0.08
10	36.91	36.54	36.49	36.80	0.17
15	53.42	52.28	51.84	52.21	0.24
20	67.53	65.69	65.54	65.79	0.13
25	78.05	77.22	76.79	77.30	0.27
35	95.71	94.50	93.93	94.52	0.34
45	103.77	102.44	102.02	102.43	0.24
f_1		1.93	2.40	1.84	
f_2		86.33	82.28	88.78	



Table 4.3: Comparison of the ISE to manual sampling and subsequent HPLC-UV analysis and ISE within the same vessel during dissolution test with Method B

Time	HPLC-UV	Electrode 1	Electrode 2	Electrode 3	SD electrodes
5	17.91	18.79	18.95	18.95	0.09
10	36.91	37.01	37.11	37.28	0.14
15	53.42	52.95	52.72	52.89	0.12
20	67.53	66.53	66.66	66.65	0.07
25	78.05	78.21	78.10	78.30	0.10
35	95.71	95.72	95.53	95.75	0.12
45	103.77	103.76	103.76	103.76	0.00
f_1		1.03	1.13	1.22	
f_2		99.77	99.83	99.86	

4.1.4 FaSSIF-V2

After conditioning the electrodes to FaSSIF-V2, the calibration curve was found to yield an R^2 exceeding 0.9995 or better, with a slope of 62.61 ± 0.63 , fulfilling the conditioning criteria. In this medium, the ISE yielded identical dissolution profiles to those obtained with manual sampling and subsequent HPLC-UV analysis. High standard deviations in the results obtained with HPLC-UV analysis were observed (see Figure 4.9 and Figure 4.10). These can likely be attributed to variations in positioning of the ISE



electrodes in the vessel and their subsequent influence on the hydrodynamics, although small variations in sample preparation could also have contributed.

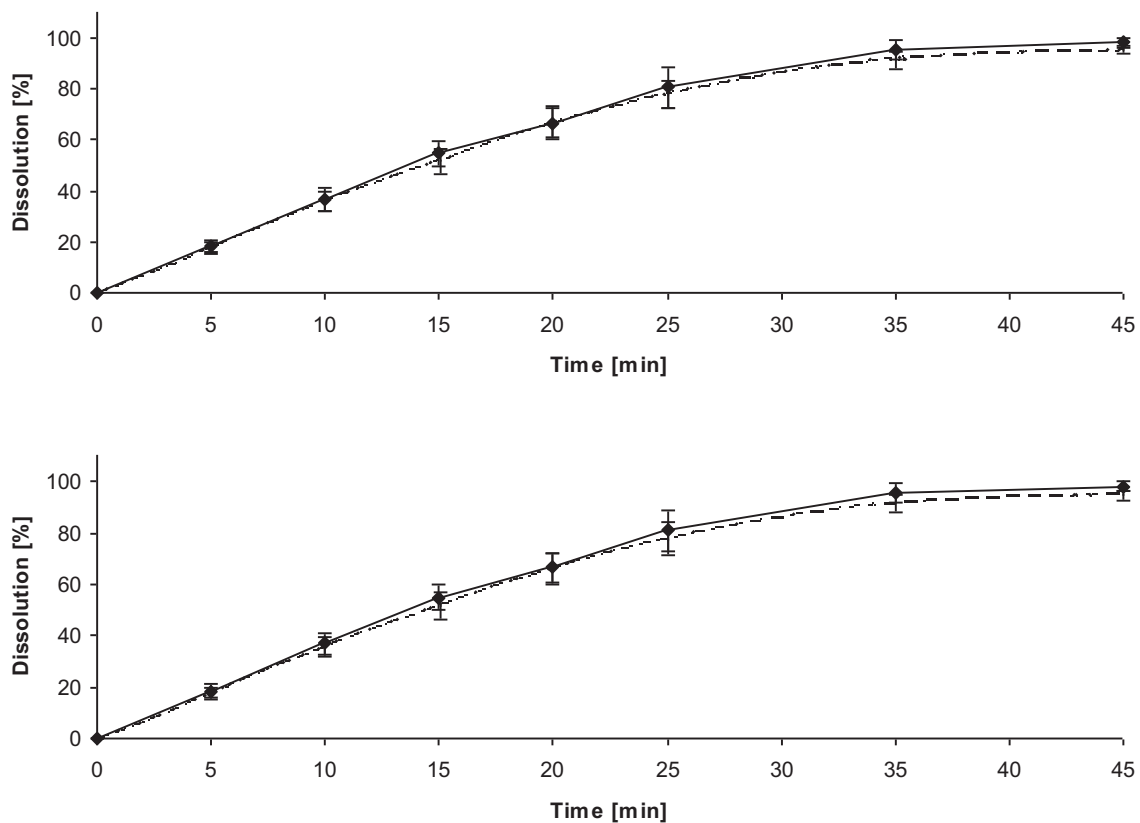


Figure 4.9: Dissolution profiles of Nustasium[®] in FaSSIF-V2 obtained by manual sampling and subsequent HPLC-UV analysis (solid line) and ISE (dotted line) Method A

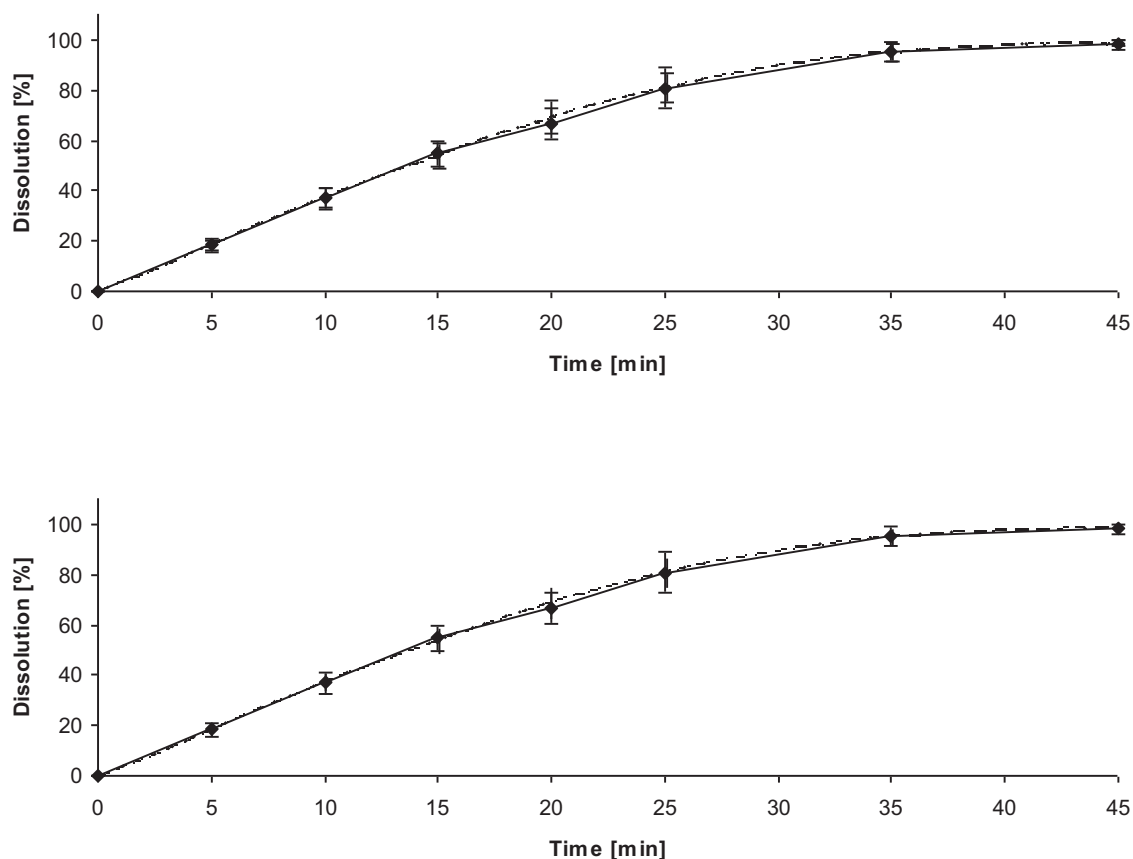


Figure 4.10: Dissolution profiles of Nustasium[®] in FaSSIF-V2 obtained by manual sampling and subsequent HPLC-UV analysis (solid line) and ISE (dotted line) Method B

4.1.5 FeSSGF

Difficulties in the measurement of the exact drug concentration in FeSSGF are often encountered, since this medium is a multi-phase system. Therefore HPLC-UV measurement is not possible unless a time-consuming and tedious sample preparation using acetonitrile to precipitate proteins followed by centrifugation is utilized [81]. Alternatively, a 25 step ISE calibration was conducted ($n = 5$) by subjecting the ISE to FeSSGF containing known concentrations of DPH. The mean slope of the resulting calibration curves was 61.15 ± 0.27 with an R^2 of 0.99978 or better, with



concentrations calculated from ISE measurement all within the range of 95% - 105% of the known concentration (Figure 4.11). Therefore the ISE can be used for on-line measurements in FeSSGF and related, milk-containing media.

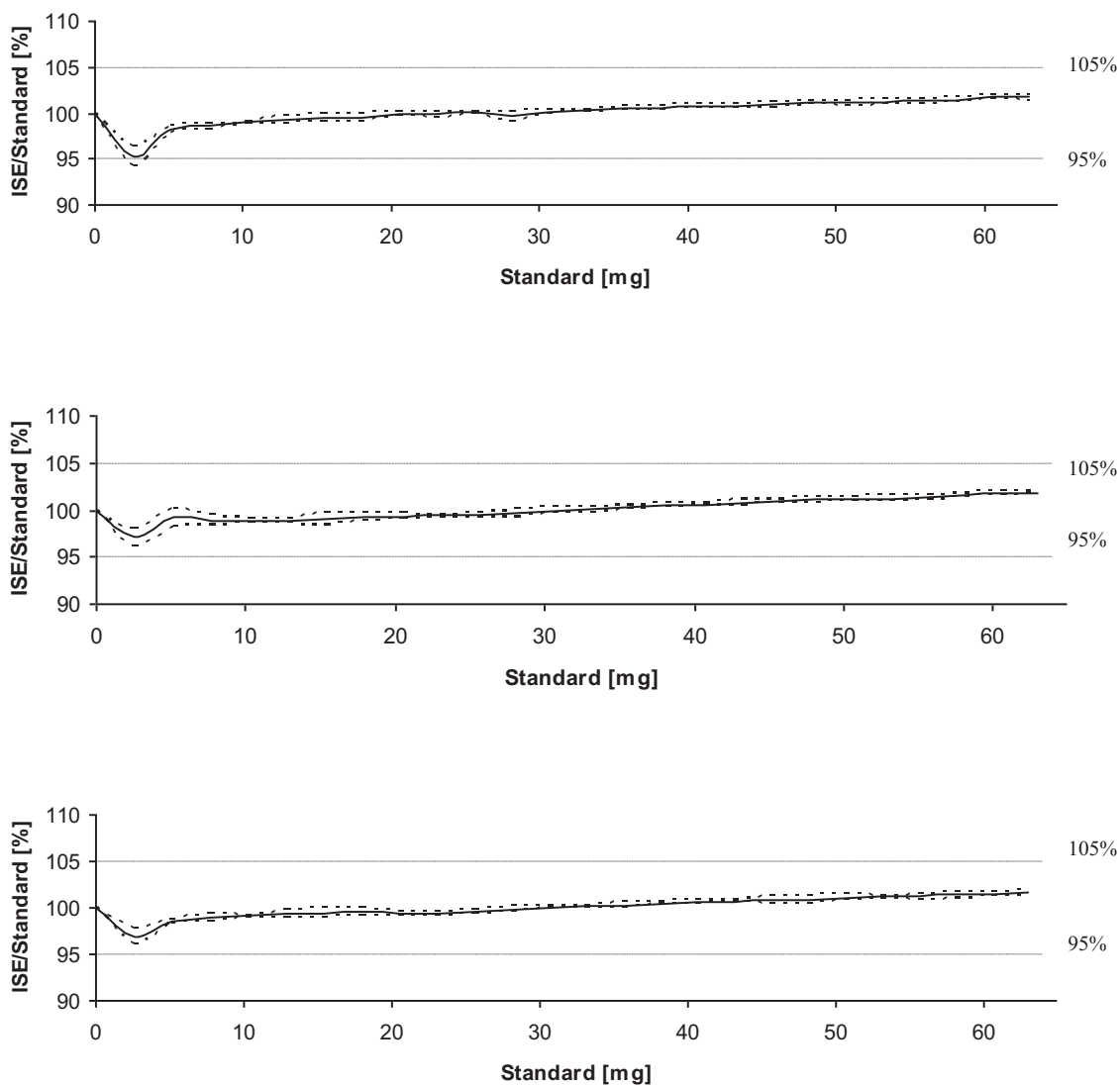


Figure 4.11: Plot of measured concentration against amount of added standard electrode 1-3. The dotted lines above and under the solid lines show the standard deviations

4.1.6 FeSSIF / FeSSIF-V2

For the conditioning of the electrode it is crucial that the surrounding medium is stable over time. In the FeSSIF media we observed an increase in turbidity over 24 hours (compare Figure 4.12). A dynamic light scattering measurement was used to confirm this visual observation and found an increased micellar size (e.g. fresh medium average 26.2 nm, after 24h at 37°C 44.1 nm for FeSSIF-V2).

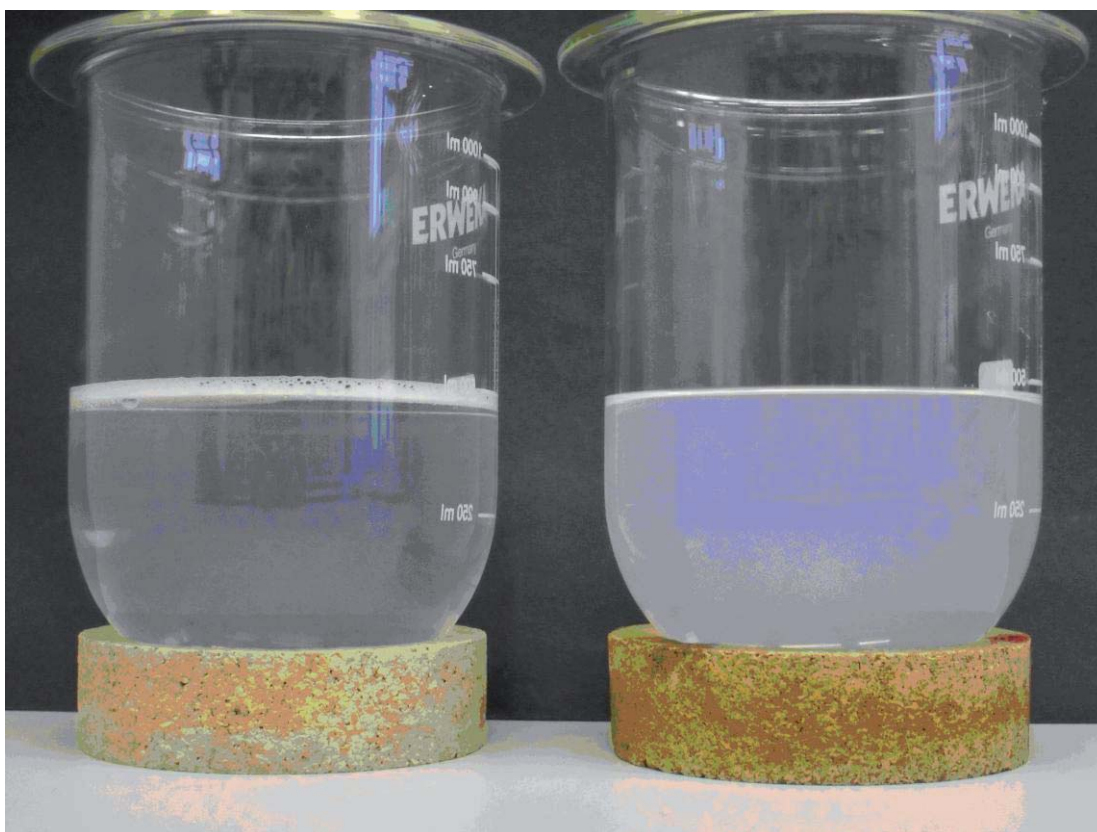


Figure 4.12: Picture of freshly prepared FeSSIF-V2 (left vessel) and FeSSIF-V2 after 24 hours at 37°C and 75 rpm (right vessel)

Using a conventional sampling method (e.g. syringe filters) these changes do not alter results (since, in the absence of a conditioning procedure, the medium does not have to be maintained at 37°C for long periods), but they can lead to different results with the ISE.



Although calibration curves were obtained with all ISEs in the biorelevant fed state media, their performance did not meet all criteria for analysis with ISE. The highest R^2 value obtained for the calibration curve was 0.99947, just failing to meet the criterion of $R^2 \geq 0.9995$. Slopes were 52.74 ± 2.47 in FeSSIF and 52.21 ± 4.10 in FeSSIF-V2, both meeting the performance criteria (max. slope of 63). The third criterion, a fast and stable plateau showing a drift of less than 0.3 mV to the next addition, was not fulfilled (e.g. drift of 0.6 mV between step 3 and 4 in Fig. 4.13).

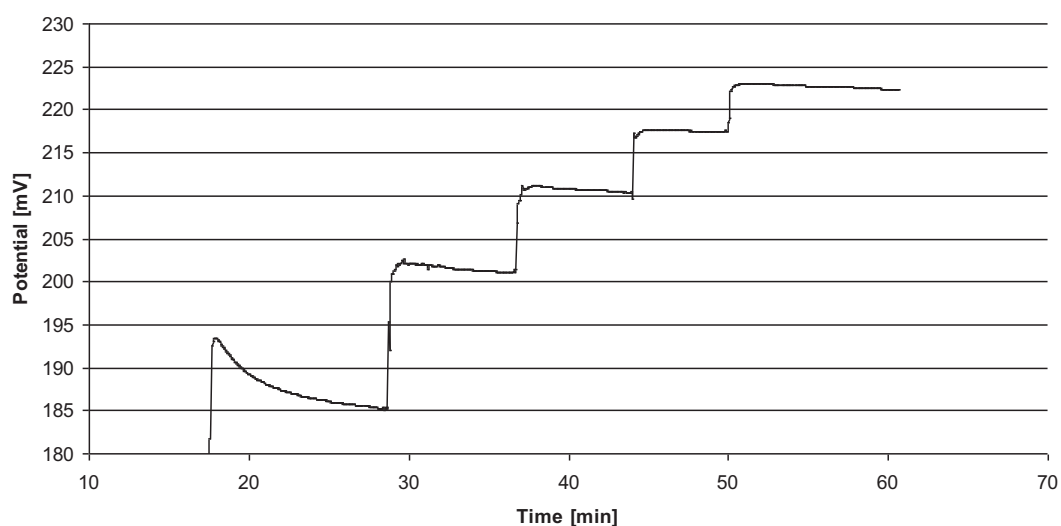


Figure 4.13: Calibration Curve of Diphenhydramine HCl in FeSSIF-V2



4.1.7 Evaluation of potential use of the ISE for nanosized drugs

Bohets and Peeters have already shown the suitability of the ISE for quality control purposes. It offers satisfactory accuracy at low cost and avoids the need for organic solvents [80, 81]. In addition, the measurements are performed on-line, enabling real-time generation of data. In consequence, the throughput of dissolution tests in quality control can be increased.

In this study, the focus was set on dissolution testing in research and development, especially with respect to measurement in biorelevant media. On-line monitoring in biorelevant media is often associated with difficulties since fiber optics and flow-through UV methods are sensitive to light scattering effects. Wavelength-independent interference of UV-absorption in simple buffers can easily be corrected by baseline offset to the entire UV-range. But micellar solutions, including all biorelevant media, show Tyndall scattering. The correction of this wavelength-dependent scattering requires complicated mathematical approaches such as multivariate analysis or second-derivative algorithm [70, 72]. Manual sampling with HPLC-UV analysis is applicable to analysis of fasted state media but more difficult to apply to the fed state media, especially for FeSSGF. The suitability of ISE for use in turbid media was demonstrated by Peeters et al. and has been further confirmed in our studies with FeSSGF as a medium containing milk. Additionally, as an off-line system, manual sampling with HPLC-UV analysis generates only a limited number of samples and the dissolution profile will not be continuous. As a non-spectroscopic on-line system without the need for sample preparation, the ISE offers the potential to circumvent these issues.



Limitations to the application of ISE-based analysis of dissolution in biorelevant media appear to be three-fold: The first is the general limitation of the ISE to ionizable compounds, recognizing that approximately 40% of drugs are neutral compounds over the physiological pH-range [28] . The second is that the ISE failed to meet all the suitability criteria for use in FaSSIF and FaSSIF-V2. Further developmental work will be needed to overcome this limitation. Third, the calibration procedure of the ISE is usually based on dilution of a concentrated stock solution. This procedure is obviously not suitable for application to very poorly soluble substances. To overcome this difficulty, the ISE Method B was adapted using a single sample analysis by HPLC-UV. This sample should be drawn just before c_{\max} is reached (i.e. at t_{25}).

Method B was applied to FaSSGF, FaSSIF and FaSSIF-V2. For all of these media, equivalence of Method B to conventional HPLC-UV analysis was established (Table 4.4). This broadens the application range for the ISE to potentially encompass even supersaturated systems of poorly soluble substances.



Table 4.4: f_1 -/ f_2 -values for each medium / each electrode in comparison to manual sampling and subsequent HPLC-UV analysis with the adapted Method B, using t_{25} instead of t_{45}

Medium	f_1	f_2
FaSSGF	1,53	83,79
FaSSIF-V2 electrode 1	2,83	86,07
FaSSIF-V2 electrode 2	3,84	72,33
FaSSIF electrode 1	1,44	83,99
FaSSIF electrode 2	1,65	79,91
FaSSIF electrode 3	6,13	51,91



4.2 Fenofibrate

4.2.1 Filter adsorption studies

The results of the filter adsorption studies conducted for fenofibrate in FaSSGF, FaSSIF, FaSSIF-V2, FeSSIF and FeSSIF-V2 are shown in Figures 4.14 to 4.18.

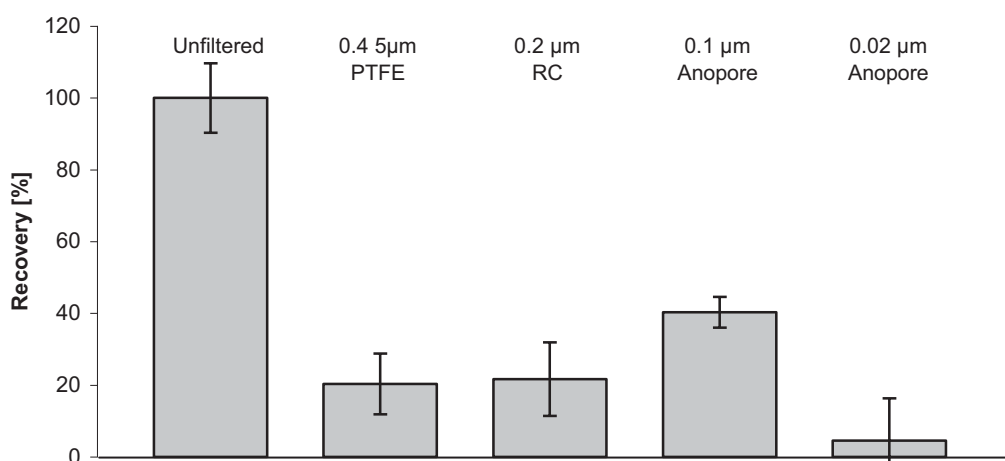


Figure 4.14: Adsorption of fenofibrate to various filter materials from a FaSSGF solution containing fenofibrate

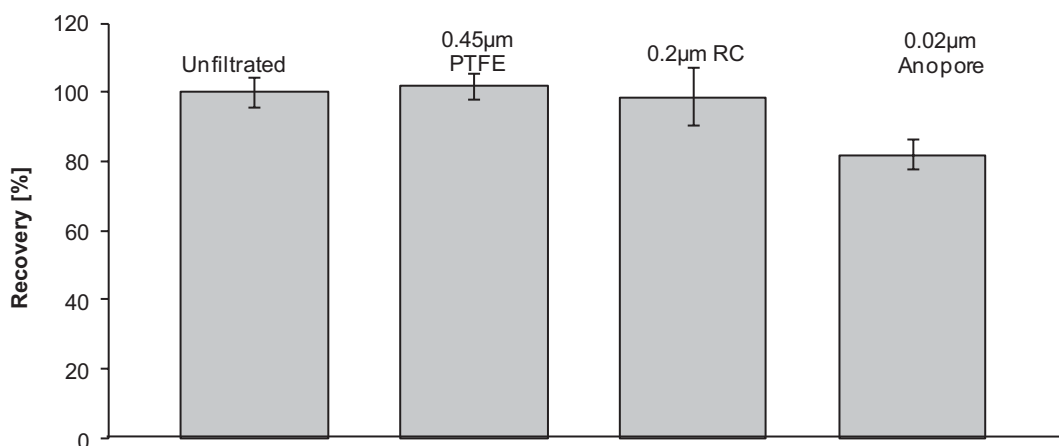


Figure 4.15: Adsorption of fenofibrate to various filter materials from a clear FaSSIF solution*

*The Anopore filter of 0.1µm is missing due to supply difficulties of the manufacturer at the time of experiments.

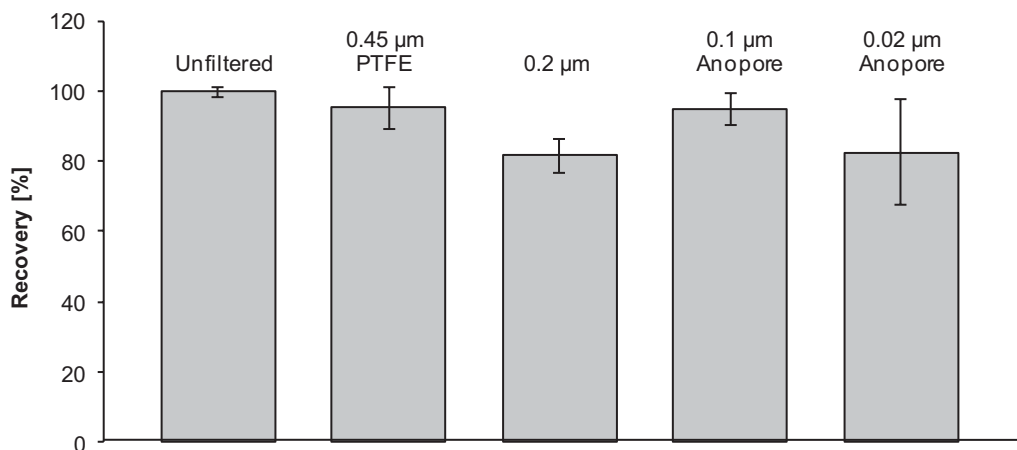


Figure 4.16: Adsorption of fenofibrate to various filter materials from a clear FaSSIF-V2 solution

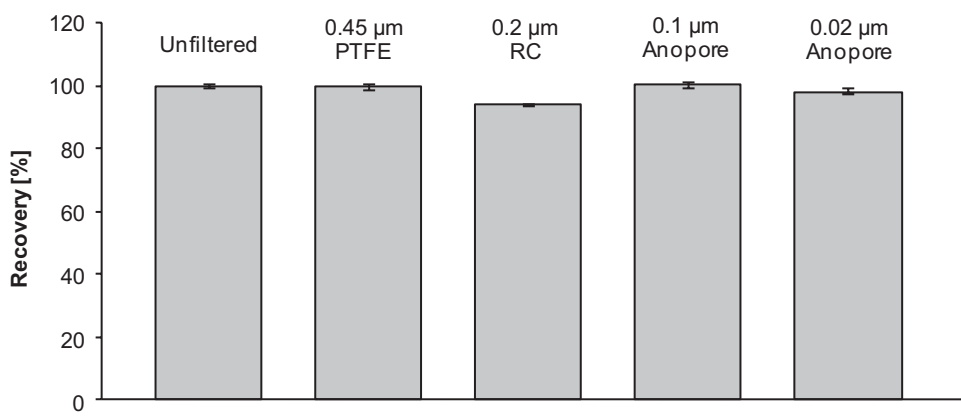


Figure 4.17: Adsorption of fenofibrate to various filter materials from a clear FeSSIF solution

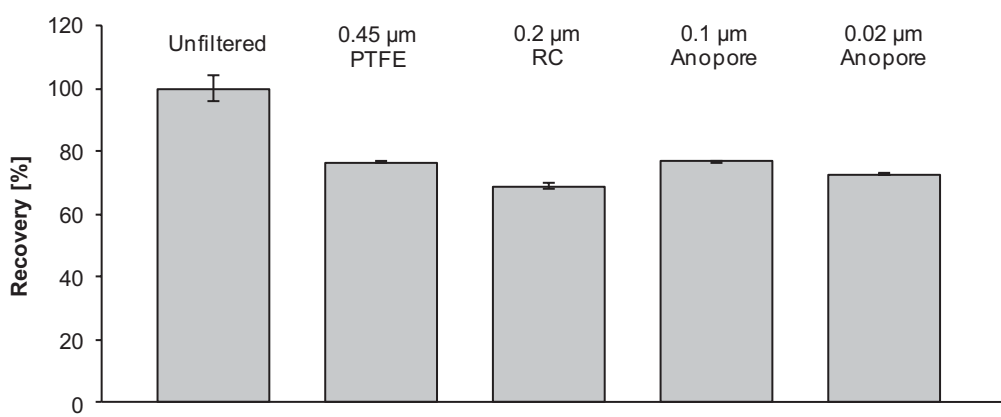


Figure 4.18: Adsorption of fenofibrate to various filter materials from a clear FeSSIF-V2 solution



The following trends were observed:

- (i) the syringe filters show comparable behavior in each medium regarding mean recovery of fenofibrate and the associated standard deviation.
- (ii) Comparing the two Anopore filters (0.1 μm and 0.02 μm), the larger filter pore size shows less adsorption in general. It is likely that this can be attributed to filtration of micelles in the medium.

In summary, this experiment shows that no filter material has a clear advantage over the others. It is hypothesized that 0.02 μm filters are already small enough to hold back micelles partly from the medium, which is an unwanted effect.



4.2.2 Solubility studies

The solubility of fenofibrate in each dissolution medium is listed in table Table 4.5.

Table 4.5: Apparent solubility (24h) of fenofibrate in various media at 37 °C in µg/ml (mean ± SD)

Medium	Solubility µg/ml (mean ± SD)
FaSSGF	0.22 ± 0.01
FaSSIF	13.7 ± 0.5
FaSSIF-V2	4.67 ± 0.25
FeSSGF	147.49 ± 93.67
FeSSIF	35.6 ± 1.0
FeSSIF-V2	78.84 ± 1.0

FeSSGF contains 50% milk and thus both protein and fat, so it is a very challenging medium in terms of analytics. The other media show remarkably low standard deviations in comparison to filter adsorption studies which were run at room temperature. This is attributed to (i) long equilibration time (24 h) and (ii) a higher temperature at which all the waxy substances are molten.



4.2.3 Dissolution in FaSSIF and FeSSIF using various filter pore sizes

The dissolution profiles of Lipidil 145 ONE[®] and Lipidil Ter[®] are shown in Figure 4.19 and in Figure 4.20:

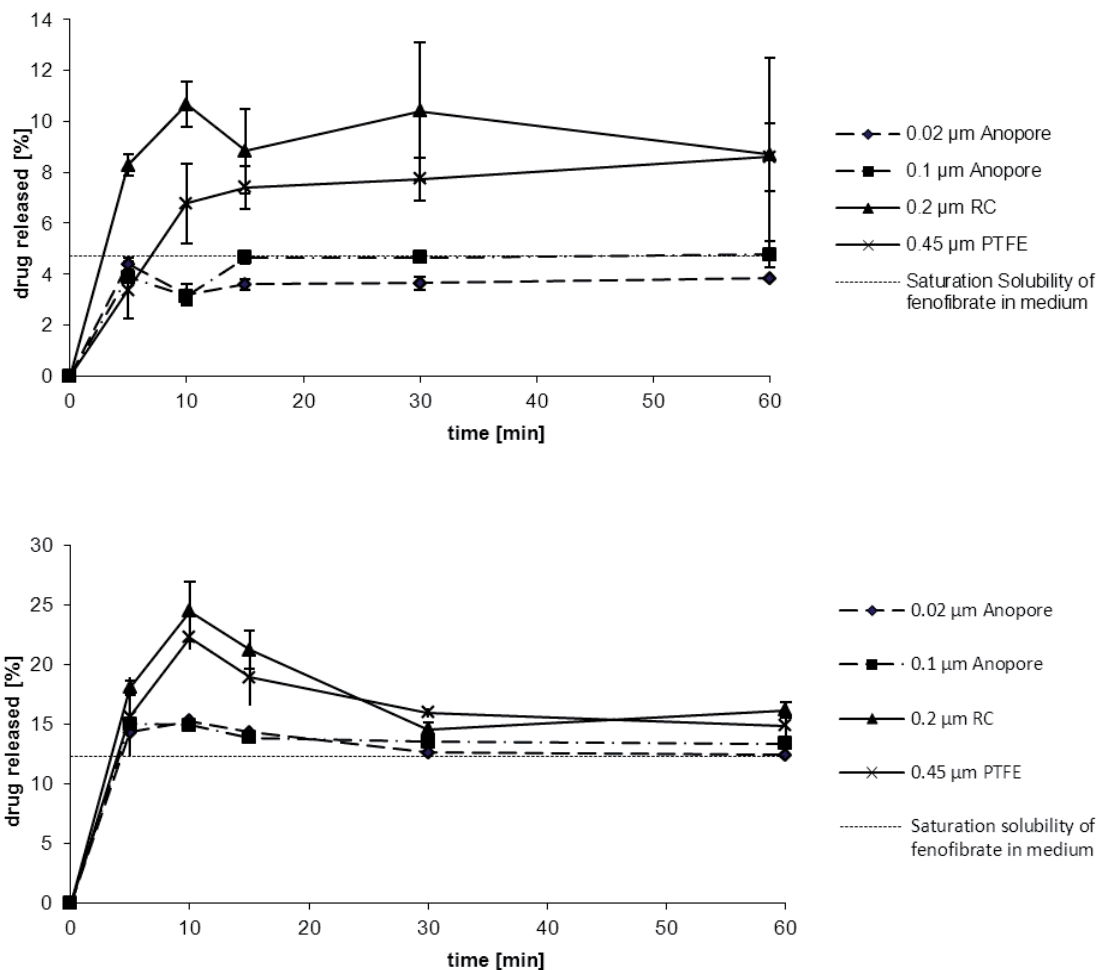


Figure 4.19: Dissolution profiles of Lipidil 145 ONE[®] in FaSSIF and FeSSIF using various filter pore sizes

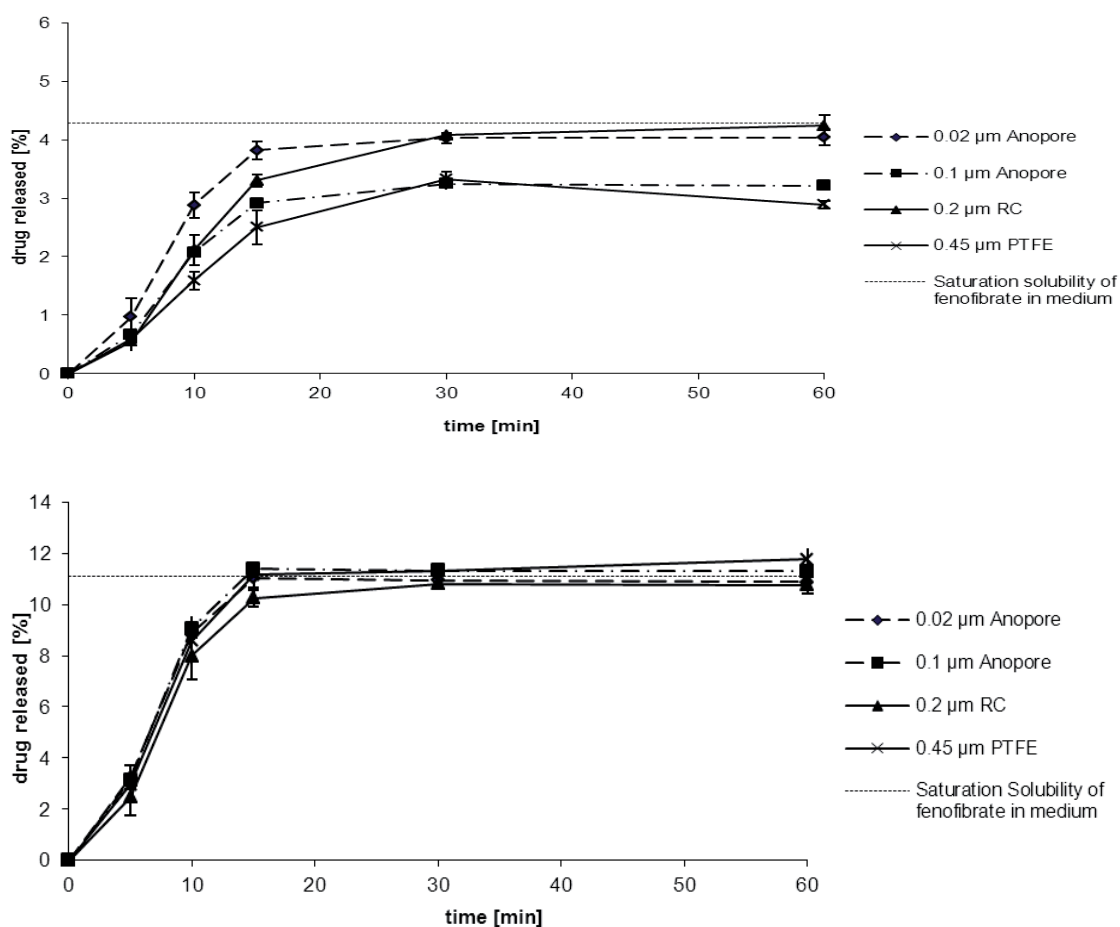


Figure 4.20: Dissolution profiles of Lipidil Ter[®] in FaSSIF and FeSSIF using various filter pore sizes

The f_2 -values for both are listed in Table 4.6.

Table 4.6: Comparison of dissolution profiles using the f_2 -value (0.1 μm pore size as reference)

Filter pore size (μm)	Lipidil 145 ONE [®]		Lipidil - Ter [®]	
	FaSSIF	FeSSIF	FaSSIF	FeSSIF
0.02	91.53	94.86	86.09	97.09
0.2	46.84	48.54	74.71	84.53
0.45	61.81	55.86	66.58	99.54



Using a pore size of 0.1 μm or less, the maximum concentration of drug achieved in solution from the nanosized formulation was commensurate with the saturation solubility of fenofibrate in FaSSIF and FeSSIF. Filtration with a pore size of 0.2 μm or 0.45 μm generated concentrations exceeding the saturation solubility. These results, in combination with the higher standard deviations, indicate that the apparent “supersaturation” is caused by colloidal fenofibrate, which is too fine to be held back by these filters. The f_2 -value of less than 50 when comparing the profiles obtained from 0.1 μm and 0.2 μm filter pore size indicates that the choice of filter pore size is crucial to the interpretation of the dissolution profiles. To separate nanosized drug from molecularly dissolved fenofibrate in Lipidil 145 ONE[®], a filter pore size of 0.1 μm or less appears to be appropriate. The use of an even smaller pore size (0.02 μm) resulted in a comparable dissolution profile. But since the filter adsorption studies indicated that the 0.02 μm pore size filter are able to filter micelles, therefore a filter pore size of 0.1 μm is recommended.

The analogous experiment with micronized fenofibrate that contains little or no colloidal fenofibrate yielded similar dissolution profiles, irrespective of filter pore size; f_2 was always greater than 65, indicating less than 5% difference between the dissolution profiles in any medium. This is commensurate with the particle size of fenofibrate ranging from 5-15 μm in Lipidil Ter[®] [51].

The results were repeated with updated biorelevant media (FaSSIF-V2 and FeSSIF-V2) using 0.1 μm and 0.2 μm filter pore sizes, leading to the same findings (compare Table 8.28 - Table 8.35).



It was observed that the results from the dissolution test are not commensurate with the results from the filter adsorption studies. It is very difficult to find a setup indicating the suitability of filters for complicated formulations as Lipidil 145 ONE[®] and Lipidil Ter[®] in such an experiment. In such cases, a direct comparison of the filter performance during the dissolution test is recommended, since the experimental setup in the filter adsorption studies is too different, e.g. in terms of solution / suspensions to filter, temperature and additional excipients present in the tablets.

Comparing the results from the dissolution tests, the filter adsorption studies (section 4.2.1) indicate more adsorption to the filter material than seen in experiments. This might be reasoned on the basis of the experimental setup which is different from the setup in dissolution testing:

- (i) a clear solution instead of a suspension was used
- (ii) the adsorption experiments were conducted at room temperature (20°C) while dissolution tests were conducted at 37°C. Especially for media containing substances with a low melting point as lecithin and glycerol monooleate this might be an issue, since recrystallization, e.g. by seed crystals seed crystals might have been formed during the test. These would be lost from the micelles, which might place the drug molecules at more risk to adsorption / precipitation.



These differences may thus explain the observed differences between filter adsorption in filter adsorption testing and dissolution testing. This hypothesis would of course have to be verified by further experiments.

4.3 Theoretical increase of dissolution rate by particle size reduction

While there is little reason to scrutinize the surface area A_{Drug} , the boundary layer δ has been subject to several studies. Higuchi et al. assume δ to be stagnant [89, 90]. In this case, Eq. 1.2 can be rewritten as follows, when decreasing particle size from 5 μm to 0.4 μm :

$$DR_{0.4\mu\text{m}} = \frac{12.25 \cdot A_{5\mu\text{m}} \cdot D_{Drug}}{\delta_{5\mu\text{m}}} \cdot (C_S - C_I)$$

Eq. 4.1

$$DR_{0.4\mu\text{m}} = 12.25 \cdot DR_{5\mu\text{m}}$$

Eq. 4.2

This implies:

$$k_D(\text{Lipidil 145 ONE}^\circ) = 12.25 k_D(\text{Lipidil - Ter}^\circ)$$

Eq. 4.3

The diffusion layer thickness δ was held constant in this calculation and the increase of surface area is the driving force for dissolution enhancement. But there are more models regarding the thickness of the boundary layer with changing particle size.



Hixson et al. assumed the diffusion boundary layer to decrease in the same manner as particle size [91].

$$DR_{0,4\mu m} = \frac{12.25 \cdot A_{5\mu m} \cdot D_{Drug}}{\frac{\delta_{5\mu m}}{12.5}} \cdot (C_S - C_I)$$

Eq. 4.4

These calculations lead to a theoretical increase of dissolution rate from factor 12.25 according to Higuchi et al, and to an increase of factor 153.125 using the model according to Hixson-Crowell.

Several other models have been applied in literature to calculate the diffusion boundary layer h with decreasing particle diameter: Niebergall et al. proposed that h correlates with the square root of radius [92], Hintz and Johnson founded the concept of a transitional particle size of 30 μm , implying that h is constantly 30 μm for particles larger than 30 μm , but the diffusion layer is equal to particle radius for particles less than 30 μm [93]. Sheng et al. found a dependency of h on the agitation of fluids [94]: 50 rpm in a dissolution vessel (paddle) results in a description of h as

$$9.91 \sqrt{d} - 23.31$$

Eq. 4.5



for particles between 6.8 μm to 106 μm . A revolution speed of 100 rpm results in a linear relationship for particles $< 23.7 \mu\text{m}$ as follows:

$$h = 1.59r$$

Eq. 4.6

A summary of the results obtained with each model can be found in Table 4.7.

Table 4.7: Calculation of change of diffusion boundary layer using various models (for particle sizes decreased in d from $5\mu\text{m}$ to $0.4\mu\text{m}$)

Author	Formula	Factor of h decrease	Factor of dissolution rate increase ($5\mu\text{m} \rightarrow 0.4\mu\text{m}$)
Higuchi [89, 90]	$h = \text{constant}$	1	12.25
Hixson-Crowell [91]	$h = r$	12.5	152.25
Niebergall [92]	$h = \sqrt{r}$	3.535	43.31
Hintz-Johnson [93]	$h = \text{constant}$ (particles $>30 \mu\text{m}$)	12.5	152.25
Sheng [94]	50 rpm: $9.91 \sqrt{d} - 23,31$	Not applicable	Not applicable
Sheng [94]	100 rpm: $1.59 r$	12.5	152.25



4.4 Comparison of dissolution rate in theory and in practice

By plotting $\ln C$ against t the dissolution rate constant k was identified. Since dissolution was incomplete, the mean dissolution time could not be calculated [95]. Instead, the mean dissolution time for the portion of drug that actually dissolved was calculated (Mean drug dissolution times, (MDTs)):

$$\text{MDTs} = \frac{1}{k}$$

Eq. 4.7

The results are listed in Table 4.8.

Table 4.8: MDTs (min) for Lipidil Ter® and Lipidil 145 ONE® in various media

	Lipidil Ter®	Lipidil 145 ONE®	Ratio
FaSSGF	6.544	1.402	4.668
FaSSIF-V2	2.933	0.494	5.937
FeSSGF*	-	-	-
FeSSIF-V2	3.004	1.041	2.886

* Impossible to measure, see section 4.1.5

The ratio of MDTs between the micronized and the nanosized formulation indicate that there is a substantial improvement in dissolution rate by nanosizing, as previously described by several authors [24, 55, 96, 97]. Nevertheless, the measured results are not commensurate with the theoretical increase according to the Noyes – Whitney equation (compare section 4.3).



The results from sections 4.3 and 4.4 indicate that the dissolution behavior of very small particles cannot be predicted by common diffusion models. It is more appropriate to use experimental data since application of the models leads to completely different results [98-101] .

4.5 Evaluation of the STELLA[®] software to generate simulated plasma profiles

In vivo plasma profiles from fenofibric acid (Lipidil 145 ONE[®] and Lipidil Ter[®], both fasted and fed state) were compared to those profiles generated from the STELLA[®]-Model above, combining the STELLA[®] software with the pharmacokinetic parameters from WinNonlin[®], as shown in Figure 4.21 to Figure 4.24 :

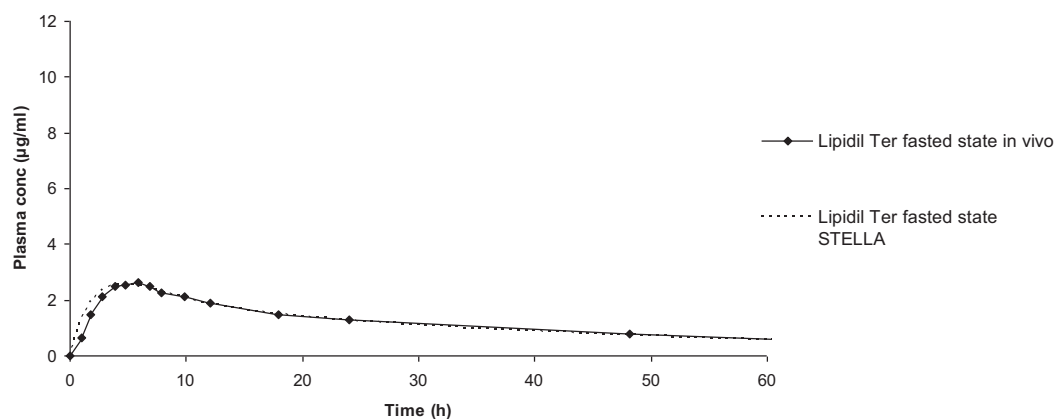


Figure 4.21: Comparison of plasma profiles, Lipidil Ter[®], fasted state

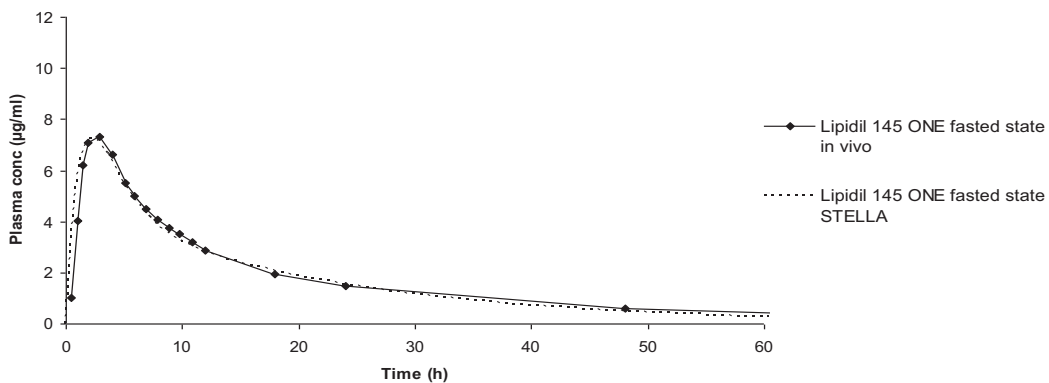


Figure 4.22: Comparison of plasma profiles, Lipidil 145 ONE[®], fasted state

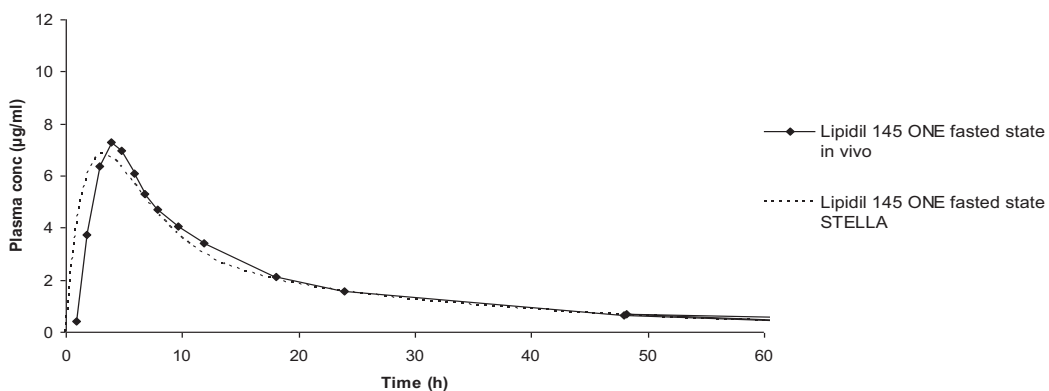


Figure 4.23: Comparison of plasma profiles, Lipidil Ter[®], fed state

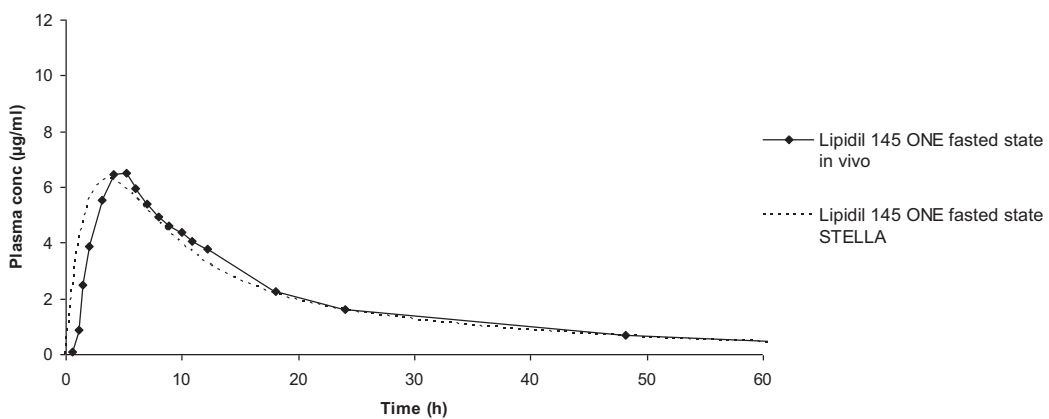


Figure 4.24: Comparison of plasma profiles, Lipidil 145 ONE[®], fed state



It is clearly shown that the STELLA[®] software is capable of accurately simulating plasma profiles when post-absorptive pharmacokinetic parameters of WinNonlin[®] are used in the model.

4.6 Discussion of the conventional approach vs. a new method for rapidly dissolving compounds

In Table 4.11 and Table 4.12 the z-values for Lipidil 145 ONE[®] and Lipidil Ter[®] in various media obtained by dissolution testing are listed. The conventional method and the new method result in very different z-values. This gives rise to the question as to which sampling points from the dissolution test should be used for simulations of plasma profiles. Fenofibrate is a substance with very low aqueous solubility. Both micronized and nanosized formulations dissolve according to the Noyes-Whitney-equation very quickly in the closed system of a dissolution vessel until they reach saturation solubility in the corresponding medium. In case of the nanosized fenofibrate, the saturation solubility is reached within three minutes. For the calculation of z at least three sampling points should be included. But for Lipidil 145 ONE[®] it is not possible to collect more than one sample per minute. For the denominator of Eq. 3.2, this means:

$2(X_s - X_0)^{\frac{2}{3}} \rightarrow 0$. This results in an increase of z and in consequence, z cannot be considered to be equal to $\frac{D\Gamma N^{1/3}}{\delta\rho^{2/3}}$. In case of Lipidil 145 ONE[®], the observed X_s was

2.8571 mg. Table 4.9 shows the dependency of z to X_s , assuming slight variations of the observed X_s up to dissolution of the entire dose.



Table 4.9: Dependence of z on X_s

Observed*/Assumed X_s	Resulting z -value
2.8571*	8.22196
2.8661	5.69162
2.9561	3.21153
3	2.85000
5	0.65818
10	0.24208
25	0.08412
50	0.04032
75	0.02652
100	0.01976
130	0.01513
145	0.01355

To evaluate the dependency of z on solubility, the z -value was calculated for another, more soluble compound, Diphenhydramine HCl. The dissolution data (not shown) was obtained by the use of the ion-selective electrode (compare section 3.3.4).

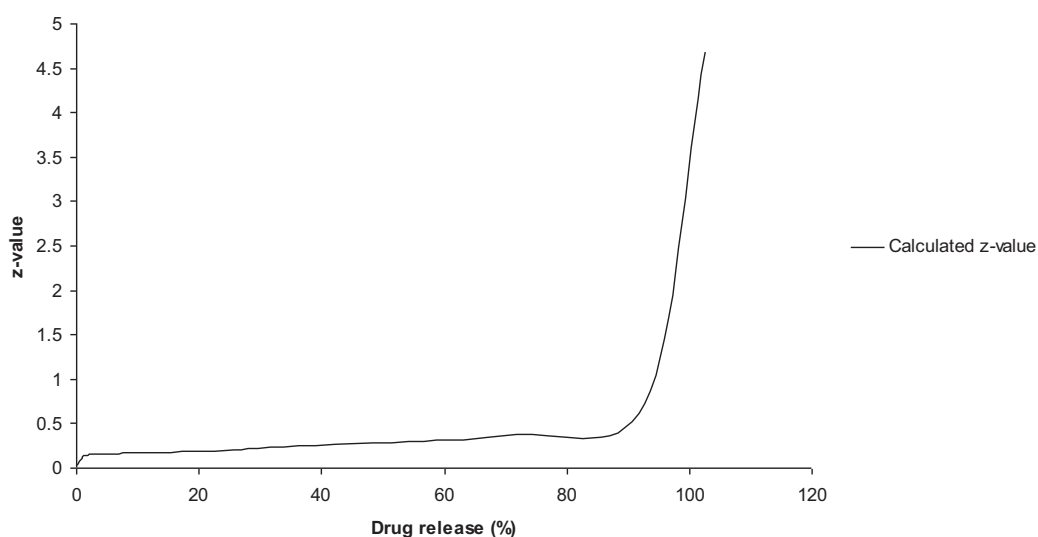


Figure 4.25: z-value in dependency of released drug

Figure 4.25 clearly shows that the z-value increases inappropriately when the last sample point used for calculation of z is over 80% dissolution, as exemplified by diphenhydramine HCl.

Table 4.9 and Figure 4.25 suggest that the data points for calculation of the z value should be taken before dissolution exceeds 80%, e.g. between 5-60%, since the z value has a relatively constant value in this region. For a very quickly dissolving drug product like the fenofibrate formulations tested, it may not be possible to draw corresponding samples quickly enough in a manual dissolution test. Thus for drug products that dissolve quickly (if incompletely) the calculation of z directly from dissolution test data leads to an overestimate of z and subsequently to inaccurate simulation of plasma profiles (compare Fig. 4.26).

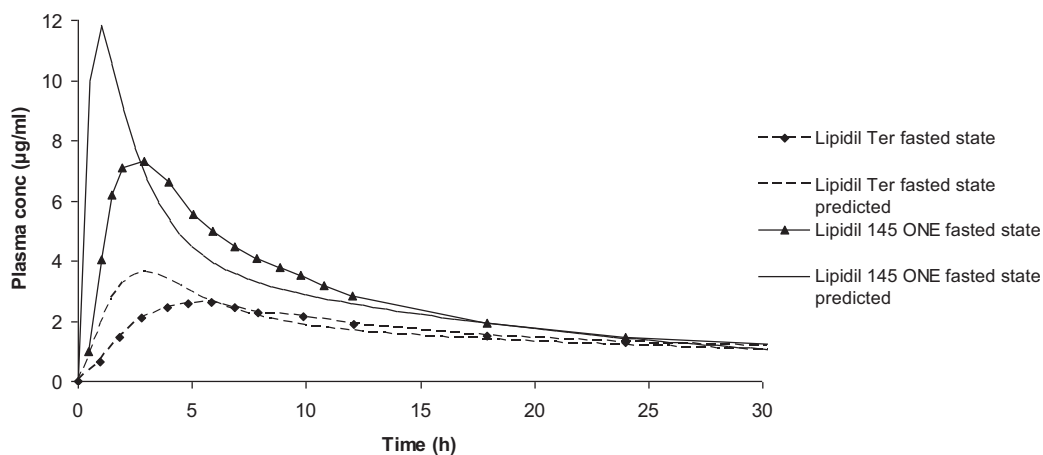


Figure 4.26: In vivo and in silico plasma profiles of fenofibric acid using the conventional z-value approach

Table 4.10: Point estimate ratios of predicted and in vivo plasma profiles

	C_{\max}	t_{\max}	AUC
Lipidil Ter [®]	1.38	0.51	0.99
Lipidil 145 ONE [®]	1.62	0.34	0.93

Figure 4.26 shows the simulated plasma profiles of Lipidil Ter[®] and Lipidil 145 ONE[®] in comparison to *in vivo* data. The point estimate ratios in Table 4.10 derived from Figure 4.26 show that the generated plasma profiles overpredict the *in vivo* profiles when z-values from the conventional approach are used for fenofibrate. For this reason, the z-values obtained by the new method described in section 3.4.3.2 were used for further simulation purposes (see also Table 4.11 and Table 4.12).



4.7 Calculation of z-values

The z-values derived from *in vitro* dissolution testing are listed in Table 4.11 and Table 4.12.

Table 4.11: z-values of Lipidil 145 ONE[®]

	z-values Lipidil 145 ONE [®]	
	Conventional method	New method
FaSSGF	6.745	0.736
FaSSIF-V2	8.222	2.209
FeSSIF	3.562	0.798
FeSSIF-V2	5.943	0.429

Table 4.12: z-values of Lipidil Ter[®]

	z-values Lipidil Ter [®]	
	Conventional method	New method
FaSSGF	0.490	0.702
FaSSIF-V2	1.223	0.348
FeSSIF	0.105	0.271
FeSSIF-V2	0.518	0.289



4.8 Simulated plasma profiles of fenofibric acid Model A

The fasted state plasma profiles generated *in silico* are compared to *in vivo* data in Figure 4.27.

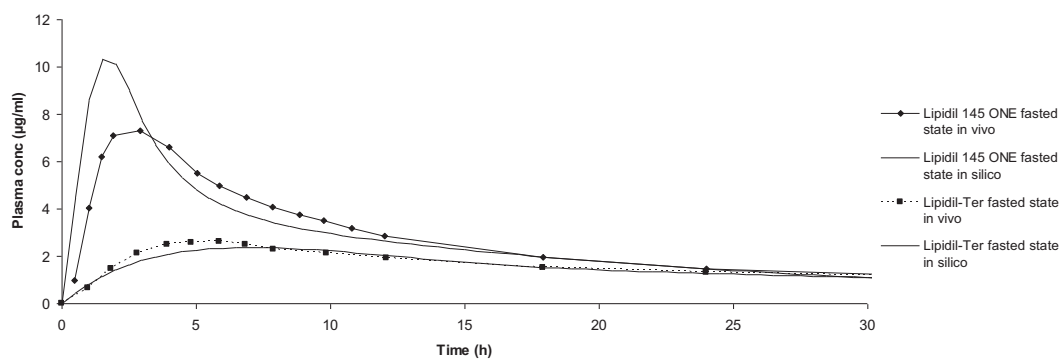


Figure 4.27: Simulated plasma profiles of Lipidil 145 ONE[®] and Lipidil Ter[®] in comparison to *in vivo* data (fasted state, Model A)

The plasma profiles for the fed state generated *in silico* are compared to *in vivo* data in Figure 4.28.

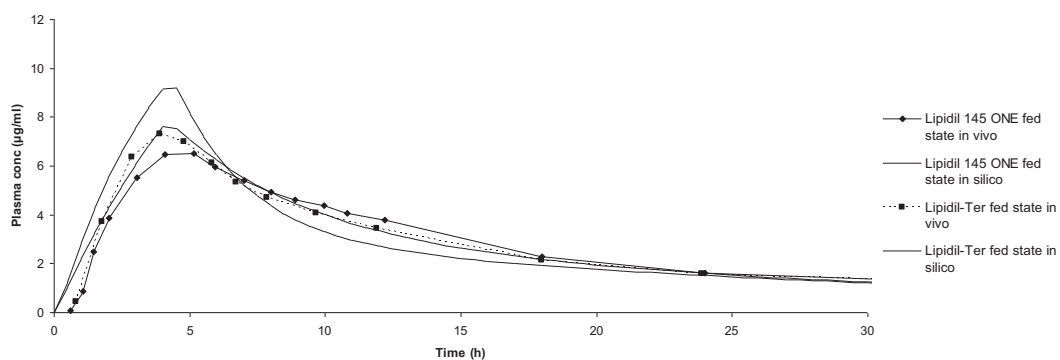


Figure 4.28: Simulated plasma profiles of Lipidil 145 ONE[®] and Lipidil Ter[®] in comparison to *in vivo* data (fed state, Model A)

For both fasted and fed state the point estimates ratios of c_{max} , t_{max} and AUC from *in silico* / *in vivo* plasma profiles are given in Table 4.13.



Table 4.13: Point estimate ratios of in silico / in vivo data Model A

	Lipidil 145 ONE [®]		Lipidil Ter [®]	
	Fasted state	Fed state	Fasted state	Fed state
C _{max}	1.41	1.16	0.91	1.32
T _{max}	0.52	0.78	1.20	0.94
AUC	0.93	0.97	0.98	0.99

Model A correlates very well to the plasma profile of the micronized Lipidil Ter[®] (Figure 4.27), indicating that for this formulation dissolution of the drug is rate-determining for its appearance in the blood.

4.8.1 Sensitivity analyses model A

4.8.1.1 Influence of gastric emptying rate

The sensitivity of the applied models to the gastric emptying rate was checked for both fasted and in the fed state. For the fasted state, the initial value (2.8^{-1}) was varied from one-fifth to five times.

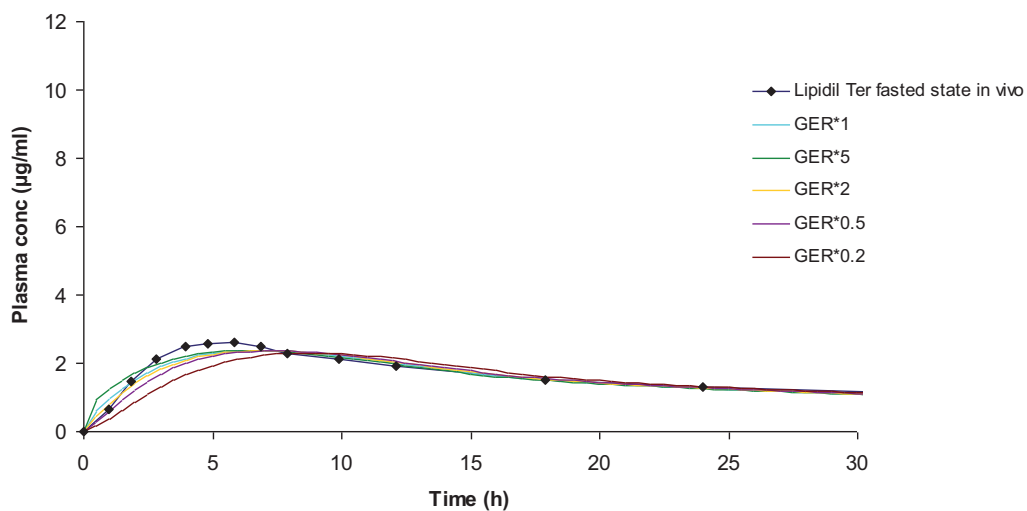


Figure 4.29: Sensitivity analysis of GER for Lipidil Ter[®] in the fasted state

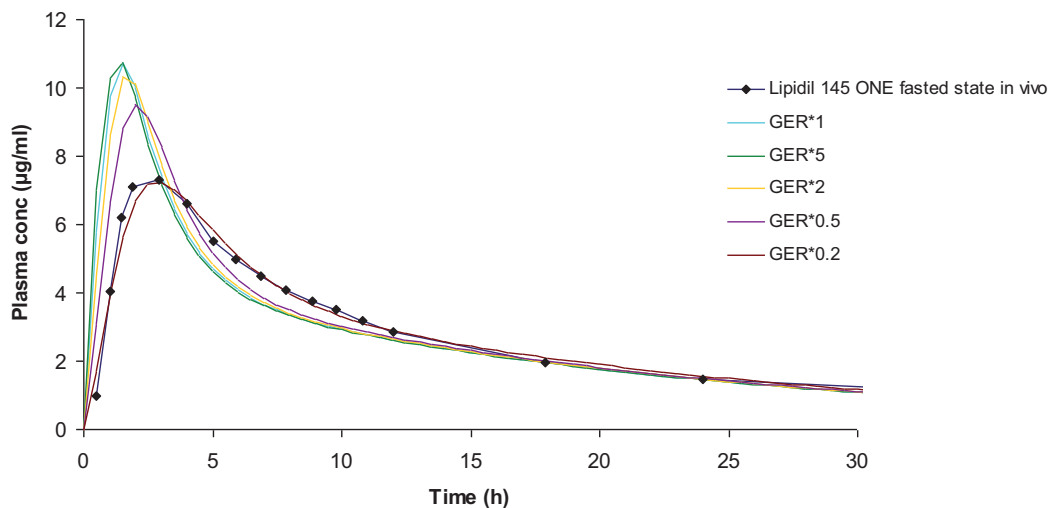


Figure 4.30: Sensitivity analysis of GER for Lipidil 145 ONE[®] in the fasted state

For the fed state, the initial value of GER (4 kcal/min) was varied from 1 kcal/min to 5 kcal/min.

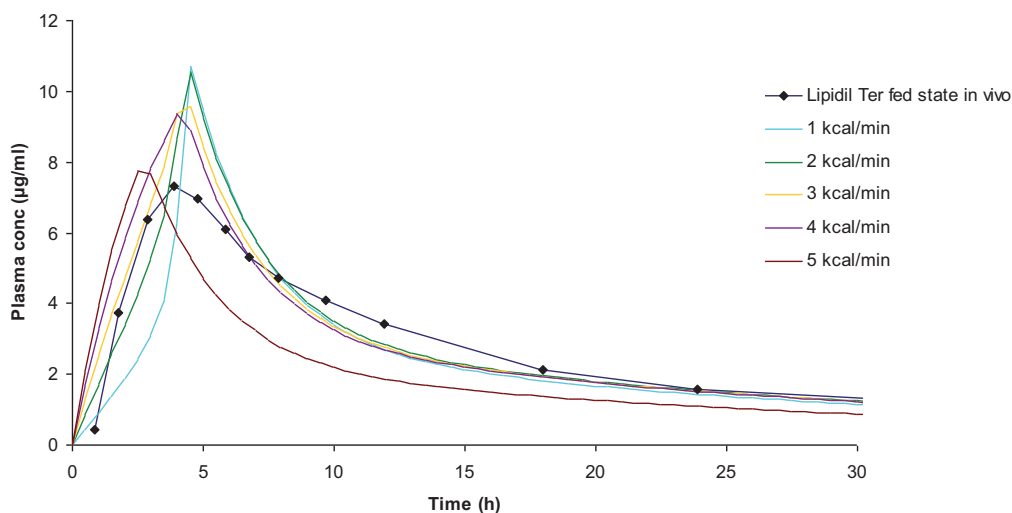


Figure 4.31: Sensitivity analysis of GER for Lipidil Ter® in the fed state

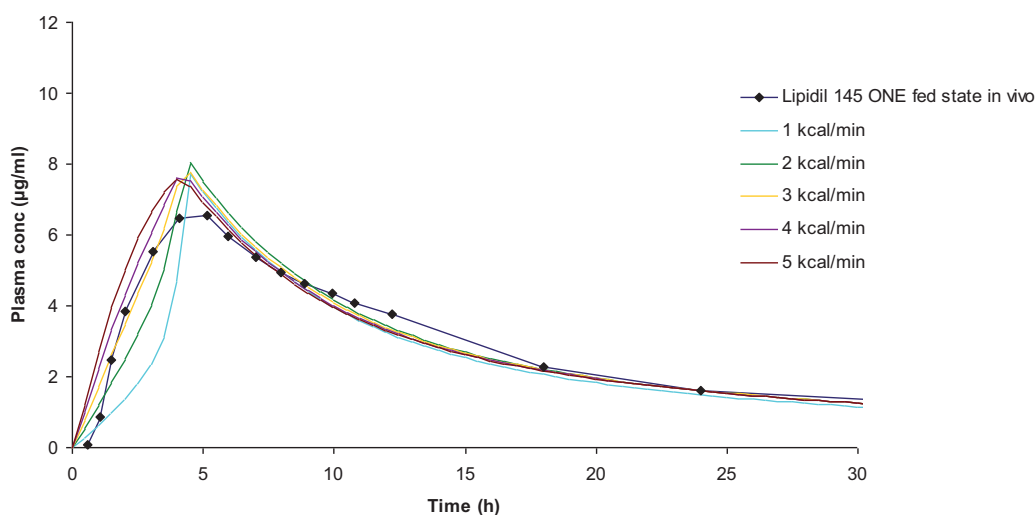


Figure 4.32: Sensitivity analysis of GER for Lipidil 145 ONE® in the fed state

The sensitivity analyses clearly show the impact of the gastric emptying rate in the fed state as the determining factor of bioavailability of the micronized formulation. The nanosized formulation shows less sensitivity to the gastric emptying rate. Neither solubility nor dissolution rate is rate determining in the fed state.



4.8.1.2 Influence of gastric dissolution rate

The sensitivity of the applied models to the gastric dissolution rate (z_{gastric}) was checked for both fasted and in the fed state.

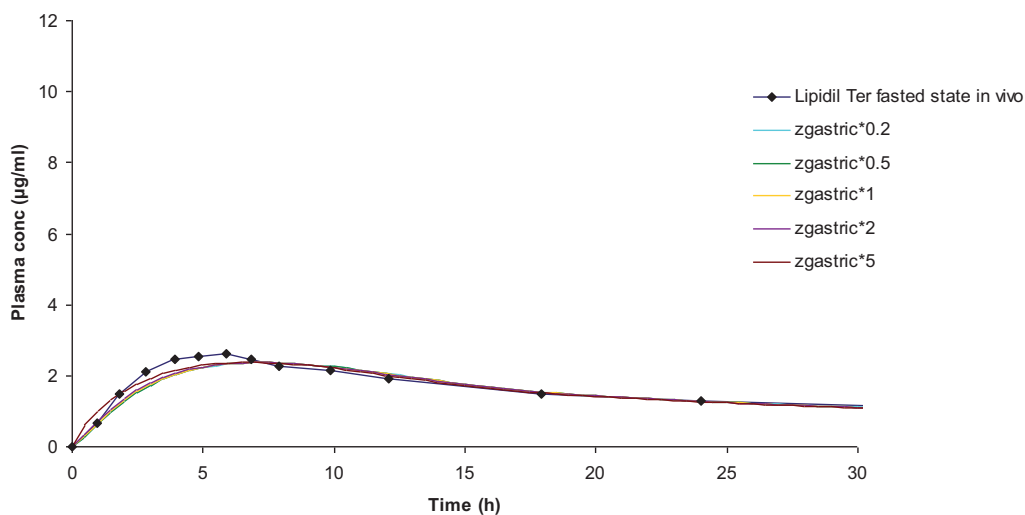


Figure 4.33: Sensitivity analysis of gastric dissolution for Lipidil Ter[®] in the fasted state

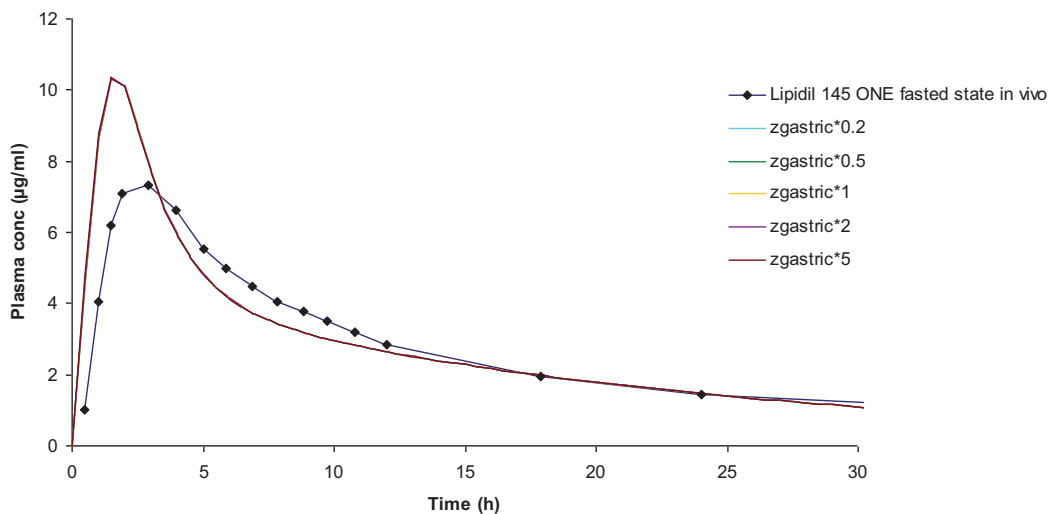


Figure 4.34: Sensitivity analysis of gastric dissolution for Lipidil 145 ONE[®] in the fasted state

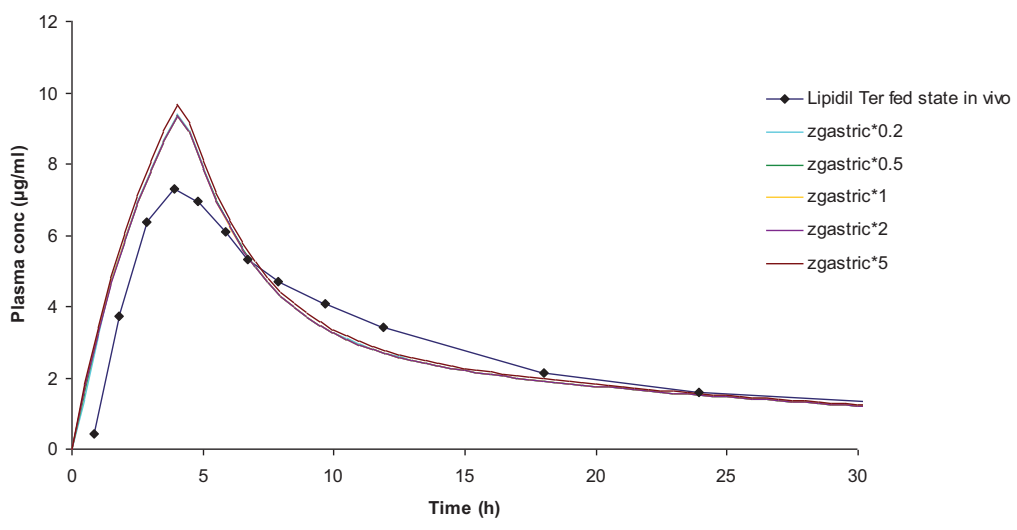


Figure 4.35: Sensitivity analysis of gastric dissolution for Lipidil Ter[®] in the fed state

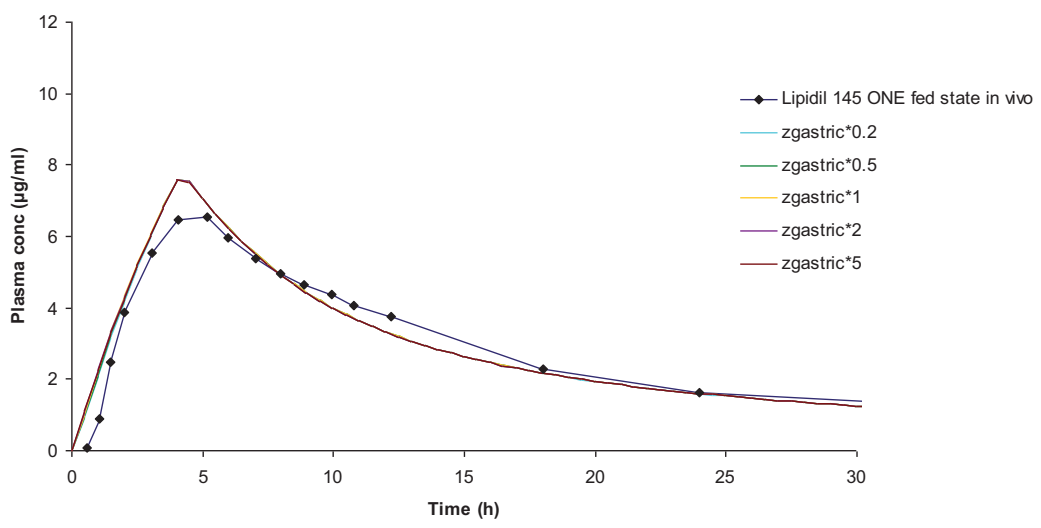


Figure 4.36: Sensitivity analysis of gastric dissolution for Lipidil 145 ONE[®] in the fed state

The sensitivity analysis of $z_{gastric}$ clearly proves that the gastric dissolution rate does not affect the simulation of plasma profiles of fenofibric acid.

4.8.1.3 Influence of intestinal dissolution rate

The sensitivity of the applied models to the intestinal dissolution rate was checked for both fasted and in the fed state.

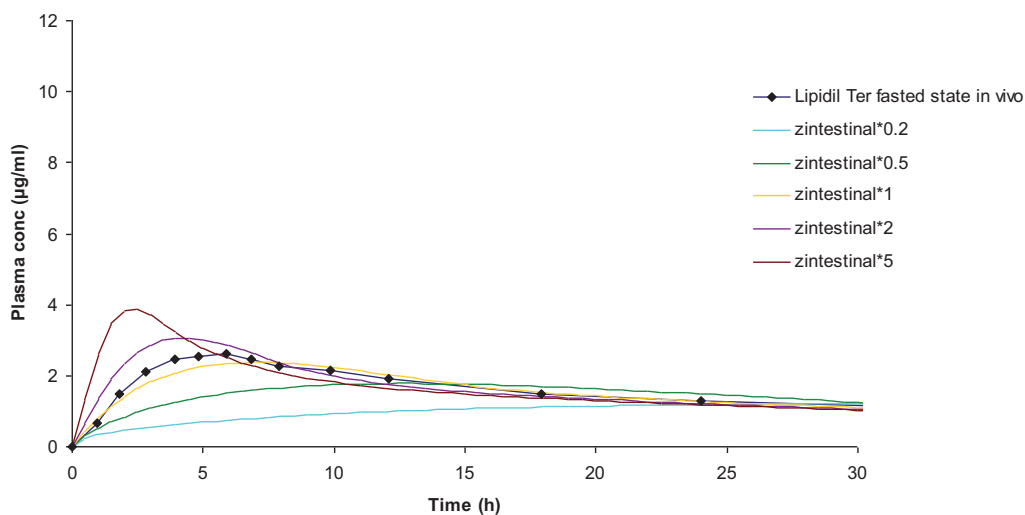


Figure 4.37: Sensitivity analysis of intestinal dissolution for Lipidil Ter[®] in the fasted state

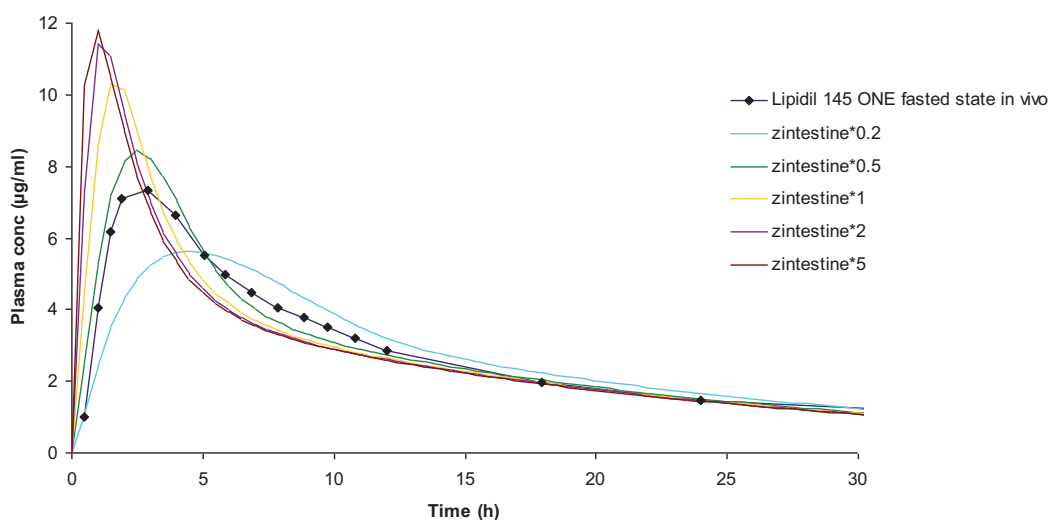


Figure 4.38: Sensitivity analysis of intestinal dissolution for Lipidil 145 ONE[®] in the fasted state

The sensitivity analysis of z_{intest} shows that intestinal dissolution is a very important parameter for both formulations in the fasted state. In case of Lipidil Ter[®] there is a good correlation between simulated plasma profiles and *in vivo* data. This clearly



supports the hypothesis that dissolution in the intestine is the rate limiting step for absorption of fenofibrate in the fasted state.

For Lipidil 145 ONE[®], the correlation is less clear. It can be seen that absorption is dependent on dissolution, but at 0.5*z there is an overprediction of c_{max} in the simulated plasma profiles. For nanoparticles it has been suggested, that a direct particle uptake through the mucosa occurs [97, 102-105]. Since Model A leads to overestimation of c_{max} taking only dissolved drug into account, the hypothesis that a direct particle uptake through the mucosa occurs seems unlikely for fenofibrate nanocrystals.

The results indicate that for Lipidil 145 ONE[®] dissolution is not the only factor that affects the rate at which fenofibrate gets absorbed. It seems more likely that dissolution is fast enough that an additional step comes into play. In Model A, instantaneous permeation across the mucosa is assumed. But even though fenofibrate is widely considered to be a BCS class II drug, recent reports suggest that permeation is likely to play a role in the absorption of fenofibrate [84, 106].

Therefore, Model B, which contains the possibility a permeability limitation, was also tested (compare 3.4.3.3).



4.9 Simulated plasma profiles of fenofibric acid model B

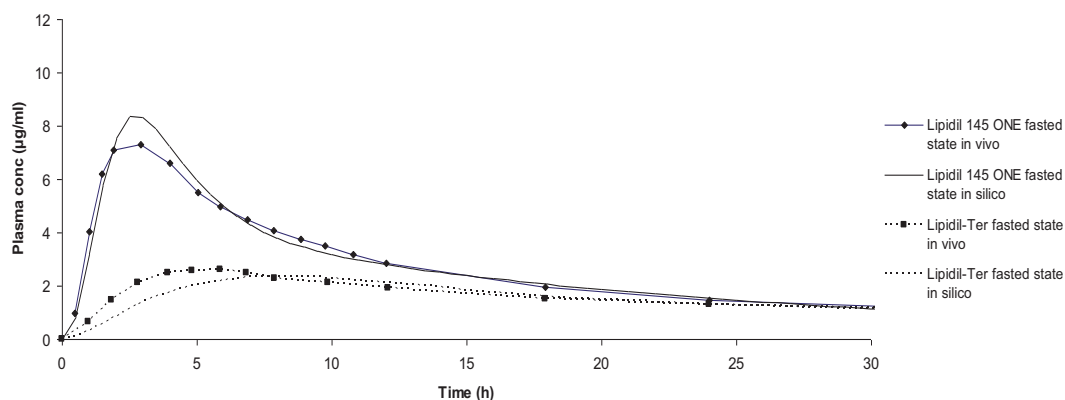


Figure 4.39: Simulated plasma profiles of Lipidil 145 ONE[®] and Lipidil Ter[®] in comparison to *in vivo* data (fasted state, Model B)

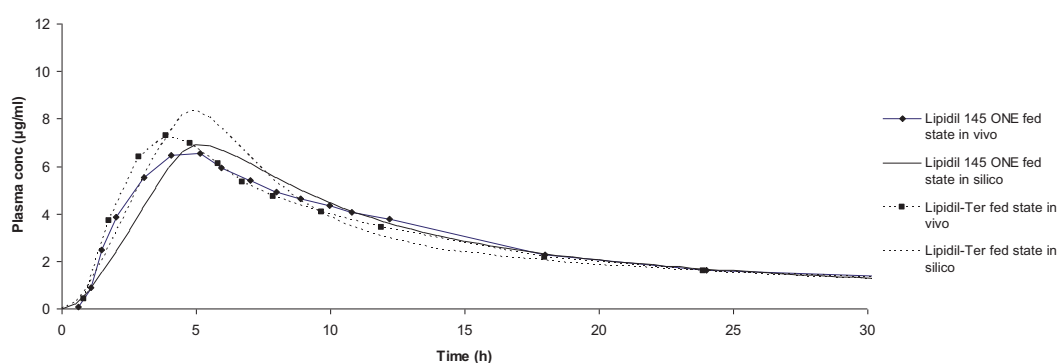


Figure 4.40: Simulated plasma profiles of Lipidil 145 ONE[®] and Lipidil Ter[®] in comparison to *in vivo* data (fed state, Model B)

Table 4.14: Point estimate ratios of *in silico* / *in vivo* data Model B

	Lipidil 145 ONE [®]		Lipidil Ter [®]	
	Fasted state	Fed state	Fasted state	Fed state
C _{max}	1.14	1.06	0.90	1.20
T _{max}	0.86	0.97	1.37	1.04
AUC	0.93	0.97	0.98	0.99

The point estimate ratios in Table 4.14 show that the correlation between *in vivo* data and simulated plasma profiles of fenofibric acid is noticeably improved for the



nanosized fenofibrate formulation using Model B. The simulated plasma profiles indicate that for micronized fenofibrate, permeation is not an issue, but for the nanosized fenofibrate, a lack of a permeation step through the intestinal mucosa seems to be responsible for the overprediction of plasma profiles with Model A. This effect comes into play when dissolution is so fast that the GI tract can no longer be considered as an open system.

4.9.1 Sensitivity analyses Model B

The sensitivity analyses for model A have shown that the intestinal dissolution rate in the fasted state and the gastric emptying rate in the fed state are the most sensitive parameters to the simulation of plasma profiles. Therefore, these parameters were tested again for Model B. Additionally, the permeability was varied from 0.5 – 1 to evaluate its effect on the simulated plasma profiles.

4.9.1.1 Influence of intestinal dissolution in the fasted state

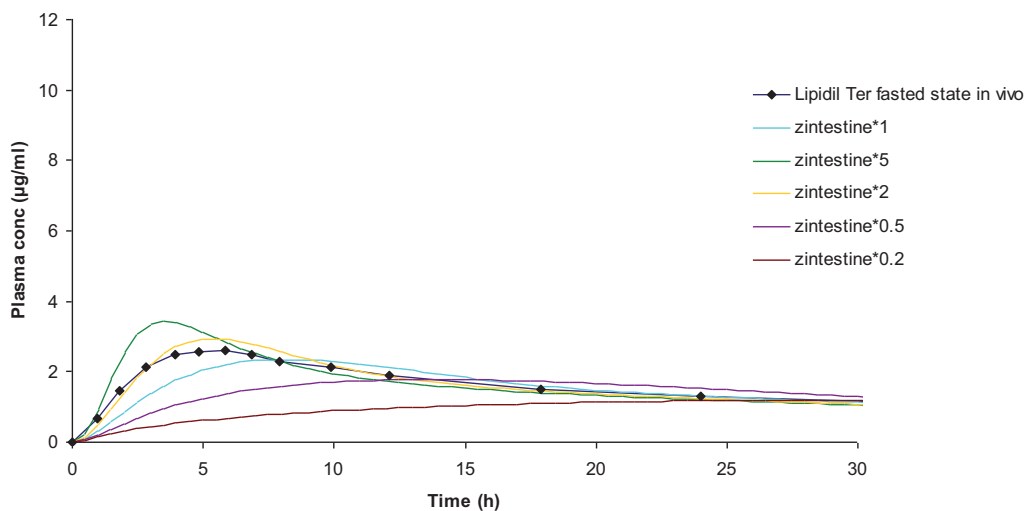


Figure 4.41: Sensitivity analysis of intestinal dissolution for Lipidil Ter[®] in the fasted state (model B)

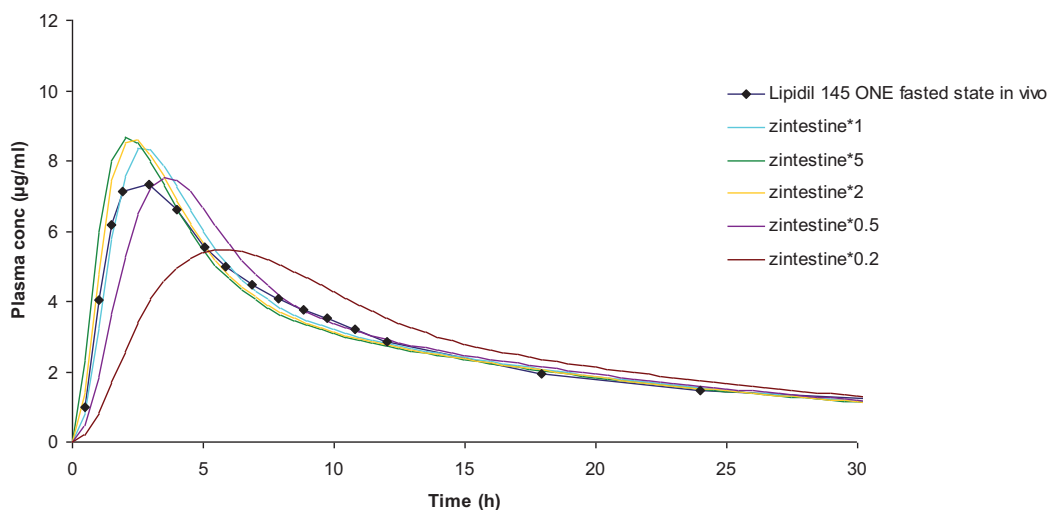


Figure 4.42: Sensitivity analysis of intestinal dissolution for Lipidil 145 ONE[®] in fasted state (model B)

Intestinal dissolution has immediate effect on the micronized fenofibrate in the fasted state. This is in congruence with the observation that dissolution BCS-class II substances is rate determining for the appearance of drug in the blood.



The nanosized drug does show such strong dependency: even a decrease of dissolution rate of 50% does not lead to a substantial change of plasma profile in the simulations. This leads to the thoughts that the degree of nanonisation is possibly even higher than necessary to achieve maximum plasma levels and jeopardizes the direct correlation of dissolution rate and drug plasma levels, as already indicated in Model A.

4.9.1.2 Influence of gastric emptying rate in the fed state

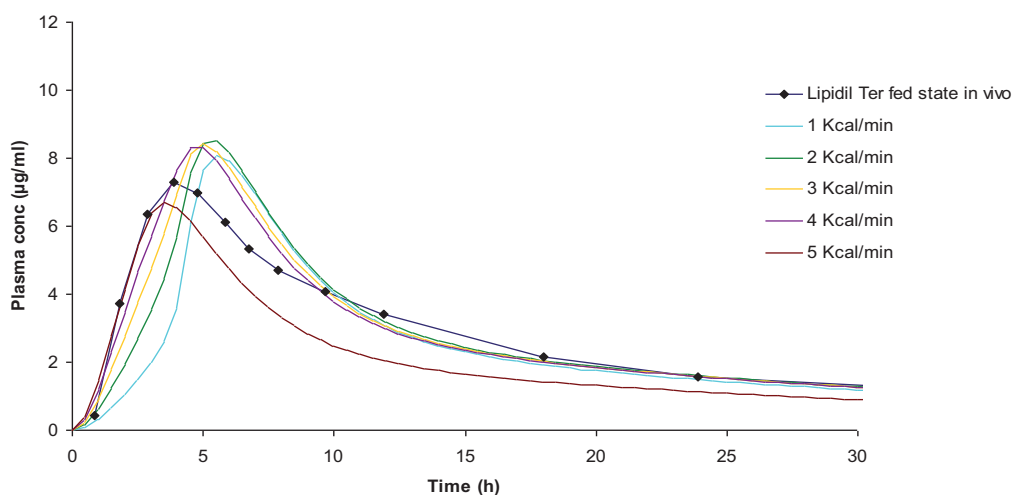


Figure 4.43: Sensitivity analysis of GER for Lipidil Ter[®] in the fed state (model B)

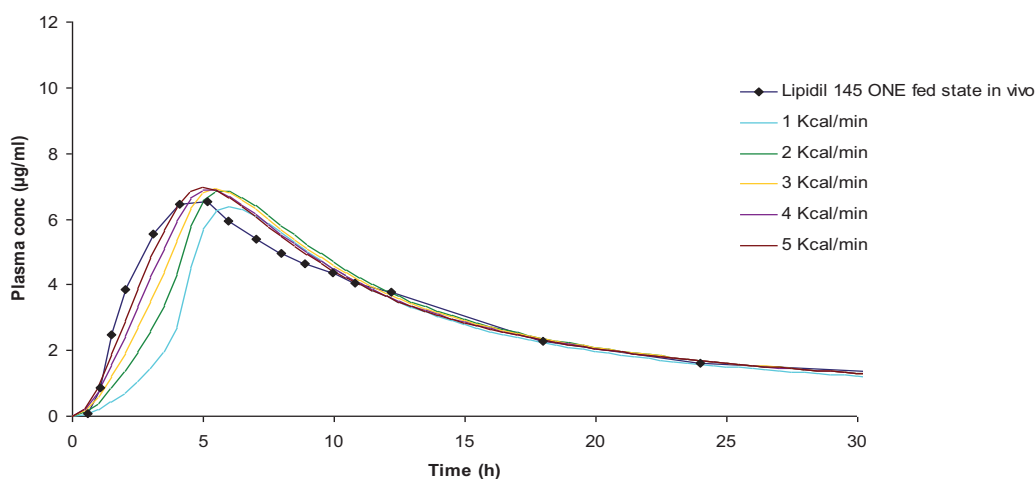


Figure 4.44: Sensitivity analysis of GER for Lipidil 145 ONE[®] in the fed state (Model B)



In the fed state, the lack of sensitivity to the choice of model can be explained by the zero order gastric emptying (GE) rate in the fed state. The GE rate seems to be an important limiting factor in the fed state for the absorption of fenofibrate: In the fed state solid drug particles enter the small intestine gradually over time, followed by rapid dissolution and absorption. So the dissolution of fenofibrate is not directly limiting to absorption but rather the rate at which fenofibrate appears in the intestine from the stomach. By contrast, due to the more rapid GE rate in the fasted state, GE plays less of a role in the overall process.

4.9.1.3 Influence of permeation rate across the intestinal mucosa

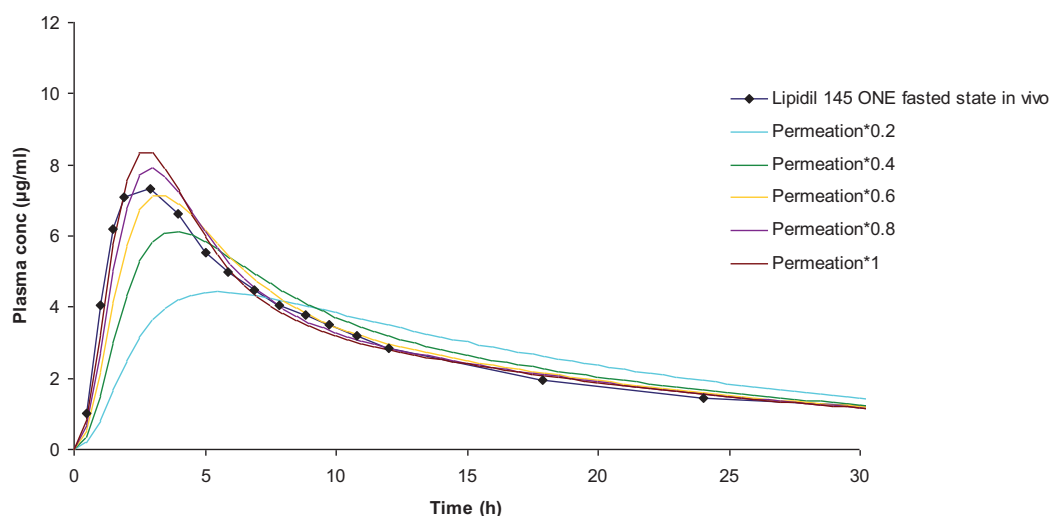


Figure 4.45: Sensitivity analysis of permeation rate for Lipidil 145 ONE[®] in the fasted state.

The sensitivity analysis of permeation across the intestinal membrane supports the hypothesis that absorption from nanosized fenofibrate is at least partly permeation controlled.



However, the simulations still slightly overpredict C_{\max} in the fasted and the fed state. Possible reasons are a) the fraction absorbed in the fed state is not 100%, b) fenofibrate gets presystemically metabolized to fenofibric acid in the intestinal membrane [85, 107, 108], a process which may be affected by food components and c) the use of a linear gastric emptying rate for simulation purposes does not reflect the *in vivo* situation perfectly. [85].

4.9.2 Discussion of STELLA[®] software

The STELLA[®] software is one of the approaches available to predict the behaviour of a drug in dependence on its dissolution rate. Other softwares include PKSim[®] and GastroPlus[®], which combine physicochemical and physiological parameters to predict the behaviour of a drug or a formulation in the body. While the physiological input data of other software are based on assumptions and means of the average population [109-111], the calculations in STELLA[®] are mainly based on the pharmacokinetic data obtained with the formulation tested and its dissolution test results in biorelevant media. Another advantage is the independence from an input value of the diffusion boundary layer h . As described in section 4.3 and 4.4 this is a sensitive parameter and, depending on which model is used, results may vary. Provided an appropriate analytical method is chosen, the calculations by STELLA[®] are more reliable than others.



4.9.2.1 Possible applications using the presented model in STELLA®

Using mainly experimental data, STELLA® enables an exact investigation of the importance of the dissolution behaviour of a drug. The consequences of a change of dissolution rate can be investigated reliably in the simulated plasma profiles. While in this study the different behaviour of micro- and nanosized fenofibrate was investigated, the software could be used for other purposes in the future. It would be possible to use the software as an indicative tool: One can predict the required particle size to obtain bioequivalence to a reference product containing nanosized drug. Whereas it is not reliable to link particle size directly to dissolution behaviour based on theories (compare chapter 4.3 and 4.4) the STELLA® software can be used to set specifications regarding the dissolution behaviour: In FaSSIF-V2, the *in vitro* $Z_{intestine}$ of Lipidil Ter® was calculated to be 0.34 whilst the corresponding value for Lipidil 145 ONE® was 2.209. The significantly higher z value for Lipidil 145 ONE® is most likely due to the nanosized particles used rather than the micronized particles of fenofibrate used in Lipidil Ter®.

A profile was constructed comparing the influence of $Z_{intestine}$ on the predicted c_{max} value (compare Figure 4.46). Using a 90% confidence interval point estimate of c_{max} , the corresponding z value is 0.6. This would suggest that formulations with a $Z_{intestine}$ higher than 0.6 are bioequivalent to Lipidil 145 ONE®. Additionally, fenofibrate formulations exceeding a z-value of 0.6 in FaSSIF-V2 *in vitro* are not expected to show a food effect *in vivo*. Results obtained for Lipidil Ter®, which had an *in vitro* $Z_{intestine}$ of 0.34 (green star), had a food effect *in vivo*. Since Lipidil 145 ONE® has a $Z_{intestine}$ value far in excess of the 0.6 cutoff value (2.209, purple star), it is likely that the particle size of

fenofibrate in Lipidil 145 ONE[®] is smaller than necessary in order to eliminate the food effect (compare Figure 4.46).

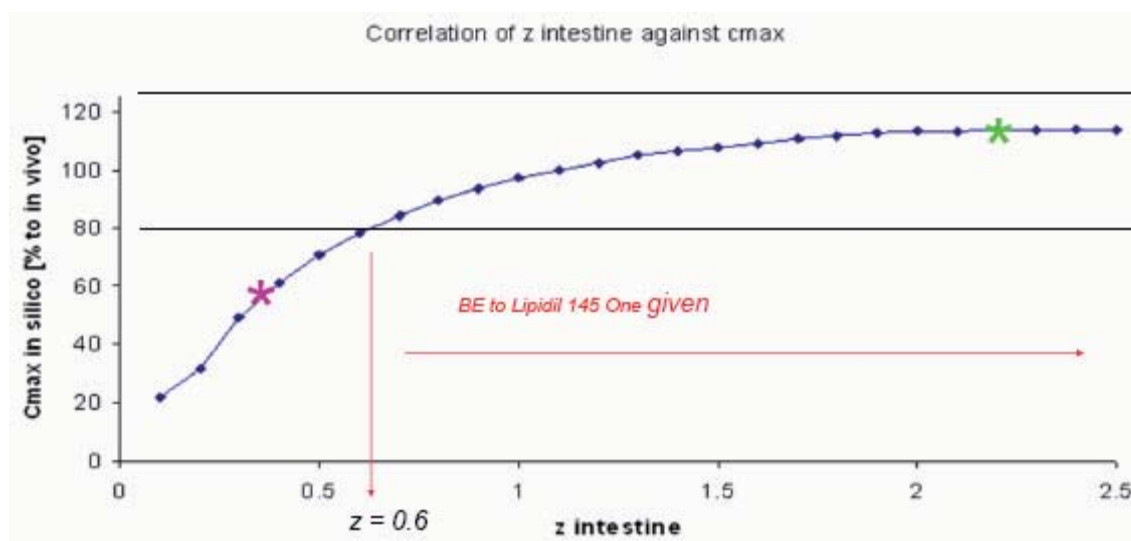


Figure 4.46: Correlation of z -values against c_{max}

4.9.2.2 Limitations of the STELLA[®] model

The model used in the STELLA[®] software is not suitable to predict plasma profiles of completely different formulations. The formulations must remain comparable, e.g. it would not be possible to predict data of a lipid formulation using the pharmacokinetic parameter of a micronized tablet. Further, if a formulation precipitates in the GI tract, the simulations of plasma profiles cannot be trusted since precipitation is not included in the present model. It should also be kept in mind that STELLA[®] can only give qualitative hints to resolve a specific problem. In this study, it was the question of whether the bioavailability of nanosized fenofibrate is affected by permeation. The sensitivity analyses indicate strongly that this is the case. But this does not lead automatically to prediction for other types of formulations.



5 General discussion of thesis

This study was conducted to clarify dissolution methodology for nanosized drugs. The main challenge that has to be considered with such formulations is the separation of undissolved from dissolved drug. This is much more difficult than with coarse or micronized drug formulations. Various analytical methods were considered.

The methods that appeared unsuitable in this study should not necessarily be abandoned altogether. For example, it appears to be possible to set up a specific method in detection of fenofibrate in turbid or milky media. Josefson et al. have developed a method to determine the content of drug in such media [72]. A prerequisite for such techniques is calibration of the system prior to dissolution testing. This calibration appears to be quite complicated and also takes some time, e.g. about 1 hour. For an extended release formulation this is acceptable, but this is surely not the case for instant release tablets, where the total time frame for dissolution is often less than 60 minutes. Nevertheless, if no other suitable method is available, this method could work for quality control purposes. But in research and development another issue comes into play: Josefson et al. strongly emphasize that comparison of dissolution via the multivariate calibration method is only possible for the same kind of tablets, e.g. same matrices. During formulation development, many excipient matrices will be tested within a short time frame, and so for each matrix a dedicated algorithm would have to be developed. It is not very likely that in these times of high throughput systems, time and effort would be dedicated to develop sophisticated correction algorithms for formulation screening, especially in early stages of development.



The method of turbidity measurement appears to be more promising for dissolution testing. But this method from Crisp et al. [75] also has its drawbacks: here too, several prerequisites have to be met. First, the drug has to be absolutely insoluble in the respective dissolution medium, otherwise the offset in the beginning cannot be set equal to 0% dissolution as a starting point. This prerequisite is in conflict with the aims and intention of dissolution testing, which is designed to show release into solution from the dosage form. To overcome the offset problem, a placebo tablet, containing the same matrix as the product to be tested could be used. If such a placebo is available, the turbidimetric-kinetic data of the dissolution test of placebo could be subtracted from a formulation of the same kind containing API, assuming no interaction of the API with the excipients.

In our study, the microdialysis system was not able to handle solutions containing any surfactant. Perhaps it is possible to design a microdialysis system that would be sufficiently robust for surfactants. However, the following points would still have to be considered: typically, the recovery and hence the accuracy of microdialysis improves when the flow rate is very low. This implies a very low yield of sample volume. For the usual analysis via HPLC-UV this might be a hindrance, since sample preparation becomes more difficult when only small volumes are available. There are two options to resolve this problem: (i) choosing a higher flow rate or (ii) to collect the dialysate over a longer time frame. The first option decreases the accuracy and a correction factor becomes necessary, the second option provides information on the concentration during a sampling frame instead of at a given sampling point, e.g. concentration at $t_8 - t_{12}$ instead of concentration at time t_{10} . This might well be



applicable to extended release formulations, but for instant release formulations such as rapidly dissolving as nanocrystals, this would be a major disadvantage regarding accuracy. All in all, intensive research is still necessary to evaluate microdialysis as analytical tool in dissolution testing of nanosized drug formulations.

The ResoScan system appears not to be suitable for dissolution testing and there does not seem to be a way forward to create a working analytical system meeting the requirements as a fast and reliable analysis of drug content.

The asymmetrical flow field-flow-fractionation is an analytical tool with great potential in analysis of nanosized drugs. During research for this thesis, the question of the particle size after redispersion in the media arose. The question was addressed to Solvay, and even though they were not able to divulge the exact method, it is likely that both Solvay[®] and Elan[®] use a fractionation method to determine the particle size of fenofibrate before and after compaction to tablets. This method might be applied to a new kind of dissolution testing, e.g. measuring the particle size and distribution of fenofibrate at predetermined time points. Although it seems that the AF4 is perhaps not the ideal tool for measuring the concentration in dissolution testing due to factors that influence dissolution, e.g. the crossflow required to create a separation field or the time needed for such an AF4 run, it appears that many other highly interesting questions can be resolved with such a system. The possible fields of applications, just to state a few, are: (i) determination of micellar size when micelles are too small for dynamic light scattering methods, (ii) the investigation of micellar behaviour in dissolution media (e.g. lipid formulations), (iii) investigation of micellar size and



bioavailability in lipid formulations, (iv) monitoring of (pH-dependent) drug precipitation.

The use of centrifugal filter devices should not be excluded due to the results in this study. As seen in the filter adsorption tests of the syringe filter, the adsorption to filter material might be dependent on many factors e.g. temperature and filter material. In a dissolution test using syringe filters, the sample is about 35°C when it is filtered. Using a centrifuge for this purpose cools down the sample considerably, likely inducing precipitation. In addition, presaturation of such a filter is virtually impossible. It would be an interesting approach to repeat the experiments using a heatable centrifuge and to compare the results to those obtained in this study. One would not be surprised if adsorption to the filter material were to decrease, since it is known from other applications, e.g. centrifugation of milk (personal communication, M. Kilic), that temperature can have a crucial influence during centrifugation of drug dissolution samples.

As an analytical “all-purpose-weapon”, this work shows that syringe filters with a pore size of 0.1 μm or 0.02 μm are most suitable of the methods evaluated. 0.1 μm is thereby preferred because not only of the risk of micelle filtration, but the application of smaller filters is very difficult to use practically. Indeed, it takes about 3 minutes to filter less than 5 ml through these filters. It was necessary to develop a sample drawing scheme that allows the analyst to have at least five minutes of time prior to the next sampling. This prolongs a dissolution test of 60 minutes with $n = 3$ to 135 minutes due



to the staggered necessary of sampling. A suitable sample withdrawal scheme can be found in Table 5.1.

*Table 5.1: Sample withdrawal scheme using Anopore filter of 0.02 μm , $n = 3$, * is for sampling point*

Time	Vessel 1	Vessel 2	Vessel 3
0	START		
5	*		
10	*		
15	*		
20			
25			
30	*		
35		START	
40		*	
45		*	
50		*	
55			
60	*		
65		*	
70			START
75			*
80			*
85			*
90			
95		*	
100			*
105			
110			
115			
120			
125			
130			*

From the foregoing discussion it is obvious that there is still a need for better methods to determine the dissolved amount of API in dissolution testing. The ISE may be a way forward, at least for ionizable drugs. Nevertheless, it is questionable if the technology to nanosize API drug particles will be widely applied to drugs for which salt formation is also possible.



The ion-selective electrode is a promising system for samples that are difficult to analyze by conventional filtration and subsequent HPLC-UV methods. It would be highly interesting to have such a system adopted to detect fenofibrate and to compare the results with those obtained by sample filtration. This is unfortunately not possible since the ISE is only applicable to ionizable substances, which is fenofibrate not. As already discussed in section 4.1.7, it is not very likely that a broad number of ionizable substances will be formulated as nanosized drug powder, since salt formation will always be preferred as option to facilitate dissolution of such compounds. But it should be kept in mind that there are already nanosized drugs on market like Aprepitant (Emend[®]), which are at least partially ionizable. In addition, use of the ISE should be investigated for other formulations like melt extrudates, which are also hard to filter in dissolution testing.

With the results of dissolution testing of fenofibrate an *in vitro* – *in silico* – *in vivo* correlation could be achieved using the STELLA[®] software. The most decisive advantage of this simulation program is the minimum of parameters required. As discussed in section 4.3 and 4.4, other simulation programs require a value for the boundary layer h . In spite of the great impact of this value on the results, one is required to make an educated guess. In some cases the outcome is very sensitive to this parameter, as shown by Willmann et al. [112]. In the current work results varied significantly, depending on which of the formulae in Table 4.7 is applied for calculation of h . The STELLA[®] software depends only on experimental results, circumventing the need for an input value for h . The results in dissolution tests in biorelevant media



combined with small filter pore size filtration were able to provide data which resulted in an acceptable *IVVC*.



6 Outlook

The work presented in this thesis suggests several follow-up projects.

6.1 Studies regarding the ISE

The ISE is suitable for the analytics of diphenhydramine HCl in dissolution testing using the biorelevant media FaSSGF, FaSSiF, FaSSiF-V2 and FeSSGF.

It was not possible to measure accurately the amount of dissolved diphenhydramine in FeSSiF and FeSSiF-V2. For these media further studies should be conducted as it is a goal of the ISE to be applicable in every dissolution medium.

The alternative way of endpoint calibration (Method B) broadens the application range of the ISE, potentially encompassing even supersaturated systems of poorly soluble substances. It would be highly interesting to apply this method to formulations which are known to create a supersaturated solution.

6.2 Filter adsorption testing

Refinement of study methods for determining adsorption of drugs to filter membranes would be appropriate. In dissolution testing none of the filters used showed any significant filter adsorption. However, when filtering a clear solution at room temperature, filter adsorption was noticeable. The reasons discussed in section 4.2.1 for the varying results should be evaluated. A future study might investigate differences in filter adsorption from biorelevant media at different temperatures.



6.3 Establishment of an *in vitro* - *in vivo* - correlation for a nanosized drug

When changing from a micronized to a nanosized formulation, the rate determining step for absorption may change from completely dissolution controlled to at least partly permeation controlled in the fasted state. In the fed state, gastric emptying appears to be rate determining for absorption of fenofibrate from both the micronized and the nanosized formulation. The presented STELLA[®] methods should be applied for other purported BCS Class II drugs (preferably also micro- and nanosized as was the case for fenofibrate in this study) to evaluate whether this is a special case or if the findings can be generalized. If they apply across the board, it might be possible to switch the behavior of many more poorly soluble drugs from BCS Class II to Class I by nanosizing.



7 Summary

The oral bioavailability of a drug substance is strongly related to its aqueous solubility. Only complete dissolution during the GI-passage can maintain an optimal bioavailability. Poor aqueous drug solubility results, according to the Nernst-Brunner equation into a slow dissolution rate, sometimes too slow for complete dissolution in the GI tract. The dissolution rate increases with decreasing particle size and therefore increasing surface area of the drug particles. In consequence,, micronization of the drug is applied to increase oral bioavailability, but often meets with modest success. Recently developed techniques were applied to decrease the particle size into the nanometer range. For some substances, pharmacokinetic parameters could be influenced decisively, e.g. the obviation of a food effect for the drugs aprepitant and fenofibrate.

The assessment of a dosage form is investigated by dissolution testing. For a reasonable assessment of such tests, a separation of solid and liquids has to be ensured within an appropriate time frame. For particle sizes of about 150 nm it appears questionable whether such separation can be succeeded by classical techniques, e.g. the use of syringe filters with a pore size of 0.45 μm .

The aims of this thesis were to investigate the suitability of various analytical techniques in analysis of dissolution tests containing nanosized drug substance.



Furthermore, a suitable analytical tool is applied to establish an *in vitro* – *in vivo* correlation of the nanosized drug fenofibrate.

At first, several techniques were investigated in theory to assess their ability to ensure a rapid and complete separation of solids and liquids. The classical dialysis, turbidity measurement and UV-measurement via fiber optics were excluded from further investigation due to various reasons, e.g. the speed of separation for dialysis. The asymmetrical flow field-flow fractionation appeared to be a promising tool, but lack of equipment precluded further investigation.

The ultrasonic resonance technology (ResoScan), the microdialysis and the use of centrifugal filter devices have shown to be inappropriate for the analytics of nanosized drugs in dissolution test. The use of syringe filters with various pore sizes and the ion-selective electrode (ISE) was promising, so these techniques were examined more intensively.

The syringe filters with various filter pore sizes were investigated for their ability to hold back colloidal drug. Fenofibrate was chosen as model drug, since this is commercially available both as micronized and nanosized formulation (Lipidil Ter® and Lipidil 145 ONE®), enabling direct comparison.

The experiments with micronized fenofibrate which contains little or no colloidal fenofibrate yielded similar dissolution profiles, irrespective of filter pore size; f_2 was



always greater than 65, indicating less than 5% difference between the dissolution profiles in any medium.

Using a pore size of 0.1 μm or less, the maximum concentration of drug achieved in solution from the nanosized formulation was commensurate with the saturation solubility of fenofibrate in all tested media. Filtration with a pore size of 0.2 μm or 0.45 μm generated concentrations exceeding the saturation solubility. These results, in combination with higher standard deviations of the analytical results, indicate that the apparent “supersaturation” is caused by colloidal fenofibrate, which is too fine to be held back by these filters. The f_2 -value of less than 50 when comparing the profiles obtained from 0.1 μm and 0.2 μm filter pore size indicates that the choice of filter pore size is crucial to the interpretation of the dissolution profiles. To separate nanosized drug from molecularly dissolved fenofibrate in Lipidil 145 ONE[®], a filter pore size of 0.1 μm or less appears to be appropriate.

It was observed that the experimental increase of dissolution rate is not congruent with common hypothesis regarding the boundary layer h for decreasing particle sizes and subsequent application of the Nernst-Brunner equation.

The initial dissolution rates of both formulations were investigated by using a filter pore size of 0.1 μm . The results were utilized in an *in silico* model (STELLA[®]) to correlate the *in vitro* results with *in vivo* data (Model A). In the preprandial state a good correlation was established for the micronized fenofibrate, while for the nanosized fenofibrate the plasma levels were overpredicted.



The model was expanded to investigate the impact of an absorption step at the intestinal membrane on the *in vitro* – *in vivo* correlation. It was found that even a minor deceleration of absorption results in varied plasma profiles caused by a lagged appearance of drug in the blood.

For both formulations the rate determining step was identified: When changing from the micronized to the nanosized formulation, the rate-determining step for absorption may change from completely dissolution-controlled to at least partly permeation-controlled in the fasted state.

In the fed state, gastric emptying appears to be rate-determining for absorption of fenofibrate from both the micronized and the nanosized formulation.

Another technique appears to be suitable for analysis of nanosized drugs in dissolution testing. The Ion-selective electrode (ISE) is a recently developed analytical system measuring the changes of the electrochemical potential in solutions. A transformation via the Nikolski – Eisenmann equation results into the concentration of the respective drug in solution. Since only dissolved drug is detected, obviating the need for separation of dissolved from undissolved drug, this system appears to be very promising in the analytics of nanocrystalline drugs.

Diphenhydramine_HCl was chosen as model substance for the ISE studies. It was the goal of investigation to test compatibility of the ISE with complex media, e.g. all biorelevant dissolution media. This is done in advance of application of the ISE in these



media for nanocrystalline drug substance. The results were compared to manual sampling, filtration and subsequent HPLC-UV analysis.

The results demonstrate that the ion-selective electrode is suitable for measurements of diphenhydramine HCl in fasted state biorelevant media (FaSSGF, FaSSIF, FaSSIF-V2) as both a stand-alone system (Method A) and in conjunction with a single point conventional assay (Method B). The results acquired are similar to those obtained by manual sampling and subsequent HPLC-UV analysis. The ISE also delivers satisfactory results in a milk-based medium (FeSSGF), in which it has distinct advantages over manual sampling with HPLC-UV analysis by obviating the need for sample preparation. The application of the ISE in FeSSIF type media will need further study.

Finally, as an on-line technology, ISE offers more efficient generation of dissolution profiles than conventional sample-based methods.



In summary it was found:

- The techniques dialysis, microdialysis, turbidity measurement, ultrasonic resonance technology, filtration via centrifugal devices and fiber optics are not suitable for the analytics of nanosized drugs in dissolution testing.
- The ISE is suitable for the analytics of nanosized API in principle. Preliminary results with diphenhydramine show equality to HPLC-UV for FaSSGF, FaSSIF and FaSSIF-V2, and superiority in FeSSGF, while still research is necessary for FeSSIF and FeSSIF-V2.
- An adaption of the methods aims to the application of the in supersaturated solutions.
- Syringe filter with pore sizes of 0.02 μm or 0.1 μm are suitable to hold back colloidal, nanocrystalline fenofibrate from biorelevant media.
- An in vitro – in vivo correlation using the STELLA[®]-Software was established for Lipidil Ter[®] and after modification of the model also for Lipidil 145 ONE[®].
- The rate determining step in the preprandial state for absorption of micronised fenofibrate is dissolution, for nanosized fenofibrate this step is shifted to absorption.



8 Appendix

Table 8.1: Dissolution of Lipidil 145 ONE® in FaSSIF, Centrifugal filter device 100 kDa

Microcon 100kDa	% Release		Conc. [$\mu\text{g/ml}$]	
Time	Mean (n=3) Lipidil ONE 145mg FaSSIF pH 6.5 75 rpm	S.D.	Mean (n=3) Lipidil ONE 145mg FaSSIF pH 6.5 75 rpm	S.D.
5	0.13	0.01	0.38	0.03
10	0.05	0.02	0.14	0.04
15	0.03	0.01	0.08	0.02
30	0.01	0.01	0.02	0.01
60	0.03	0.02	0.08	0.05

Table 8.2: Dissolution of Lipidil Ter® in FaSSIF, Centrifugal filter device 100 kDa

Microcon 100 kDa	% Release		Conc. [$\mu\text{g/ml}$]	
Time	Mean (n=3) Lipidil Ter 160 mg FaSSIF pH 6.5 75 rpm	S.D.	Mean (n=3) Lipidil Ter 160mg FaSSIF pH 6.5 75 rpm	S.D.
5	0.17	0.03	0.55	0.08
10	0.11	0.03	0.34	0.08
15	0.09	0.02	0.28	0.05
30	0.06	0.06	0.32	n.a.
60	0.11	0.00	0.37	0.01

Table 8.3: Dissolution of Lipidil 145 ONE® in FeSSIF, Centrifugal filter device 100 kDa

Microcon 100kDa	% Release		Conc. [$\mu\text{g/ml}$]	
Time	Mean (n=3) Lipidil ONE 145mg FeSSIF pH 5.0 75 rpm	S.D.	Mean (n=3) Lipidil ONE 145mg FeSSIF pH 5.0 75 rpm	S.D.
5	10.85	0.61	31.47	1.77
10	10.35	0.38	30.03	1.09
15	11.48	0.34	33.30	0.99
30	12.15	0.20	35.53	0.40
60	12.11	0.45	35.11	1.32



Table 8.4: Dissolution of Lipidil Ter® in FeSSIF, Centrifugal filter device 100 kDa

Microcon 100kDa	% Release		Conc. [$\mu\text{g/ml}$]	
Time	Mean (n=3) Lipidil Ter 160 mg FeSSIF pH 5.0 75 rpm	S.D.	Mean (n=3) Lipidil Ter 160 mg FeSSIF pH 5.0 75 rpm	S.D.
5	4.65	0.39	14.87	1.24
10	7.56	0.37	24.21	1.19
15	8.70	0.23	27.84	0.74
30	9.22	0.43	30.31	0.26
60	8.71	0.14	27.88	0.46

Table 8.5: Comparison of filter adsorption of Lipidil Ter® in FaSSIF, 0.2 μm RC compared to centrifugal filter device 100 kDa

FaSSIF	Lipidil Ter filtrated through 0.2 μm RC		Lipidil Ter filtrated through Microcon 100kDa	
	% Release	Conc. [$\mu\text{g/ml}$]	% Release	Conc. [$\mu\text{g/ml}$]
	Lipidil Ter 160 mg	Lipidil Ter 160 mg	Lipidil Ter 160 mg	Lipidil Ter 160 mg
A	3.97	12.71	0.04	0.14
B	4.03	12.89	0.05	0.16
C	4.05	12.95	2.38*	7.62*
Mean	4.02	12.85	0.82	2.64
s.d	0.04	0.12	1.35	4.31

*more liquid was found in Eppendorf-vial than in other experiments, indicating a damaged filter membrane

Table 8.6: Comparison of filter adsorption of Lipidil Ter® in FeSSIF, 0.2 μm RC compared to centrifugal filter device 100 kDa

FeSSIF	Lipidil Ter filtrated through 0.2 μm RC		Lipidil Ter filtrated through Microcon 100kDa	
	% Release	Conc. [$\mu\text{g/ml}$]	% Release	Conc. [$\mu\text{g/ml}$]
	Lipidil Ter 160 mg	Lipidil Ter 160 mg	Lipidil Ter 160 mg	Lipidil Ter 160 mg
A	8.16	26.12	6.27	20.07
B	8.09	25.87	6.08	19.45
C	8.52	27.28	6.64	21.24
Mean	8.26	26.42	6.33	20.25
s.d	0.23	0.75	0.28	0.91



Table 8.7: Filteradsorption from clear FaSSGF - solution with various filter

Filteradsorption	FaSSGF Unfiltered	0.02 µm Anopore	0.1µm Anopore	0.2µm RC	0.45µm PTFE
Mean %	100.00	4.55	40.33	21.66	20.32
s.d.	9.65	11.57	4.28	10.25	8.45

Table 8.8: Filteradsorption from clear FaSSIF - solution with various filters

Filteradsorption	FaSSIF Unfiltered	0.02 µm Anopore	0.1µm Anopore	0.2µm RC	0.45µm PTFE
Mean %	100.00	81.92	-	98.66	101.94
s.d.	9.65	4.25	-	8.38	3.73

Table 8.9: Filteradsorption from clear FaSSIF-V2 – solution with various filters

Filteradsorption	FaSSIF Unfiltered	0.02 µm Anopore	0.1µm Anopore	0.2µm RC	0.45µm PTFE
Mean %	100.00	82.6	94.92	81.81	94.43
s.d.	9.65	15.11	4.58	4.88	6.14

Table 8.10: Filteradsorption from clear FeSSIF – solution with various filters

Filteradsorption	FaSSIF Unfiltered	0.02 µm Anopore	0.1µm Anopore	0.2µm RC	0.45µm PTFE
Mean %	100.00	98.08	100.14	94.04	99.54
s.d.	0.58	0.85	1.22	0.27	1.05

Table 8.11: Filteradsorption from clear FeSSIF-V2 – solution with various filters

Filteradsorption	FaSSIF Unfiltered	0.02 µm Anopore	0.1µm Anopore	0.2µm RC	0.45µm PTFE
Mean %	100.00	72.49	76.63	68.79	76.50
s.d.	4.18	0.35	0.42	0.87	0.34



Table 8.12: Dissolution of Lipidil 145 ONE® in FaSSIF, 0.02 µm Anopore

Anopore 0.02	% Release		Conc. [µg/ml]	
Time	Mean (n=3) Lipidil ONE 145mg FaSSIF pH 6.5 75 rpm	S.D.	Mean (n=3) Lipidil ONE 145mg FaSSIF pH 6.5 75 rpm	S.D.
5	4.40	0.24	12.76	0.71
10	3.18	0.41	9.22	1.20
15	3.60	0.22	10.44	0.63
30	3.64	0.27	10.64	1.09
60	3.84	n.a	11.14	n.a.

Table 8.13: Dissolution of Lipidil 145 ONE® in FaSSIF, 0.1 µm Anopore

Anopore 0.1	% Release		Conc. [µg/ml]	
Time	Mean (n=3) Lipidil ONE 145mg FaSSIF pH 6.5 75 rpm	S.D.	Mean (n=3) Lipidil ONE 145mg FaSSIF pH 6.5 75 rpm	S.D.
5	3.89	0.24	11.27	0.69
10	3.12	0.27	9.06	0.79
15	4.65	0.25	13.49	0.72
30	4.65	n.a.	13.49	n.a.
60	4.78	0.52	13.85	1.50

Table 8.14: Dissolution of Lipidil 145 ONE® in FaSSIF, 0.2 µm RC

RC 0.2	% Release		Conc. [µg/ml]	
time	Mean (n=3) Lipidil ONE 145mg FaSSIF pH 6.5 75 rpm	S.D.	Mean (n=3) Lipidil ONE 145mg FaSSIF pH 6.5 75 rpm	S.D.
5	8.28	0.43	24.01	1.24
10	10.66	0.89	30.92	2.57
15	8.82	1.66	25.58	4.80
30	10.39	2.72	33.88	6.40
60	8.70	3.78	25.22	10.96



Table 8.15: Dissolution of Lipidil 145 ONE® in FaSSIF, 0.45 µm RC

PTFE 0.45	% Release		Conc. [µg/ml]	
time	Mean (n=3) Lipidil ONE 145mg FaSSIF pH 6.5 75 rpm	S.D.	Mean (n=3) Lipidil ONE 145mg FaSSIF pH 6.5 75 rpm	S.D.
5	3.37	1.13	9.76	3.28
10	6.77	1.56	19.62	4.52
15	7.41	0.84	21.50	2.43
30	7.72	0.86	23.41	2.51
60	8.61	1.33	24.96	3.86

Table 8.16: Dissolution of Lipidil Ter® in FaSSIF, 0.02 µm Anopore

Anopore 0.02	% Release		Conc. [µg/ml]	
time	Mean (n=3) Lipidil Ter 160 mg FaSSIF pH 6.5 75 rpm	S.D.	Mean (n=3) Lipidil Ter 160mg FaSSIF pH 6.5 75 rpm	S.D.
5	0.97	0.31	3.12	0.98
10	2.88	0.22	9.21	0.70
15	3.82	0.15	12.23	0.49
30	4.03	0.09	12.81	0.36
60	4.04	0.14	12.93	0.45

Table 8.17: Dissolution of Lipidil Ter® in FaSSIF, 0.1 µm Anopore

Anopore 0.1	% Release		Conc. [µg/ml]	
time	Mean (n=3) Lipidil Ter 160 mg FaSSIF pH 6.5 75 rpm	S.D.	Mean (n=3) Lipidil Ter 160mg FaSSIF pH 6.5 75 rpm	S.D.
5	0.67	0.29	2.16	0.93
10	2.08	0.08	6.65	0.24
15	2.92	0.10	9.34	0.32
30	3.25	0.10	10.54	0.28
60	3.21	0.05	10.29	0.17



Table 8.18: Dissolution of Lipidil Ter® in FaSSIF, 0.2 µm RC

RC 0.2	% Release		Conc. [µg/ml]	
time	Mean (n=3) Lipidil Ter 160 mg FaSSIF pH 6.5 75 rpm	S.D.	Mean (n=3) Lipidil Ter 160mg FaSSIF pH 6.5 75 rpm	S.D.
5	0.55	0.02	1.76	0.06
10	2.12	0.26	6.77	0.82
15	3.30	0.10	10.56	0.32
30	4.08	0.00	13.05	0.02
60	4.24	0.19	13.56	0.60

Table 8.19: Dissolution of Lipidil Ter® in FaSSIF, 0.45 µm Anopore

PTFE 0.45	% Release		Conc. [µg/ml]	
time	Mean (n=3) Lipidil Ter 160 mg FaSSIF pH 6.5 75 rpm	S.D.	Mean (n=3) Lipidil Ter 160mg FaSSIF pH 6.5 75 rpm	S.D.
5	0.60	0.02	1.91	0.06
10	1.59	0.15	5.10	0.49
15	2.50	0.30	8.00	0.95
30	3.33	0.12	10.59	0.53
60	2.89	0.07	9.25	0.21

Table 8.20: Dissolution of Lipidil 145 ONE® in FeSSIF, 0.02 µm Anopore

Anopore 0.02	% Release		Conc. [µg/ml]	
time	Mean (n=3) Lipidil ONE 145mg FeSSIF pH 5.0 75 rpm	S.D.	Mean (n=3) Lipidil ONE 145mg FeSSIF pH 5.0 75 rpm	S.D.
5	14.35	0.53	41.62	1.54
10	15.26	0.34	44.24	0.99
15	14.32	0.39	41.53	1.13
30	12.64	0.21	36.65	0.60
60	12.44	0.28	36.08	0.80

Table 8.21: Dissolution of Lipidil 145 ONE® in FeSSIF, 0.1 µm Anopore

Anopore 0.1	% Release		Conc. [µg/ml]	
time	Mean (n=3) Lipidil ONE 145mg FeSSIF pH 5.0 75 rpm	S.D.	Mean (n=3) Lipidil ONE 145mg FeSSIF pH 5.0 75 rpm	S.D.
5	15.05	0.43	43.64	1.25
10	14.94	0.26	43.33	0.75
15	13.86	0.19	40.20	0.54
30	13.54	1.01	39.26	2.92
60	13.36	0.64	38.73	1.87



Table 8.22: Dissolution of Lipidil 145 ONE® in FeSSIF, 0.2 µm RC

RC 0.2	% Release		Conc. [µg/ml]	
time	Mean (n=3) Lipidil ONE 145mg FeSSIF pH 5.0 75 rpm	S.D.	Mean (n=3) Lipidil ONE 145mg FeSSIF pH 5.0 75 rpm	S.D.
5	18.07	0.58	52.41	1.68
10	24.48	2.48	70.99	7.20
15	21.25	1.61	61.62	4.67
30	14.58	0.59	42.29	1.71
60	16.17	0.66	46.89	1.92

Table 8.23: Dissolution of Lipidil 145 ONE® in FeSSIF, 0.45 µm RC

PTFE 0.45	% Release		Conc. [µg/ml]	
time	Mean (n=3) Lipidil ONE 145mg FeSSIF pH 5.0 75 rpm	S.D.	Mean (n=3) Lipidil ONE 145mg FeSSIF pH 5.0 75 rpm	S.D.
5	15.64	3.31	45.34	9.60
10	22.25	1.03	64.53	2.99
15	18.95	2.43	54.96	7.04
30	15.97	0.38	46.31	1.11
60	14.87	1.58	43.11	4.58

Table 8.24: Dissolution of Lipidil Ter® in FeSSIF, 0.02 µm Anopore

Anopore 0.02	% Release		Conc. [µg/ml]	
time	Mean (n=3) Lipidil Ter 160 mg FeSSIF pH 5.0 75 rpm	S.D.	Mean (n=3) Lipidil Ter 160 mg FeSSIF pH 5.0 75 rpm	S.D.
5	3.23	0.47	10.35	1.49
10	8.91	0.22	28.51	0.70
15	11.04	0.37	35.33	1.20
30	10.95	0.17	34.72	0.16
60	10.88	0.32	34.82	1.04

Table 8.25: Dissolution of Lipidil Ter® in FeSSIF, 0.1 µm Anopore

Anopore 0.1	% Release		Conc. [µg/ml]	
time	Mean (n=3) Lipidil Ter 160 mg FeSSIF pH 5.0 75 rpm	S.D.	Mean (n=3) Lipidil Ter 160 mg FeSSIF pH 5.0 75 rpm	S.D.
5	3.15	0.15	10.07	0.47
10	9.07	0.49	29.02	1.57
15	11.39	0.14	36.46	0.45
30	11.33	0.08	36.40	0.06
60	11.32	0.44	36.21	1.40



Table 8.26: Dissolution of Lipidil Ter® in FeSSIF, 0.2 µm RC

RC 0.2	% Release		Conc. [µg/ml]	
time	Mean (n=3) Lipidil Ter 160 mg FeSSIF pH 5.0 75 rpm	S.D.	Mean (n=3) Lipidil Ter 160 mg FeSSIF pH 5.0 75 rpm	S.D.
5	2.45	0.70	7.85	2.24
10	8.00	0.93	25.61	2.98
15	10.25	0.32	32.79	1.02
30	10.81	0.14	34.81	0.28
60	10.77	0.36	34.45	1.14

Table 8.27: Dissolution of Lipidil Ter® in FeSSIF, 0.45 µm PTFE

PTFE 0.45	% Release		Conc. [µg/ml]	
time	Mean (n=3) Lipidil Ter 160 mg FeSSIF pH 5.0 75 rpm	S.D.	Mean (n=3) Lipidil Ter 160 mg FeSSIF pH 5.0 75 rpm	S.D.
5	2.94	0.14	9.41	0.46
10	8.58	0.36	27.45	1.16
15	11.16	0.20	35.70	0.63
30	11.33	0.09	36.43	0.05
60	11.78	0.41	37.69	1.30

Table 8.28: Dissolution of Lipidil 145 ONE® in FaSSIF – V2, 0.1 µm Anopore

Anopore 0.1	% Release		Conc. [µg/ml]	
time	Mean (n=3) Lipidil ONE 145mg FaSSIF- V2 pH 6.5 75 rpm	S.D.	Mean (n=3) Lipidil ONE 145mg FaSSIF- V2 pH 6.5 75 rpm	S.D.
5	1.91	0.04	5.55	0.12
10	1.63	0.08	4.73	0.22
15	1.52	0.13	4.42	0.37
30	1.46	0.01	4.23	0.03
60	1.44	0.05	4.17	0.14

Table 8.29: Dissolution of Lipidil 145 ONE® in FaSSIF – V2, 0.2 µm RC

RC 0.2	% Release		Conc. [µg/ml]	
time	Mean (n=3) Lipidil ONE 145mg FaSSIF- V2 pH 6.5 75 rpm	S.D.	Mean (n=3) Lipidil ONE 145mg FaSSIF- V2 pH 6.5 75 rpm	S.D.
5	3.86	0.74	11.21	2.14
10	4.64	2.17	13.46	6.28
15	2.71	0.78	7.87	2.25
30	2.71	1.63	7.86	5.76
60	2.46	0.44	7.14	1.26

Table 8.30: Dissolution of Lipidil Ter® in FaSSIF – V2, 0.1 µm Anopore

Anopore 0.1	% Release		Conc. [µg/ml]	
time	Mean (n=3) Lipidil ONE 145mg FaSSIF-V2 pH 6.5 75 rpm	S.D.	Mean (n=3) Lipidil ONE 145mg FaSSIF-V2 pH 6.5 75 rpm	S.D.
5	0.87	0.04	2.77	0.12
10	1.28	0.07	4.08	0.21
15	1.35	0.08	4.31	0.26
30	1.33	0.06	4.37	0.01
60	1.35	0.04	4.31	0.11

Table 8.31: Dissolution of Lipidil Ter® in FaSSIF – V2, 0.2 µm RC

RC 0.2	% Release		Conc. [µg/ml]	
time	Mean (n=3) Lipidil ONE 145mg FaSSIF-V2 pH 6.5 75 rpm	S.D.	Mean (n=3) Lipidil ONE 145mg FaSSIF-V2 pH 6.5 75 rpm	S.D.
5	1.21	0.08	3.87	0.25
10	1.63	0.02	5.23	0.05
15	1.71	0.06	5.49	0.18
30	1.68	0.04	5.38	0.12
60	1.62	0.07	5.18	0.23

Table 8.32: Dissolution of Lipidil 145 ONE® in FeSSIF – V2, 0.1 µm Anopore

Anopore 0.1	% Release		Conc. [µg/ml]	
time	Mean (n=3) Lipidil ONE 145mg FeSSIF- V2 pH 5.8 75 rpm	S.D.	Mean (n=3) Lipidil ONE 145mg FeSSIF- V2 pH 5.8 75 rpm	S.D.
5	25.14	1.70	72.92	4.94
10	26.39	1.05	76.53	3.05
15	25.02	0.51	72.55	1.48
30	24.40	2.26	66.38	0.20
60	21.82	0.60	63.28	1.74



Table 8.33: Dissolution of Lipidil 145 ONE® in FeSSIF – V2, 0.2 µm RC

RC 0.2	% Release		Conc. [µg/ml]	
time	Mean (n=3) Lipidil ONE 145mg FeSSIF- V2 pH 5.8 75 rpm	S.D.	Mean (n=3) Lipidil ONE 145mg FeSSIF- V2 pH 5.8 75 rpm	S.D.
5	20.49	3.55	59.43	10.31
10	26.41	8.42	76.59	24.41
15	27.76	1.83	80.51	5.31
30	25.17	1.00	73.00	2.64
60	23.62	1.08	68.49	3.13

Table 8.34: Dissolution of Lipidil Ter® in FeSSIF – V2, 0.1µm Anopore

Anopore 0.1	% Release		Conc. [µg/ml]	
time	Mean (n=3) Lipidil ONE 145mg FeSSIF-V2 pH 5.8 75 rpm	S.D.	Mean (n=3) Lipidil ONE 145mg FeSSIF-V2 pH 5.8 75 rpm	S.D.
5	4.82	0.33	15.44	1.05
10	16.01	0.73	51.24	2.33
15	21.48	0.30	68.74	0.95
30	23.43	0.55	74.98	1.75
60	23.18	0.27	74.18	0.87

Table 8.35: Dissolution of Lipidil Ter® in FeSSIF – V2, 0.2 µm RC

RC 0.2	% Release		Conc. [µg/ml]	
time	Mean (n=3) Lipidil ONE 145mg FeSSIF-V2 pH 5.8 75 rpm	S.D.	Mean (n=3) Lipidil ONE 145mg FeSSIF-V2 pH 5.8 75 rpm	S.D.
5	4.33	0.93	13.85	2.97
10	14.88	0.88	47.63	2.82
15	19.53	0.38	62.49	1.20
30	20.53	0.14	65.68	0.46
60	20.26	0.41	64.84	1.30



Table 8.36: Initial Dissolution of Lipidil 145 ONE® in FaSSGF, 0.1 µm Anopore

Anopore 0.1µm	% Release		Conc. [µg/ml]	
time	Mean (n=3) Lipidil ONE 145mg FaSSGF pH 1.6 75 rpm	S.D.	Mean (n=3) Lipidil ONE 145mg FaSSGF pH 1.6 75 rpm	S.D.
1	0.08	0.01	0.23	0.04
2	0.22	0.04	0.63	0.12
3	0.34	0.05	0.97	0.15
4	0.21	0.08	0.61	0.22
5	0.21	0.03	0.60	0.10
10	0.18	0.00	0.52	0.01
15	0.18	0.01	0.53	0.03

Table 8.37: Initial Dissolution of Lipidil Ter® in FaSSGF, 0.2 µm RC

RC 0.2µm	% Release		Conc. [µg/ml]	
time	Mean (n=3) Lipidil Ter 160mg FaSSGF pH 1.6 75 rpm	S.D.	Mean (n=3) Lipidil ONE 145mg FaSSGF pH 1.6 75 rpm	S.D.
1	0.16	0.11	0.35	0.56
2	0.43	0.29	0.72	1.11
3	0.66	0.45	1.07	1.67
4	0.41	0.28	1.43	2.67
5	0.40	0.28	1.71	2.85
10	0.35	0.24	3.34	5.77
15	0.36	0.25	5.01	8.65

Table 8.38: Initial Dissolution of Lipidil 145 ONE® in FaSSIF - V2, 0.1 µm Anopore

Anopore 0.1µm	% Release		Conc. [µg/ml]	
time	Mean (n=3) Lipidil ONE 145mg FaSSIF V2 pH 6.5 75 rpm	S.D.	Mean (n=3) Lipidil ONE 145mg blankFaSSIF V2 pH 6.5 75 rpm	S.D.
1	0.75	0.15	2.18	0.44
2	1.55	0.18	4.51	0.53
3	1.97	0.02	5.71	0.06
4	1.90	0.05	5.51	0.05
5	1.85	0.07	5.38	0.21

Table 8.39: Initial Dissolution of Lipidil Ter® in FaSSIF - V2 0.2 µm RC

RC 0.2µm	% Release		Conc. [µg/ml]	
time	Mean (n=3) Lipidil ONE 145mg blankFaSSIF V2 pH 6.5 75 rpm	S.D.	Mean (n=3) Lipidil ONE 145mg blankFaSSIF V2 pH 6.5 75 rpm	S.D.
1	0.33	0.19	0.97	0.54
2	1.40	0.55	4.07	1.60
3	2.60	0.40	7.54	1.17
4	3.51	0.65	10.18	1.21
5	3.27	0.73	9.49	2.11

Table 8.40: Initial Dissolution of Lipidil 145 ONE® in FeSSIF - V2, 0.1 µm Anopore

Anopore 0.1µm	% Release		Conc. [µg/ml]	
time	Mean (n=3) Lipidil ONE 145mg FeSSIF V2 pH 5.8 75 rpm	S.D.	Mean (n=3) Lipidil ONE 145mg FeSSIF V2 pH 5.8 75 rpm	S.D.
1	0.50	0.41	1.46	1.20
2	5.25	1.66	15.24	4.82
3	11.30	3.63	32.78	10.54
4	17.26	4.35	50.06	16.05
5	22.57	3.77	65.46	10.94

Table 8.41: Initial Dissolution of Lipidil Ter® in FeSSIF - V2, 0.2 µm RC

RC 0.2µm	% Release		Conc. [µg/ml]	
time	Mean (n=3) Lipidil ONE 145mg FeSSIF V2 pH 5.8 75 rpm	S.D.	Mean (n=3) Lipidil ONE 145mg FeSSIF V2 pH 5.8 75 rpm	S.D.
1	0.62	0.34	1.80	0.99
2	4.37	3.11	12.68	9.03
3	10.69	7.31	31.01	21.18
4	16.79	9.29	48.69	35.28
5	21.05	7.97	61.03	23.11



```
□ dissolved_stom(t) = dissolved_stom(t - dt) + (dissolution_stom - liquid_emptying) * dt
INIT dissolved_stom = 0
INFLOWS:
  ☞ dissolution_stom = IF (Dose)>0 AND ((dissolved_stom)/(vfluid))<0.000976 THEN(0.736333518
    *500*1*((Dose)^(2/3))*(0.000976-((dissolved_stom)/(vfluid)))) ELSE(0)
OUTFLOWS:
  ☞ liquid_emptying = IF(dissolved_stom)>0 AND(vfluid)>0 THEN(dissolved_stom)*2.8 ELSE(0)
□ Dose(t) = Dose(t - dt) + (- dissolution_stom - solid_emptying) * dt
INIT Dose = 128.094
OUTFLOWS:
  ☞ dissolution_stom = IF (Dose)>0 AND ((dissolved_stom)/(vfluid))<0.000976 THEN(0.736333518
    *500*1*((Dose)^(2/3))*(0.000976-((dissolved_stom)/(vfluid)))) ELSE(0)
  ☞ solid_emptying = IF(Dose)>0 AND(vfluid)>0 THEN(Dose)*2.8 ELSE(0)
□ perip(t) = perip(t - dt) + (k12 - k21) * dt
INIT perip = 0
INFLOWS:
  ☞ k12 = plasma*0.290364
OUTFLOWS:
  ☞ k21 = perip*0.194355
□ plasma(t) = plasma(t - dt) + (k21 + dissolution_intestine_z_2_208998 + liquid_emptying - k12 - k10) * dt
INIT plasma = 0
INFLOWS:
  ☞ k21 = perip*0.194355
  ☞ dissolution_intestine_z_2_208998 = IF(solid_intestine)>0
    THEN(2.20899811*2.856666667*1*(solid_intestine)^(2/3)) ELSE(0)
  ☞ liquid_emptying = IF(dissolved_stom)>0 AND(vfluid)>0 THEN(dissolved_stom)*2.8 ELSE(0)
OUTFLOWS:
  ☞ k12 = plasma*0.290364
  ☞ k10 = plasma*0.144507
□ solid_intestine(t) = solid_intestine(t - dt) + (solid_emptying - dissolution_intestine_z_2_208998) * dt
INIT solid_intestine = 0
INFLOWS:
  ☞ solid_emptying = IF(Dose)>0 AND(vfluid)>0 THEN(Dose)*2.8 ELSE(0)
OUTFLOWS:
  ☞ dissolution_intestine_z_2_208998 = IF(solid_intestine)>0
    THEN(2.20899811*2.856666667*1*(solid_intestine)^(2/3)) ELSE(0)
□ vfluid(t) = vfluid(t - dt) + (- vfge) * dt
INIT vfluid = 240
OUTFLOWS:
  ☞ vfge = IF(vfluid)>0 THEN(vfluid)*2.8 ELSE(0)
○ plascon = 1000*plasma/vcf
○ vcf = 7802.094472
```

Figure 8.1: Equation Set STELLA[®] for Lipidil 145 ONE[®], fasted state, Model A



```
□ dissolved_stom(t) = dissolved_stom(t - dt) + (dissolution_stom - liquid_emptying) * dt
  INIT dissolved_stom = 0
  INFLOWS:
    -> dissolution_stom = IF (Dose)>0 AND ((dissolved_stom)/(vfluid))<0.000976 THEN(0.736333518
      *500*1*((Dose)^(2/3))*(0.000976-((dissolved_stom)/(vfluid)))) ELSE(0)
  OUTFLOWS:
    -> liquid_emptying = IF(dissolved_stom)>0 AND(vfluid)>0 THEN(dissolved_stom)*2.8 ELSE(0)
□ Dose(t) = Dose(t - dt) + (- dissolution_stom - solid_emptying) * dt
  INIT Dose = 128.094
  OUTFLOWS:
    -> dissolution_stom = IF (Dose)>0 AND ((dissolved_stom)/(vfluid))<0.000976 THEN(0.736333518
      *500*1*((Dose)^(2/3))*(0.000976-((dissolved_stom)/(vfluid)))) ELSE(0)
    -> solid_emptying = IF(Dose)>0 AND(vfluid)>0 THEN(Dose)*2.8 ELSE(0)
□ GI_Lumen(t) = GI_Lumen(t - dt) + (liquid_emptying + dissolution_intestine_z_2_208998 - Absorption) * dt
  INIT GI_Lumen = 0

  INFLOWS:
    -> liquid_emptying = IF(dissolved_stom)>0 AND(vfluid)>0 THEN(dissolved_stom)*2.8 ELSE(0)
    -> dissolution_intestine_z_2_208998 = IF(solid_intestine)>0
      THEN(2.20899811*2.856666667*1*(solid_intestine)^(2/3)) ELSE(0)
  OUTFLOWS:
    -> Absorption = GI_Lumen
□ perip(t) = perip(t - dt) + (k12 - k21) * dt
  INIT perip = 0
  INFLOWS:
    -> k12 = plasma*0.290364
  OUTFLOWS:
    -> k21 = perip*0.194355
□ plasma(t) = plasma(t - dt) + (k21 + Absorption - k12 - k10) * dt
  INIT plasma = 0
  INFLOWS:
    -> k21 = perip*0.194355
    -> Absorption = GI_Lumen
  OUTFLOWS:
    -> k12 = plasma*0.290364
    -> k10 = plasma*0.144507
□ solid_intestine(t) = solid_intestine(t - dt) + (solid_emptying - dissolution_intestine_z_2_208998) * dt
  INIT solid_intestine = 0
  INFLOWS:
    -> solid_emptying = IF(Dose)>0 AND(vfluid)>0 THEN(Dose)*2.8 ELSE(0)
  OUTFLOWS:
    -> dissolution_intestine_z_2_208998 = IF(solid_intestine)>0
      THEN(2.20899811*2.856666667*1*(solid_intestine)^(2/3)) ELSE(0)
□ vfluid(t) = vfluid(t - dt) + (- vfge) * dt
  INIT vfluid = 240
  OUTFLOWS:
    -> vfge = IF(vfluid)>0 THEN(vfluid)*2.8 ELSE(0)
○ plascon = 1000*plasma/vcf
○ vcf = 7802.094472
```

Figure 8.2: Equation Set STELLA[®] for Lipidil 145 ONE[®], fasted state, Model B



```
liqstom(t) = liqstom(t - dt) + (disstom - gsl) * dt
INIT liqstom = 0
INFLOWS:
  disstom = IF (stomtablet)>0 AND ((liqstom)/(vfluid))<0.003113333THEN(0.7
    *500*1*((stomtablet)^(2/3))*(0.003113333-((liqstom)/(vfluid)))) ELSE(0)
OUTFLOWS:
  gsl = IF(liqstom)>0 AND(vfluid)>0 THEN(liqstom)*2.8 ELSE(0)
perip(t) = perip(t - dt) + (k12 - k21) * dt
INIT perip = 0
INFLOWS:
  k12 = plasma*0.151728
OUTFLOWS:
  k21 = perip*0.130123
plasma(t) = plasma(t - dt) + (k21 + Dissolution_with__z_0_3483821 + gsl - k12 - k10) * dt
INIT plasma = 0
INFLOWS:
  k21 = perip*0.130123
  Dissolution_with__z_0_3483821 = IF(si)>0 THEN(0.348382084*2.753333333*1*(si)^(2/3))
    ELSE(0)
  gsl = IF(liqstom)>0 AND(vfluid)>0 THEN(liqstom)*2.8 ELSE(0)
OUTFLOWS:
  k12 = plasma*0.151728
  k10 = plasma*0.053687
si(t) = si(t - dt) + (gss - Dissolution_with__z_0_3483821) * dt
INIT si = 0
INFLOWS:
  gss = IF(stomtablet)>0 AND(vfluid)>0 THEN(stomtablet)*2.8 ELSE(0)
OUTFLOWS:
  Dissolution_with__z_0_3483821 = IF(si)>0 THEN(0.348382084*2.753333333*1*(si)^(2/3))
    ELSE(0)
stomtablet(t) = stomtablet(t - dt) + (- disstom - gss) * dt
INIT stomtablet = 141.345
OUTFLOWS:
  disstom = IF (stomtablet)>0 AND ((liqstom)/(vfluid))<0.003113333THEN(0.7
    *500*1*((stomtablet)^(2/3))*(0.003113333-((liqstom)/(vfluid)))) ELSE(0)
  gss = IF(stomtablet)>0 AND(vfluid)>0 THEN(stomtablet)*2.8 ELSE(0)
vfluid(t) = vfluid(t - dt) + (- vfge) * dt
INIT vfluid = 240
OUTFLOWS:
  vfge = IF(vfluid)>0 THEN(vfluid)*2.8 ELSE(0)
plascon = 1000*plasma/vcf
vcf = 26610.418737
```

Figure 8.3: Equation Set STELLA[®] for Lipidil Ter[®], fasted state, Model A



- $GI_Lumen(t) = GI_Lumen(t - dt) + (Dissolution_with_z_0_3483821 + gsl - Absorption) * dt$
INIT $GI_Lumen = 0$
INFLOWS:
 - ☞ $Dissolution_with_z_0_3483821 = IF(si) > 0 THEN(0.348382084 * 2.753333333 * 1 * (si)^{(2/3)})$
ELSE(0)
 - ☞ $gsl = IF(liqstom) > 0 AND(vfluid) > 0 THEN(liqstom)^{2.8} ELSE(0)$OUTFLOWS:
 - ☞ $Absorption = GI_Lumen$
- $liqstom(t) = liqstom(t - dt) + (disstom - gsl) * dt$
INIT $liqstom = 0$
INFLOWS:
 - ☞ $disstom = IF(stomtablet) > 0 AND ((liqstom)/(vfluid)) < 0.003113333 THEN(2.105138163 * 500 * 1 * ((stomtablet)^{(2/3)}) * (0.003113333 - ((liqstom)/(vfluid)))) ELSE(0)$OUTFLOWS:
 - ☞ $gsl = IF(liqstom) > 0 AND(vfluid) > 0 THEN(liqstom)^{2.8} ELSE(0)$
- $perip(t) = perip(t - dt) + (k12 - k21) * dt$
INIT $perip = 0$
INFLOWS:
 - ☞ $k12 = plasma * 0.151728$OUTFLOWS:
 - ☞ $k21 = perip * 0.130123$
- $plasma(t) = plasma(t - dt) + (k21 + Absorption - k12 - k10) * dt$
INIT $plasma = 0$
INFLOWS:
 - ☞ $k21 = perip * 0.130123$
 - ☞ $Absorption = GI_Lumen$OUTFLOWS:
 - ☞ $k12 = plasma * 0.151728$
 - ☞ $k10 = plasma * 0.053687$
- $si(t) = si(t - dt) + (gss - Dissolution_with_z_0_3483821) * dt$
INIT $si = 0$
INFLOWS:
 - ☞ $gss = IF(stomtablet) > 0 AND(vfluid) > 0 THEN(stomtablet)^{2.8} ELSE(0)$OUTFLOWS:
 - ☞ $Dissolution_with_z_0_3483821 = IF(si) > 0 THEN(0.348382084 * 2.753333333 * 1 * (si)^{(2/3)})$
ELSE(0)
- $stomtablet(t) = stomtablet(t - dt) + (-disstom - gss) * dt$
INIT $stomtablet = 141.345$
OUTFLOWS:
 - ☞ $disstom = IF(stomtablet) > 0 AND ((liqstom)/(vfluid)) < 0.003113333 THEN(2.105138163 * 500 * 1 * ((stomtablet)^{(2/3)}) * (0.003113333 - ((liqstom)/(vfluid)))) ELSE(0)$
 - ☞ $gss = IF(stomtablet) > 0 AND(vfluid) > 0 THEN(stomtablet)^{2.8} ELSE(0)$
- $vfluid(t) = vfluid(t - dt) + (-vfge) * dt$
INIT $vfluid = 240$
OUTFLOWS:
 - ☞ $vfge = IF(vfluid) > 0 THEN(vfluid)^{2.8} ELSE(0)$
- $plascon = 1000 * plasma / vcf$
- $vcf = 26610.418737$

Figure 8.4: Equation Set STELLA[®] for Lipidil Ter[®], fasted state, Model B



- $liqstom(t) = liqstom(t - dt) + (disstom - gsl) * dt$
INIT $liqstom = 0$
INFLOWS:
 - ☞ $disstom = IF ((liqstom)/(vfluid)) < 0.14749 AND (vfluid) > 0 and (time) > 0 THEN (0.0542 * 500 * 1 * ((stomtablet)^{(2/3)}) * (0.14749 - ((liqstom)/(vfluid)))) ELSE (0)$OUTFLOWS:
 - ☞ $gsl = IF (liqstom) > 0 AND (vfluid) > 0 and (time) > 0 THEN (liqstom) * 177.8 / vfluid ELSE (0)$
- $perip(t) = perip(t - dt) + (k12 - k21) * dt$
INIT $perip = 0$
INFLOWS:
 - ☞ $k12 = plasma * 0.065608$OUTFLOWS:
 - ☞ $k21 = perip * 0.084826$
- $plasma(t) = plasma(t - dt) + (gsl + di + k21 - k12 - k10) * dt$
INIT $plasma = 0$
INFLOWS:
 - ☞ $gsl = IF (liqstom) > 0 AND (vfluid) > 0 and (time) > 0 THEN (liqstom) * 177.8 / vfluid ELSE (0)$
 - ☞ $di = IF (si) > 0 THEN (0.4291 * 32.73266667 * 1 * (si)^{(2/3)}) ELSE (0)$
 - ☞ $k21 = perip * 0.084826$OUTFLOWS:
 - ☞ $k12 = plasma * 0.065608$
 - ☞ $k10 = plasma * 0.080146$
- $si(t) = si(t - dt) + (gss - di) * dt$
INIT $si = 0$
INFLOWS:
 - ☞ $gss = IF (stomtablet) > 0 AND (vfluid) > 0 and (time) > 0 THEN (stomtablet) * 177.8 / vfluid ELSE (0)$OUTFLOWS:
 - ☞ $di = IF (si) > 0 THEN (0.4291 * 32.73266667 * 1 * (si)^{(2/3)}) ELSE (0)$
- $stomtablet(t) = stomtablet(t - dt) + (- disstom - gss) * dt$
INIT $stomtablet = 128.094$
OUTFLOWS:
 - ☞ $disstom = IF ((liqstom)/(vfluid)) < 0.14749 AND (vfluid) > 0 and (time) > 0 THEN (0.0542 * 500 * 1 * ((stomtablet)^{(2/3)}) * (0.14749 - ((liqstom)/(vfluid)))) ELSE (0)$
 - ☞ $gss = IF (stomtablet) > 0 AND (vfluid) > 0 and (time) > 0 THEN (stomtablet) * 177.8 / vfluid ELSE (0)$
- $vfluid(t) = vfluid(t - dt) + (- vfge) * dt$
INIT $vfluid = 740$
OUTFLOWS:
 - ☞ $vfge = IF (TIME) < 4.16 THEN 177.8 ELSE (0)$
- $plascon = 1000 * plasma / vcf$
- $vcf = 12477.068877$

Figure 8.5: Equation Set STELLA© for Lipidil 145 ONE®, fed state, Model A



```
liqstom(t) = liqstom(t - dt) + (disstom - gsl) * dt
INIT liqstom = 0
INFLOWS:
  ⚡ disstom = IF ((liqstom)/(vfluid))<0.14749 AND(vfluid)>0 and (time)>0 THEN(0.797950436
    *500*1*((stomtablet)^(2/3))*(0.14749)-((liqstom)/(vfluid))) ELSE(0)
OUTFLOWS:
  ⚡ gsl = IF(liqstom)>0 AND(vfluid)>0 and (time)>0 THEN(liqstom)* 177.8/vfluid ELSE(0)
Noname_1(t) = Noname_1(t - dt) + (gsl + di - Noname_2) * dt
INIT Noname_1 = 0
INFLOWS:
  ⚡ gsl = IF(liqstom)>0 AND(vfluid)>0 and (time)>0 THEN(liqstom)* 177.8/vfluid ELSE(0)
  ⚡ di = IF(si)>0 THEN(0.0858
    *32.73266667*1*(si)^(2/3)) ELSE(0)
OUTFLOWS:
  ⚡ Noname_2 = Noname_1
perip(t) = perip(t - dt) + (k12 - k21) * dt
INIT perip = 0
INFLOWS:
  ⚡ k12 = plasma*0.065608
OUTFLOWS:
  ⚡ k21 = perip*0.084826
plasma(t) = plasma(t - dt) + (k21 + Noname_2 - k12 - k10) * dt
INIT plasma = 0
INFLOWS:
  ⚡ k21 = perip*0.084826
  ⚡ Noname_2 = Noname_1
OUTFLOWS:
  ⚡ k12 = plasma*0.065608
  ⚡ k10 = plasma*0.080146
si(t) = si(t - dt) + (gss - di) * dt
INIT si = 0
INFLOWS:
  ⚡ gss = IF(stomtablet)>0 AND(vfluid)>0 and (time)>0 THEN (stomtablet)* 177.8/vfluid ELSE(0)
OUTFLOWS:
  ⚡ di = IF(si)>0 THEN(0.0858
    *32.73266667*1*(si)^(2/3)) ELSE(0)
stomtablet(t) = stomtablet(t - dt) + (- disstom - gss) * dt
INIT stomtablet = 128.094
OUTFLOWS:
  ⚡ disstom = IF ((liqstom)/(vfluid))<0.14749 AND(vfluid)>0 and (time)>0 THEN(0.797950436
    *500*1*((stomtablet)^(2/3))*(0.14749)-((liqstom)/(vfluid))) ELSE(0)
  ⚡ gss = IF(stomtablet)>0 AND(vfluid)>0 and (time)>0 THEN (stomtablet)* 177.8/vfluid ELSE(0)
vfluid(t) = vfluid(t - dt) + (- vfge) * dt
INIT vfluid = 740
OUTFLOWS:
  ⚡ vfge = IF (TIME)<4.16 THEN 177.8 ELSE(0)
plascon = 1000*plasma/vcf
vcf = 12477.068877
```

Figure 8.6: Equation Set STELLA© for Lipidil 145 ONE®, fed state, Model B



```
liqstom(t) = liqstom(t - dt) + (disstom - gsl) * dt
INIT liqstom = 0
INFLOWS:
  disstom = IF ((liqstom)/(vfluid)<0.14749 AND(vfluid)>0 and (time)>0 THEN(0.288785769
    *500*1*((stomtablet)^(2/3))*(0.14749 -((liqstom)/(vfluid)))) ELSE(0)
OUTFLOWS:
  gsl = IF(liqstom)>0 AND(vfluid)>0 and (time)>0 THEN(liqstom)* 177.8/vfluid ELSE(0)
perip(t) = perip(t - dt) + (k12 - k21) * dt
INIT perip = 0
INFLOWS:
  k12 = plasma*0.1759
OUTFLOWS:
  k21 = perip*0.1051
plasma(t) = plasma(t - dt) + (gsl + di + k21 - k12 - k10) * dt
INIT plasma = 0
INFLOWS:
  gsl = IF(liqstom)>0 AND(vfluid)>0 and (time)>0 THEN(liqstom)* 177.8/vfluid ELSE(0)
  di = IF(si)>0 THEN(0.288785769
    *37.4967*1*(si)^(2/3)) ELSE(0)
  k21 = perip*0.1051
OUTFLOWS:
  k12 = plasma*0.1759
  k10 = plasma*0.1280
si(t) = si(t - dt) + (gss - di) * dt
INIT si = 0
INFLOWS:
  gss = IF(stomtablet)>0 AND(vfluid)>0 and (time)>0 THEN (stomtablet)* 177.8/vfluid ELSE(0)
OUTFLOWS:
  di = IF(si)>0 THEN(0.288785769
    *37.4967*1*(si)^(2/3)) ELSE(0)
stomtablet(t) = stomtablet(t - dt) + (- disstom - gss) * dt
INIT stomtablet = 141.345
OUTFLOWS:
  disstom = IF ((liqstom)/(vfluid)<0.14749 AND(vfluid)>0 and (time)>0 THEN(0.288785769
    *500*1*((stomtablet)^(2/3))*(0.14749 -((liqstom)/(vfluid)))) ELSE(0)
  gss = IF(stomtablet)>0 AND(vfluid)>0 and (time)>0 THEN (stomtablet)* 177.8/vfluid ELSE(0)
vfluid(t) = vfluid(t - dt) + (- vfge) * dt
INIT vfluid = 740
OUTFLOWS:
  vfge = IF (TIME)<4.16 THEN 177.8 ELSE(0)
plascon = 1000*plasma/vcf
vcf = 8763.11
```

Figure 8.7: Equation Set STELLA® for Ter®, fed state, Model A



```
liqstom(t) = liqstom(t - dt) + (disstom - gsl) * dt
INIT liqstom = 0
INFLOWS:
  disstom = IF ((liqstom)/(vfluid))<0.14749 AND(vfluid)>0 and (time)>0 THEN(0.288785769
    *500*1*((stomtablett)^(2/3))*(0.14749)-((liqstom)/(vfluid))) ELSE(0)
OUTFLOWS:
  gsl = IF(liqstom)>0 AND(vfluid)>0 and (time)>0 THEN(liqstom)*177.8/vfluid ELSE(0)
Noname_1(t) = Noname_1(t - dt) + (gsl + di - Noname_2) * dt
INIT Noname_1 = 0
INFLOWS:
  gsl = IF(liqstom)>0 AND(vfluid)>0 and (time)>0 THEN(liqstom)*177.8/vfluid ELSE(0)
  di = IF(si)>0 THEN(0.288785769
    *37.4967*1*(si)^(2/3)) ELSE(0)
OUTFLOWS:
  Noname_2 = Noname_1
perip(t) = perip(t - dt) + (k12 - k21) * dt
INIT perip = 0
INFLOWS:
  k12 = plasma*0.1759
OUTFLOWS:
  k21 = perip*0.1051
plasma(t) = plasma(t - dt) + (k21 + Noname_2 - k12 - k10) * dt
INIT plasma = 0
INFLOWS:
  k21 = perip*0.1051
  Noname_2 = Noname_1
OUTFLOWS:
  k12 = plasma*0.1759
  k10 = plasma*0.1280
si(t) = si(t - dt) + (gss - di) * dt
INIT si = 0
INFLOWS:
  gss = IF(stomtablett)>0 AND(vfluid)>0 and (time)>0 THEN (stomtablett)*177.8/vfluid ELSE(0)
OUTFLOWS:
  di = IF(si)>0 THEN(0.288785769
    *37.4967*1*(si)^(2/3)) ELSE(0)
stomtablett(t) = stomtablett(t - dt) + (- disstom - gss) * dt
INIT stomtablett = 141.345
OUTFLOWS:
  disstom = IF ((liqstom)/(vfluid))<0.14749 AND(vfluid)>0 and (time)>0 THEN(0.288785769
    *500*1*((stomtablett)^(2/3))*(0.14749)-((liqstom)/(vfluid))) ELSE(0)
  gss = IF(stomtablett)>0 AND(vfluid)>0 and (time)>0 THEN (stomtablett)*177.8/vfluid ELSE(0)
vfluid(t) = vfluid(t - dt) + (- vfge) * dt
INIT vfluid = 740
OUTFLOWS:
  vfge = IF (TIME)<4.16 THEN 177.8 ELSE(0)
plascon = 1000*plasma/vcf
vcf = 8763.11
```

Figure 8.8: Equation Set STELLA© for Ter®, fed state, Model B



Table 8.42: Filteradsorption of Diphenhydramine (DPH) to 0.2 µm RC filter in various media

Filteradsorption DPH to 0.2µm RC	FaSSIF Unfiltered	FaSSIF 0.2µm	FaSSIF - V2 Unfiltered	FaSSIF - V2 0.2µm	FeSSIF Unfiltered	FeSSIF 0.2µm	FeSSIF - V2 Unfiltered	FeSSIF - V2 0.2µm	FaSSGF Unfiltered	FaSSGF 0.2µm
Mean %	100.0	95.4	100.0	98.6	100.0	99.1	100.0	100.6	100.0	100.3
s.d.	1.30	2.83	0.00	1.81	1.81	1.87	1.41	3.03	4.54	1.24

Table 8.43: Dissolution of DPH in FaSSGF, HPLC method

FaSSGF time [min]	n = 1 [%]	n = 2 [%]	n = 3 [%]	mean [%]	s.d.
5	18.39	20.63	20.00	19.67	1.15
10	36.77	39.23	39.91	38.64	1.65
15	53.55	57.43	59.53	56.83	3.04
20	71.53	73.41	77.68	74.21	3.15
25	87.42	82.84	88.05	86.10	2.84
35	99.09	92.90	99.96	97.32	3.85
45	99.41	96.33	102.02	99.25	2.85

Table 8.44: Dissolution of DPH in FaSSGF, ISE method A

FaSSGF time [min]	n = 1 [%]	n = 2 [%]	n = 3 [%]	mean [%]	s.d.
5	19.90	18.39	19.77	19.35	0.84
10	38.98	36.77	37.03	37.59	1.21
15	57.50	52.61	53.21	54.44	2.66
20	72.97	70.75	67.55	70.42	2.73
25	85.09	83.46	78.78	82.44	3.27
35	97.33	96.58	90.47	94.79	3.76
45	98.83	97.32	93.65	96.60	2.66

Table 8.45: Dissolution of DPH in FaSSGF, ISE method B

FaSSGF time [min]	n = 1 [%]	n = 2 [%]	n = 3 [%]	mean [%]	s.d.
5.00	18.48	20.20	15.84	18.17	2.20
10.00	37.84	40.90	32.88	37.21	4.05
15.00	55.84	57.35	47.86	53.68	5.10
20.00	73.05	73.68	61.95	69.56	6.60
25.00	84.45	83.95	74.28	80.90	5.73
35.00	97.63	96.00	91.02	94.88	3.45
45.00	100.50	97.75	98.21	98.82	1.47



Table 8.46: Dissolution of DPH in FaSSiF-V2, HPLC method

FaSSiF-V2 time [min]	n = 1 [%]	n = 2 [%]	n = 3 [%]	mean [%]	s.d.
5	19.68	20.15	15.49	18.44	2.56
10	39.32	39.53	31.74	36.86	4.44
15	57.59	57.96	48.96	54.84	5.09
20	70.13	69.79	59.76	66.56	5.89
25	86.24	84.84	71.65	80.91	8.05
35	99.42	95.21	91.50	95.38	3.96
45	100.50	97.40	96.80	98.23	1.98

Table 8.47: Dissolution of DPH in FaSSiF-V2, ISE Electrode 1, method A

FaSSiF-V2 time [min]	n = 1 [%]	n = 2 [%]	n = 3 [%]	mean [%]	s.d.
5	17.88	19.45	15.29	17.54	2.10
10	36.61	39.37	31.73	35.90	3.87
15	54.03	55.21	46.19	51.81	4.90
20	70.67	70.93	59.79	67.13	6.36
25	81.71	80.82	71.70	78.07	5.54
35	94.45	92.42	87.84	91.57	3.39
45	97.23	94.11	94.79	95.38	1.64

Table 8.48: Dissolution of DPH in FaSSiF-V2, ISE Electrode 1, method B

FaSSiF-V2 time [min]	n = 1 [%]	n = 2 [%]	n = 3 [%]	mean [%]	s.d.
5	18.48	20.20	15.84	18.17	2.20
10	37.84	40.90	32.88	37.21	4.05
15	55.84	57.35	47.86	53.68	5.10
20	73.05	73.68	61.95	69.56	6.60
25	84.45	83.95	74.28	80.90	5.73
35	97.63	96.00	91.02	94.88	3.45
45	100.50	97.75	98.21	98.82	1.47

Table 8.49: Dissolution of DPH in FaSSiF-V2, ISE Electrode 2, method A

FaSSiF-V2 time [min]	n = 1 [%]	n = 2 [%]	n = 3 [%]	mean [%]	s.d.
5	17.77	19.30	14.87	17.31	2.25
10	36.32	39.11	31.39	35.61	3.91
15	54.11	55.33	45.54	51.66	5.33
20	69.25	70.28	59.01	66.18	6.23
25	81.70	80.81	70.72	77.74	6.10
35	94.28	92.57	87.56	91.47	3.49
45	96.73	93.94	93.22	94.63	1.86



Table 8.50: Dissolution of DPH in FaSSIF-V2, ISE Electrode 2, method B

FaSSIF-V2, time [min]	n = 1 [%]	n = 2 [%]	n = 3 [%]	mean [%]	s.d.
5	18.46	19.99	15.45	17.97	2.31
10	37.73	40.54	32.61	36.96	4.02
15	56.22	57.35	47.30	53.62	5.51
20	71.94	72.86	61.29	68.70	6.43
25	84.88	83.78	73.44	80.70	6.32
35	97.95	95.98	90.93	94.95	3.62
45	100.50	97.40	96.80	98.23	1.99

Table 8.51: Dissolution of DPH in FaSSIF, HPLC method

FaSSIF time [min]	n = 1 [%]	n = 2 [%]	n = 3 [%]	mean [%]	s.d.
5	24.56	26.79	23.54	24.96	1.66
10	48.34	51.65	47.61	49.20	2.15
15	69.28	72.99	68.66	70.31	2.34
20	90.27	85.73	85.20	87.07	2.78
25	97.82	97.59	95.52	96.98	1.27
35	102.33	101.44	102.68	102.15	0.63
45	105.76	102.30	105.82	104.63	2.01

Table 8.52: Dissolution of DPH in FaSSIF, ISE Electrode 1, method A

FaSSIF time [min]	n = 1 [%]	n = 2 [%]	n = 3 [%]	mean [%]	s.d.
5	25.77	26.52	25.60	25.96	0.49
10	50.99	52.45	50.45	51.30	1.04
15	72.07	72.00	70.52	71.53	0.87
20	88.64	85.58	86.43	86.88	1.58
25	98.12	93.46	97.77	96.45	2.60
35	103.98	96.60	103.98	101.52	4.26
45	103.98	96.95	103.98	101.64	4.06

Table 8.53: Dissolution of DPH in FaSSIF, ISE Electrode 1, method B

FaSSIF, time [min]	n = 1 [%]	n = 2 [%]	n = 3 [%]	mean [%]	s.d.
5	26.21	28.11	26.07	26.79	1.14
10	51.86	55.75	51.35	52.99	2.41
15	71.46	74.60	70.22	72.09	2.26
20	88.54	88.80	86.37	87.90	1.33
25	98.72	97.94	98.06	98.24	0.42
35	105.76	101.93	105.82	104.50	2.23
45	105.76	102.30	105.82	104.63	2.02



Table 8.54: Dissolution of DPH in FaSSIF, ISE Electrode 2, method A

FaSSIF, el.2 time [min]	n = 1 [%]	n = 2 [%]	n = 3 [%]	mean [%]	s.d.
5	25.90	27.67	26.11	26.56	0.97
10	50.60	52.66	50.07	51.11	1.37
15	70.75	71.50	68.98	70.41	1.29
20	87.67	85.26	85.47	86.13	1.33
25	97.41	92.93	96.35	95.56	2.34
35	103.99	96.67	103.61	101.42	4.12
45	104.36	97.02	103.61	101.66	4.04

Table 8.55: Dissolution of DPH in FaSSIF, ISE Electrode 2, method B

FaSSIF time [min]	n = 1 [%]	n = 2 [%]	n = 3 [%]	mean [%]	s.d.
5	25.957	28.346	26.28	26.86	1.30
10	51.281	54.734	50.766	52.26	2.16
15	71.172	74.307	69.937	71.81	2.25
20	88.198	88.791	86.35	87.78	1.27
25	98.71	97.584	98.053	98.12	0.57
35	105.76	101.929	105.437	104.38	2.12
45	106.145	102.3	105.82	104.76	2.13

Table 8.56: Dissolution of DPH in FaSSIF, ISE Electrode 3, method A

FaSSIF time [min]	n = 1 [%]	n = 2 [%]	n = 3 [%]	mean [%]	s.d.
5	26.26	26.95	26.45	26.55	0.36
10	50.99	51.88	50.44	51.10	0.73
15	71.29	71.09	69.77	70.71	0.83
20	87.83	84.72	85.95	86.16	1.57
25	97.47	92.48	96.77	95.57	2.71
35	103.61	96.27	103.61	101.16	4.24
45	103.98	96.62	103.98	101.53	4.25

Table 8.57: Dissolution of DPH in FaSSIF, ISE Electrode 3, method B

FaSSIF time [min]	n = 1 [%]	n = 2 [%]	n = 3 [%]	mean [%]	s.d.
5	26.32	28.79	26.73	27.28	1.32
10	51.67	55.28	51.33	52.76	2.19
15	71.73	75.09	70.49	72.44	2.38
20	88.37	89.24	86.85	88.15	1.21
25	98.78	97.98	98.49	98.42	0.40
35	105.76	101.93	105.82	104.50	2.23
45	105.76	102.67	106.20	104.88	1.93

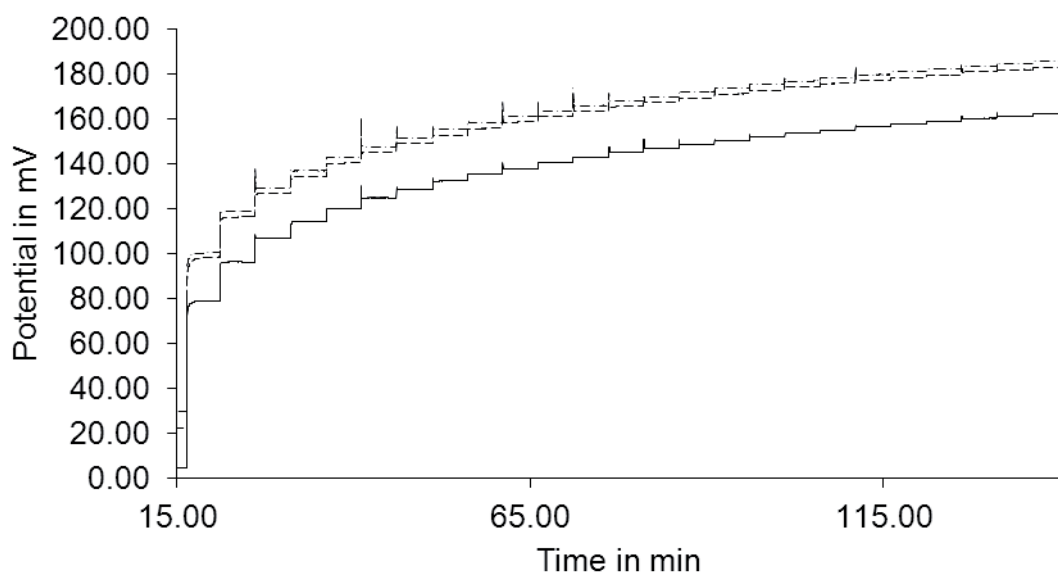


Figure 8.9: Example of 25-step calibration potential / time



9 References

- [1] A. Dokoumetzidis, P. Macheras, A century of dissolution research: From Noyes and Whitney to the Biopharmaceutics Classification System, *International Journal of Pharmaceutics*, 321 (2006) 1-11.
- [2] J.L. Cohen, B.B. Hubert, L.J. Leeson, C.T. Rhodes, J.R. Robinson, T.J. Roseman, E. Shefter, The Development of USP Dissolution and Drug Release Standards, *Pharmaceutical Research*, 7 (1990) 983-987.
- [3] J. Lindenbaum, M.H. Mellow, M. Blackstone, V.P. Butler, Variation in Biologic Availability of Digoxin from 4 Preparations, *New England Journal of Medicine*, 285 (1971) 1344-&.
- [4] E.J. Fraser, J.W. Poston, R.H. Leach, Bioavailability of Digoxin, *Lancet*, 2 (1972) 541-&.
- [5] E.J. Fraser, R.H. Leach, J.W. Poston, A.M. Bold, L.S. Culank, A.B. Lipede, Dissolution-Rates and Bioavailability of Digoxin Tablets, *Lancet*, 1 (1973) 1393-1393.
- [6] A.J. Jounela, P.J. Pentikainen, A. Sothmann, Effect of Particle-Size on Bioavailability of Digoxin, *Eur J Clin Pharmacol*, 8 (1975) 365-370.
- [7] J.B. Dressman, G.L. Amidon, C. Reppas, V.P. Shah, Dissolution testing as a prognostic tool for oral drug absorption: Immediate release dosage forms, *Pharm Res*, 15 (1998) 11-22.
- [8] P. Shah, V. Jogani, P. Mishra, A.K. Mishra, T. Bagchi, A. Misra, In vitro assessment of acyclovir permeation across cell monolayers in the presence of absorption enhancers, *Drug Dev Ind Pharm*, 34 (2008) 279-288.
- [9] M. Thanou, J.C. Verhoef, H.E. Junginger, Oral drug absorption enhancement by chitosan and its derivatives, *Adv Drug Deliv Rev*, 52 (2001) 117-126.
- [10] A.M. Kaushal, P. Gupta, A.K. Bansal, Amorphous drug delivery systems: molecular aspects, design, and performance, *Crit Rev Ther Drug Carrier Syst*, 21 (2004) 133-193.
- [11] R.S. Cvetkovic, K.L. Goa, Lopinavir/ritonavir: a review of its use in the management of HIV infection, *Drugs*, 63 (2003) 769-802.
- [12] A. Noyes, Whitney, W. , The rate of solution of solid substances in their own solutions., *J. Am. Chem. Soc.*, 19 (1897) 930-934.
- [13] J. Boni, Improvements to biorelevant dissolution testing: lyophilized media, buffer alternatives and miniaturized apparatus, in: Department for Biochemistry, Chemics and Pharmaceutics, Johann Wolfgang Goethe-Universitaet, Frankfurt, 2009.
- [14] E. Galia, E. Nicolaidis, D. Horter, R. Lobenberg, C. Reppas, J.B. Dressman, Evaluation of various dissolution media for predicting in vivo performance of class I and II drugs, *Pharm Res*, 15 (1998) 698-705.
- [15] E. Jantratid, N. Janssen, C. Reppas, J.B. Dressman, Dissolution Media Simulating Conditions in the Proximal Human Gastrointestinal Tract: An Update, *Pharm Res*, 25 (2008) 1663-1676.
- [16] Y. Shono, E. Jantratid, N. Janssen, F. Kesisoglou, Y. Mao, M. Vertzoni, C. Reppas, J.B. Dressman, Prediction of food effects on the absorption of celecoxib based on biorelevant dissolution testing coupled with physiologically based pharmacokinetic modeling, *Eur J Pharm Biopharm*, 73 (2009) 107-114.
- [17] E. Nicolaidis, M. Symillides, J.B. Dressman, C. Reppas, Biorelevant dissolution testing to predict the plasma profile of lipophilic drugs after oral administration, *Pharm Res*, 18 (2001) 380-388.



-
- [18] E. Jantratid, S. Prakongpan, G.L. Amidon, J.B. Dressman, Feasibility of biowaiver extension to biopharmaceutics classification system class III drug products: cimetidine, *Clin Pharmacokinet*, 45 (2006) 385-399.
- [19] S. Strauch, E. Jantratid-And, J.B. Dressman, Comparison of WHO and US FDA biowaiver dissolution test conditions using bioequivalent doxycycline hyclate drug products, *Journal of Pharmacy and Pharmacology*, 61 (2009) 331-337.
- [20] S. Strauch, E. Jantratid, M. Stahl, L. Rago, J.B. Dressman, The biowaiver procedure: its application to antituberculosis products in the WHO prequalification programme, *J Pharm Sci*, 100 (2011) 822-830.
- [21] G.L. Amidon, H. Lennernas, V.P. Shah, J.R. Crison, A theoretical basis for a biopharmaceutic drug classification: the correlation of in vitro drug product dissolution and in vivo bioavailability, *Pharm Res*, 12 (1995) 413-420.
- [22] C.Y. Wu, L.Z. Benet, Predicting drug disposition via application of BCS: transport/absorption/ elimination interplay and development of a biopharmaceutics drug disposition classification system, *Pharm Res*, 22 (2005) 11-23.
- [23] M. Lindenberg, C. Wiegand, J. Dressman, Comparison of the Adsorption of Several Drugs to Typical Filter Materials, *Dissolution Tech.*, 12 (2005) 22-25.
- [24] B.E. Rabinow, Nanosuspensions in drug delivery, *Nat. Rev. Drug Discovery*, 3 (2004) 785-796.
- [25] S.M. Berge, L.D. Bighley, D.C. Monkhouse, Pharmaceutical Salts, *Journal of Pharmaceutical Sciences*, 66 (1977) 1-19.
- [26] P.L. Gould, Salt Selection for Basic Drugs, *International Journal of Pharmaceutics*, 33 (1986) 201-217.
- [27] S. Agharkar, S. Lindenbaum, T. Higuchi, Enhancement of Solubility of Drug Salts by Hydrophilic Counterions - Properties of Organic Salts of an Antimalarial Drug, *Journal of Pharmaceutical Sciences*, 65 (1976) 747-749.
- [28] G.S. Paulekuhn, J.B. Dressman, C. Saal, Trends in active pharmaceutical ingredient salt selection based on analysis of the Orange Book Database, *Journal of Medicinal Chemistry*, 50 (2007) 6665-6672.
- [29] R.J. Bastin, M.J. Bowker, B.J. Slater, Salt selection and optimisation procedures for pharmaceutical new chemical entities, *Organic Process Research & Development*, 4 (2000) 427-435.
- [30] T. Loftsson, S.B. Vogensen, M.E. Brewster, F. Konradsdottir, Effects of cyclodextrins on drug delivery through biological membranes, *J Pharm Sci*, 96 (2007) 2532-2546.
- [31] T. Loftsson, D. Hreinsdottir, M. Masson, Evaluation of cyclodextrin solubilization of drugs, *International Journal of Pharmaceutics*, 302 (2005) 18-28.
- [32] T. Loftsson, D. Duchene, Cyclodextrins and their pharmaceutical applications, *International Journal of Pharmaceutics*, 329 (2007) 1-11.
- [33] S. Klein, Zoeller, T., Molekulare Zuckertüten für Arzneistoffe, *Pharmazeutische Zeitung*, (2008).
- [34] S. Klein, M.F. Wempe, T. Zoeller, N.L. Buchanan, J.L. Lambert, M.G. Ramsey, K.J. Edgar, C.M. Buchanan, Improving glyburide solubility and dissolution by complexation with hydroxybutenyl-beta-cyclodextrin, *Journal of Pharmacy and Pharmacology*, 61 (2009) 23-30.
- [35] V. Stella, J. Haslam, N. Yata, H. Okada, S. Lindenbaum, T. Higuchi, Enhancement of Bioavailability of a Hydrophobic Amine Anti-Malarial by Formulation with Oleic-



- Acid in a Soft Gelatin Capsule, *Journal of Pharmaceutical Sciences*, 67 (1978) 1375-1377.
- [36] C.J.H. Porter, W.N. Charman, In vitro assessment of oral lipid based formulations, *Advanced Drug Delivery Reviews*, 50 (2001) S127-S147.
- [37] C.W. Pouton, Formulation of poorly water-soluble drugs for oral administration: Physicochemical and physiological issues and the lipid formulation classification system, *European Journal of Pharmaceutical Sciences*, 29 (2006) 278-287.
- [38] L. SMB, Lidose, in, Brussels, 2011.
- [39] B. Rodriguez-Spong, C.P. Price, A. Jayasankar, A.J. Matzger, N. Rodriguez-Hornedo, General principles of pharmaceutical solid polymorphism: a supramolecular perspective, *Adv Drug Deliv Rev*, 56 (2004) 241-274.
- [40] A.W. Newman, S.R. Byrn, Solid-state analysis of the active pharmaceutical ingredient in drug products, *Drug Discov Today*, 8 (2003) 898-905.
- [41] S.R. Chemburkar, J. Bauer, K. Deming, H. Spiwek, K. Patel, J. Morris, R. Henry, S. Spanton, W. Dziki, W. Porter, J. Quick, P. Bauer, J. Donaubauber, B.A. Narayanan, M. Soldani, D. Riley, K. McFarland, Dealing with the impact of ritonavir polymorphs on the late stages of bulk drug process development, *Organic Process Research & Development*, 4 (2000) 413-417.
- [42] J. Breitenbach, Melt extrusion: from process to drug delivery technology, *Eur J Pharm Biopharm*, 54 (2002) 107-117.
- [43] J. Jinno, N. Kamada, M. Miyake, K. Yamada, T. Mukai, M. Odomi, H. Toguchi, G.G. Liversidge, K. Higaki, T. Kimura, Effect of particle size reduction on dissolution and oral absorption of a poorly water-soluble drug, cilostazol, in beagle dogs, *J Control Release*, 111 (2006) 56-64.
- [44] G.G. Liversidge, K.C. Cundy, Particle-Size Reduction for Improvement of Oral Bioavailability of Hydrophobic Drugs .1. Absolute Oral Bioavailability of Nanocrystalline Danazol in Beagle Dogs, *International Journal of Pharmaceutics*, 125 (1995) 91-97.
- [45] J.B. Dressman, D. Fleisher, Mixing-tank model for predicting dissolution rate control or oral absorption, *J Pharm Sci*, 75 (1986) 109-116.
- [46] J. Oliver, *Genial Italienisch*, 4 ed., Starnberg: Dorling Kindersley 2006.
- [47] S.J. Martin A., Cammarata A., *Physikalische Pharmazie*, Wissenschaftliche Verlagsgesellschaft, Stuttgart, 1987.
- [48] F.K. Bauer K., Führer C., *Lehrbuch der pharmazeutischen Technologie*, Wissenschaftliche Verlagsgesellschaft, Stuttgart, 1999.
- [49] M. Sugimoto, T. Okagaki, S. Narisawa, Y. Koida, K. Nakajima, Improvement of dissolution characteristics and bioavailability of poorly water-soluble drugs by novel cogrinding method using water-soluble polymer, *International Journal of Pharmaceutics*, 160 (1998) 11-19.
- [50] M. Otsuka, T. Ofusa, Y. Matsuda, Dissolution improvement of water-insoluble glybuzole by co-grinding and co-melting with surfactants and their physicochemical properties, *Colloids and Surfaces B-Biointerfaces*, 10 (1998) 217-226.
- [51] J.P. Guichard, P. Blouquin, Y. Qing, A new formulation of fenofibrate: Suprabioavailable tablets, *Current Medical Research and Opinion*, 16 (2000) 134-138.
- [52] M. Vogt, K. Kunath, J.B. Dressman, Dissolution enhancement of fenofibrate by micronization, cogrinding and spray-drying: Comparison with commercial preparations, *Eur J Pharm Biopharm*, 68 (2008) 283-288.



- [53] M. Vogt, M. Vertzoni, K. Kunath, C. Reppas, J.B. Dressman, Cogrounding enhances the oral bioavailability of EMD 57033, a poorly water soluble drug, in dogs, *Eur J Pharm Biopharm*, 68 (2008) 338-345.
- [54] E. Merisko-Liversidge, G.G. Liversidge, E.R. Cooper, Nanosizing: a formulation approach for poorly-water-soluble compounds, *Eur J Pharm Sci*, 18 (2003) 113-120.
- [55] F. Kesisoglou, S. Panmai, Y. Wu, Nanosizing--oral formulation development and biopharmaceutical evaluation, *Adv Drug Deliv Rev*, 59 (2007) 631-644.
- [56] J.U. Junghanns, R.H. Muller, Nanocrystal technology, drug delivery and clinical applications, *Int J Nanomedicine*, 3 (2008) 295-309.
- [57] C.M. Keck, R.H. Muller, Drug nanocrystals of poorly soluble drugs produced by high pressure homogenisation, *Eur J Pharm Biopharm*, 62 (2006) 3-16.
- [58] P. SkyePharma, IDD-P Microparticle, in, 2011.
- [59] R. Sauron, M. Wilkins, V. Jessent, A. Dubois, C. Maillot, A. Weil, Absence of a food effect with a 145 mg nanoparticle fenofibrate tablet formulation, *Int J Clin Pharmacol Ther*, 44 (2006) 64-70.
- [60] A. Solvay, Fachinfo Lipidil-Ter 160 mg, in, 2007.
- [61] A.J. Humberstone, C.J.H. Porter, W.N. Charman, A physicochemical basis for the effect of food on the absolute oral bioavailability of halofantrine, *J Pharm Sci*, 85 (1996) 525-529.
- [62] Y. Wu, A. Loper, E. Landis, L. Hettrick, L. Novak, K. Lynn, C. Chen, K. Thompson, R. Higgins, U. Batra, S. Shelukar, G. Kwei, D. Storey, The role of biopharmaceutics in the development of a clinical nanoparticle formulation of MK-0869: a Beagle dog model predicts improved bioavailability and diminished food effect on absorption in human, *Int J Pharm*, 285 (2004) 135-146.
- [63] Z.M. Miao, S.X. Cheng, X.Z. Zhang, R.X. Zhuo, Study on drug release behaviors of poly-alpha,beta-[n-(2-hydroxyethyl)-L-aspartamide]-g-poly(epsilon-caprolactone) nano- and microparticles, *Biomacromolecules*, 7 (2006) 2020-2026.
- [64] N. Chidambaram, D.J. Burgess, A novel in vitro release method for submicron sized dispersed systems, *AAPS PharmSci*, 1 (1999) E11.
- [65] J.C. Goodman, Clinical microdialysis in neuro-oncology: principles and applications, *Chin J Cancer*, 30 (2011) 173-181.
- [66] K.P. Shah, M. Chang, C.M. Riley, Automated analytical systems for drug development studies. II--A system for dissolution testing, *J Pharm Biomed Anal*, 12 (1994) 1519-1527.
- [67] K.P. Shah, M. Chang, C.M. Riley, Automated analytical systems for drug development studies. 3. Multivessel dissolution testing system based on microdialysis sampling, *J Pharm Biomed Anal*, 13 (1995) 1235-1241.
- [68] K.P. Shah, J. Zhou, R. Lee, R.L. Schowen, R. Elsbernd, J.M. Ault, J.F. Stobaugh, M. Slavik, C.M. Riley, Automated analytical systems for drug development studies. I--A system for the determination of drug stability, *J Pharm Biomed Anal*, 12 (1994) 993-1001.
- [69] A.K. Dash, P.W. Haney, M.J. Garavalia, Development of an in vitro dissolution method using microdialysis sampling technique for implantable drug delivery systems, *J Pharm Sci*, 88 (1999) 1036-1040.
- [70] J. Johansson, M. Cauchi, M. Sundgren, Multiple fiber-optic dual-beam UV/Vis system with application to dissolution testing, *Journal of Pharmaceutical and Biomedical Analysis*, 29 (2002) 469-476.



- [71] K.C. Roinestad, FS; Palermo, PJ; Bynum, K, Detection systems and methods for predicting the dissolution curve of a drug from a pharmaceutical dosage form in: P. Inc. (Ed.), Euro-Celtique, S.A. (Luxembourg, LU) United States of America, 2001.
- [72] M. Josefson, E. Johansson, A. Torstensson, Optical fiber spectrometry in turbid solutions by multivariate calibration applied to tablet dissolution testing, *Anal Chem*, 60 (1988) 2666-2671.
- [73] F. Liu, Embry, Cantu, Pack, Technical Evaluation of a Fiber-Optic Probe Dissolution System, *Diss. Tech.*, 15 (2008) 10-20.
- [74] M.W. Wunderlich, T.; Dressman, J. B., Practical considerations when using fiber optics for dissolution testing., *Dissolution Technol.*, 10 (2003) 17-19.
- [75] M.T. Crisp, C.J. Tucker, T.L. Rogers, R.O. Williams, 3rd, K.P. Johnston, Turbidimetric measurement and prediction of dissolution rates of poorly soluble drug nanocrystals, *J Control Release*, 117 (2007) 351-359.
- [76] Y. Shono, Forecasting in vivo oral absorption and food effect of micronized and nanosized aprepitant formulations in humans, *Eur. J. Pharm. Biopharm.*, (2010).
- [77] T.H. Klein, C, Charakterisierung von Biopolymeren, Proteinen, Partikeln und Kolloiden mit Feldflussfraktionierung, *GIT Laborfachzeitschrift*, 11 (1999) 1224 - 1228.
- [78] C.B. Hürzeler, B, Größencharakterisierung von Biopolymeren und Biopartikeln mit Feldflussfraktionierung und on-line dynamischer Lichtstreuung, *Artikel GIT Laborfachzeitschrift*, 3 (2000) 271 - 274.
- [79] T. Klein, Postnova Analytics - Company Presentation, in: I.o.P.T.-U. Frankfurt (Ed.), Postnova Analytics, Frankfurt, 2008.
- [80] H. Bohets, K. Vanhoutte, R. De Maesschalck, P. Cockaerts, B. Vissers, L.J. Nagels, Development of in situ ion selective sensors for dissolution, *Analytica Chimica Acta*, 581 (2007) 181-191.
- [81] K. Peeters, R. De Maesschalck, H. Bohets, K. Vanhoutte, L. Nagels, In situ dissolution testing using potentiometric sensors, *Eur J Pharm Sci*, 34 (2008) 243-249.
- [82] E. Mutschler, *Arzneimittelwirkungen*, Wissenschaftliche Verlagsgesellschaft mbH Stuttgart, Stuttgart, 2001.
- [83] Martindale, Martindale. *The extra pharmacopeia*, Council of The Pharmaceutical Society of Great Britain, London, 1982.
- [84] P. Buch, P. Languth, M. Kataoka, S. Yamashita, IVIVC in Oral Absorption for Fenofibrate Immediate Release Tablets Using a Dissolution/Permeation System, *J Pharm Sci*, 98 (2009) 2001-2009.
- [85] A. Hanafy, H. Spahn-Langguth, G. Vergnault, P. Grenier, M. Tubic Grozdanis, T. Lenhardt, P. Langguth, Pharmacokinetic evaluation of oral fenofibrate nanosuspensions and SLN in comparison to conventional suspensions of micronized drug, *Adv Drug Deliv Rev*, 59 (2007) 419-426.
- [86] T. O'Hara, A. Dunne, J. Butler, J. Devane, A review of methods used to compare dissolution profile data, *Pharmaceut Sci Tech Today*, 1 (1998) 214-223.
- [87] FDA, *Guidance for Industry: Dissolution testing of immediate-release solid oral dosage forms*, 1997.
- [88] E. Nicolaides, Contribution to the prediction of absorption of lipophilic drugs based on in vitro dissolution data, in: *National and Kapodistrian University of Athens*, Athens, 2000.



-
- [89] W.I. Higuchi, E.N. Hiestand, Dissolution Rates of Finely Divided Drug Powders .1. Effect of a Distribution of Particle Sizes in a Diffusion-Controlled Process, *Journal of Pharmaceutical Sciences*, 52 (1963) 67-&.
- [90] W.I. Higuchi, E.N. Hiestand, E.L. Rowe, Dissolution Rates of Finely Divided Drug Powders .2. Micronized Methylprednisolone, *Journal of Pharmaceutical Sciences*, 52 (1963) 162-&.
- [91] A.W. Hixson, S.J. Baum, Agitation - Mass transfer coefficients in liquid-solid agitation systems, *Industrial and Engineering Chemistry*, 33 (1941) 478-485.
- [92] P.J. Niebergall, J.E. Goyan, G. Milosovich, Dissolution Rate Studies .2. Dissolution of Particles under Conditions of Rapid Agitation, *Journal of Pharmaceutical Sciences*, 52 (1963) 236-&.
- [93] R.J. Hintz, K.C. Johnson, The Effect of Particle-Size Distribution on Dissolution Rate and Oral Absorption, *International Journal of Pharmaceutics*, 51 (1989) 9-17.
- [94] J.J. Sheng, P.J. Sirois, J.B. Dressman, G.L. Amidon, Particle Diffusional Layer Thickness in a USP Dissolution Apparatus II: A Combined Function of Particle Size and Paddle Speed, *Journal of Pharmaceutical Sciences*, 97 (2008) 4815-4829.
- [95] E. Rinaki, A. Dokoumetzidis, P. Macheras, The mean dissolution time depends on the dose/solubility ratio, *Pharmaceutical Research*, 20 (2003) 406-408.
- [96] M. Perrut, J. Jung, F. Leboeuf, Enhancement of dissolution rate of poorly-soluble active ingredients by supercritical fluid processes. Part I: Micronization of neat particles, *Int J Pharm*, 288 (2005) 3-10.
- [97] R.H. Muller, C. Jacobs, O. Kayser, Nanosuspensions as particulate drug formulations in therapy. Rationale for development and what we can expect for the future, *Adv Drug Deliv Rev*, 47 (2001) 3-19.
- [98] S. Willmann, K. Thelen, C. Becker, J.B. Dressman, J. Lippert, Mechanism-based prediction of particle size-dependent dissolution and absorption: cilostazol pharmacokinetics in dogs, *Eur J Pharm Biopharm*, 76 (2010) 83-94.
- [99] R. Takano, K. Sugano, A. Higashida, Y. Hayashi, M. Machida, Y. Aso, S. Yamashita, Oral absorption of poorly water-soluble drugs: Computer simulation of fraction absorbed in humans from a miniscale dissolution test, *Pharmaceutical Research*, 23 (2006) 1144-1156.
- [100] K. Sugano, Possible reduction of effective thickness of intestinal unstirred water layer by particle drifting effect, *International Journal of Pharmaceutics*, 387 (2010) 103-109.
- [101] J. Jinno, N. Kamada, M. Miyake, K. Yamada, T. Mukai, M. Odomi, H. Toguchi, G.G. Liversidge, K. Higaki, T. Kimura, In vitro-in vivo correlation for wet-milled tablet of poorly water-soluble cilostazol, *J Control Release*, 130 (2008) 29-37.
- [102] N.W. Thomas, P.G. Jenkins, K.A. Howard, M.W. Smith, E.C. Lavelle, J. Holland, S.S. Davis, Particle uptake and translocation across epithelial membranes, *J Anat*, 189 (Pt 3) (1996) 487-490.
- [103] F. Delie, Evaluation of nano- and microparticle uptake by the gastrointestinal tract, *Adv Drug Deliv Rev*, 34 (1998) 221-233.
- [104] A.T. Florence, The oral absorption of micro- and nanoparticulates: neither exceptional nor unusual, *Pharm Res*, 14 (1997) 259-266.
- [105] J.D. Smart, The basics and underlying mechanisms of mucoadhesion, *Adv Drug Deliv Rev*, 57 (2005) 1556-1568.



-
- [106] J. Brouwers, M.E. Brewster, P. Augustijns, Supersaturating drug delivery systems: The answer to solubility-limited oral bioavailability?, *J Pharm Sci*, 98 (2009) 2549-2572.
- [107] K. Tziomalos, V.G. Athyros, Fenofibrate: a novel formulation (Triglide (TM)) in the treatment of lipid disorders: a review, *International Journal of Nanomedicine*, 1 (2006) 129-147.
- [108] M.J. Chapman, Pharmacology of Fenofibrate, *American Journal of Medicine*, 83 (1987) 21-25.
- [109] D. Fleisher, C. Li, Y. Zhou, L.H. Pao, A. Karim, Drug, meal and formulation interactions influencing drug absorption after oral administration - Clinical implications, *Clin Pharmacokinet*, 36 (1999) 233-254.
- [110] V. Karalis, P. Macheras, A. Van Peer, V.P. Shah, Bioavailability and Bioequivalence: Focus on physiological factors and variability, *Pharmaceutical Research*, 25 (2008) 1956-1962.
- [111] A. Karamanlis, R. Chaikornin, S. Doran, M. Bellon, F.D. Bartholomeusz, J.M. Wishart, K.L. Jones, M. Horowitz, C.K. Rayner, Effects of protein on glycemic and incretin responses and gastric emptying after oral glucose in healthy subjects, *American Journal of Clinical Nutrition*, 86 (2007) 1364-1368.
- [112] S. Willmann, K. Thelen, C. Becker, J.B. Dressman, J. Lippert, Mechanism-based prediction of particle size-dependent dissolution and absorption: cilostazol pharmacokinetics in dogs, *Eur J Pharm Biopharm*, 76 83-94.



10 Summary (German)

Die vorliegende Arbeit untersucht das Auflösungsverhalten von nanonisierten Arzneistoffen in Tabletten hinsichtlich deren Analytik

Die Beurteilung der festen Arzneiform erfolgt durch den Dissolutionstest. Für eine sinnvolle Beurteilung muss die Trennung von festen und gelösten Bestandteilen in einem geeigneten Zeitrahmen sichergestellt sein. Bei Partikelgrößen von etwa 150 nm, wie bei nanonisierten Substanzen üblich, erscheint es fraglich, ob über herkömmliche Methoden wie z.B. die Nutzung eines 0.45 µm Spritzenaufsatzfilters eine solche Trennung erfolgen kann.

In dieser Studie wurden verschiedene analytische Techniken untersucht und auf ihre Eignung beurteilt, in einem Dissolutionstest nanokristalliner Arzneistoffe eingesetzt zu werden.

Zunächst wurden verschiedene analytische Systeme in Theorie auf ihre Eignung untersucht, ob die entsprechende Technik zur schnellen Trennung von festen und gelösten Bestandteilen überhaupt geeignet ist. Nach dieser Untersuchung konnten die klassische Dialyse, die Trübungsmessung sowie die UV-spektroskopische Analytik über Glasfaseroptik aus mehreren Gründen ausgeschlossen werden, z.B. die Dialyse dadurch, dass eine schnelle Trennung der festen von den gelösten Bestandteilen nicht gewährleistet ist. Die asymmetrische Fluss-Feldfluss-Fraktionierung erscheint



vielversprechend, jedoch war kein entsprechendes Gerät verfügbar um diese Technik auf ihre Eignung weiter zu untersuchen.

Die Ultraschall-Resonanz-Technologie (ResoScan), die Mikrodialyse sowie der Einsatz von Zentrifugalfiltern haben sich als ungeeignet für die Analytik von Dissolutionstests erwiesen. Der Einsatz von Spritzenaufsatzfiltern mit verschiedenen Porengrößen sowie die Ionen-selektive Elektrode schienen vielversprechend, daher wurden diese Techniken intensiver untersucht.

Die Spritzenaufsatzfilter mit Porengrößen von $0.0 \mu\text{m}$ – $0.45\mu\text{m}$ wurden auf ihre Eignung untersucht, kolloidalen Arzneistoff ($> 1000\mu\text{m}$) zurückzuhalten. Fenofibrat wurde als Modellsubstanz gewählt, da es kommerziell sowohl als mikronisierte als auch als nanonisierte Formulierung erhältlich ist und so ein direkter Vergleich ermöglicht wird.

Die Experimente mit mikronisiertem Fenofibrat, welches wenig oder kein kolloidales Fenofibrat enthält, resultierten unabhängig von der gewählten Filterporengröße in gleiche Dissolutionprofile. Der f_2 – Wert war immer größer 65, somit beträgt der Unterschied zwischen den einzelnen Profilen weniger als 5%, unabhängig vom gewählten Medium.

Bei der Dissolution des nanonisierten Fenofibrat wurde mit einer Porengröße von $0,1 \mu\text{m}$ oder weniger jeweils die Sättigungslöslichkeit im jeweiligen Medium getroffen.



Wurden 0,2 μm oder 0,45 μm als Porengröße gewählt, wurde die Sättigungslöslichkeit des Fenofibrats im Medium weit übertroffen. Diese Beobachtungen, kombiniert mit den jeweils hohen Standardabweichungen der einzelnen Testpunkte zeigen, dass diese „Übersättigung“ durch kolloidales Fenofibrat verursacht wurden, welches zu fein ist um von den Filtern zurückgehalten zu werden. Die f_2 – Werte waren im Vergleich zum Profil aus der 0,1 μm -Filtration kleiner 50. Somit ist die Wahl der richtigen Filtergröße unerlässlich für die sinnvolle Beurteilung eines Dissolutionprofils.

Um nanonisierten von gelöstem Arzneistoff zu trennen, scheint eine Filtergröße von 0,1 μm oder weniger geeignet.

Es konnte weiterhin beobachtet werden, dass die experimentell bestimmten Dissolutionraten nicht mit den üblichen Hypothesen zur Verringerung der Diffusionsschicht h bei abnehmendem Partikelradius in Einklang gebracht werden können. Somit erscheint die ausschließlich theoretische Anwendung der Nernst-Brunner Gleichung als nicht zielführend zur Ermittlung der Auflösraten.

Für beide Formulierungen wurden die initialen Auflösraten ermittelt. Anschließend wurden diese in ein Computermodell (STELLA[®], Model A) eingesetzt, um eine Korrelation mit *in vivo* - Daten durchzuführen. Im präprandialen Status konnte eine gute Korrelation für das mikronisierte Fenofibrat gefunden werden, während die Plasmalevel für die nanonisierte Fenofibrat zu hoch berechnet wurden. Daher wurde das Modell erweitert, um den Einfluss eines Absorptionsschrittes an der intestinalen Membran untersuchen zu können (Modell B). Es konnte gezeigt werden, dass sogar



kleine Verzögerungen der Absorption und damit des Erscheinens der Substanz im Plasma einen großen Einfluss auf die Plasmaprofile haben.

Für beide Formulierungen konnten so die geschwindigkeitsbestimmenden Schritte ermittelt werden: Wenn die Formulierung von mikronisiert auf nanonisiert wechselt, ändert sich der geschwindigkeitsbestimmende Schritt von vollständig von der Auflösungsgeschwindigkeit bestimmt, hin zu zumindest teilweise absorptionsbestimmt (präprandial). Im postprandialen Zustand gilt für beide Formulierungen, dass hauptsächlich die Magenentleerungsrate geschwindigkeitsbestimmend ist.

Für die Studien mit der Ionen-selektive Elektrode wurde Diphenhydramin-HCl als Modellsubstanz gewählt. Ziel der Untersuchung war es, die Kompatibilität der Elektrode mit komplexen Dissolutionmedien, wie z.B. alle biorelevanten Medien nachzuweisen. Dieses dient zur Vorbereitung zu weiteren Dissolutionstudien mit nanokristallinem Arzneistoff in diesen Medien. Die Resultate wurden mit Dissolutionprofilen verglichen, welche mit herkömmlichen manuellem Sampling und anschließender HPLC-UV Analyse erhalten wurden.

Es zeigte sich, dass sich die Ionen-selektive Elektrode zur Analytik der Dissolution von Diphenhydramin-HCl in den biorelevanten Medien eignet, welche den präprandialen Zustand simulieren (FaSSGF, FaSSIF, FaSSIF-V2). Dabei kann das System alleine (Methode A) oder unterstützend zu einer Ein-Punkt-Analyse via HPLC-UV eingesetzt werden (Methode B). Die Elektrode liefert ebenfalls zufriedenstellende Ergebnisse in



milchbasiertem Medium (FeSSGF), zeigt dabei sogar Vorteile gegenüber dem manuellen Sampling und der anschließenden HPLC-UV Methode da keine Trennung von festen und flüssigen Bestandteilen und damit keine Probenaufbereitung notwendig ist. Die Anwendung in postprandialen Medien (FeSSIF und FeSSIF-V2) konnte noch nicht etabliert werden und muss Ziel weiterer Studien sein.

Als eine Online-Technologie bietet die Ionen-selektive Elektrode eine effizientere Generierung von Dissolutionprofilen als herkömmliche Methoden mit manuellem Sampling.



Zusammenfassend lässt sich feststellen:

- Die Techniken Dialyse, Mikro dialyse, Trübheitsmessung, Ultraschall-Resonanz, Zentrifugalfiltration sowie die UV-Messung via Glasfaser sind nicht für die Dissolutionanalytik von nanonisierten Arzneistoffen geeignet.
- Spritzenaufsatzfilter mit Porengrößen von 0,02 µm oder 0,1 µm sind geeignet, kolloidales Fenofibrat aus biorelevanten Medien zu filtern.
- Via der Software STELLA[®] konnte eine in vitro – in vivo Korrelation für mikronisiertes und nanonisiertes Fenofibrat etabliert werden.
- Für mikronisiertes Fenofibrat im nüchternen Zustand ist der geschwindigkeitsbestimmende Schritt für die Absorption die Dissolution, während eine Nanonisierung den Schritt hin zur Absorption verlagert
- Die Ionen-selektive Elektrode ist prinzipiell geeignet für die Analytik von nanonisiertem Arzneistoff. Erste Ergebnisse mit Diphenhydramin zeigten, dass in FaSSGF, FaSSIF und FaSSIF-V2 die Ergebnisse gleichwertig zur herkömmlichen Methode sind, während die Elektrode in FeSSGF sogar überlegen scheint. Für FeSSIF und FeSSIF-V2 ist noch weitere Forschung notwendig.
- Eine Adaption der Methodik erlaubt den Einsatz der Elektrode als unterstützendes System für die herkömmliche Methode.



11 Curriculum vitae

Persönliche Daten

Name	Daniel Jünemann
Geburtsdatum	08.01.1981
Geburtsort	Lingen (Ems)
Nationalität	deutsch
Familienstand	ledig
Beruf:	Apotheker

Studium

11.2006	Dritter Abschnitt der Pharmazeutischen Prüfung und Erlangung der Approbation
05.2006 – 10.2006	Pharmaziepraktikant, <i>Rosen-Apotheke</i> , Frankfurt
11.2005 – 04.2006	Pharmaziepraktikant, <i>Merck KGaA</i> Darmstadt
SS 2005	Zweiter Abschnitt der Pharmazeutischen Prüfung
SS 2003	Erster Abschnitt der Pharmazeutischen Prüfung
WS 2001 – SS 2005	Studium der Pharmazie, <i>Goethe-Universität Frankfurt</i> , Frankfurt

Meine akademischen Lehrer waren die Professoren:

T. Dingermann, J.B. Dressman, J. Kreuter, D. Steinhilber, M. Schubert-Zsilavic, W.E. Müller, G. Lamprecht, H. Stark, R. Marschalek, H. Blume, M. Karas



Schulbildung:

2000	Abitur, <i>Gymnasium Georgianum</i> , Lingen (Ems)
1998 – 2000	Gymnasium Georgianum, Lingen (Ems)
1991 – 1998	Franziskugymnasium Lingen (Ems)
1987 – 1991	Grundschule Leschede, Emsbüren

Beruflicher Werdegang

Seit 07.2010	Project Manager, <i>Midas Pharma GmbH</i> , Ingelheim,
12.2006 – 06.2010	Wissenschaftlicher Mitarbeiter, <i>Institut für Pharmazeutische Technologie</i> , <i>Goethe-Universität Frankfurt</i> , Frankfurt AK Dressman, Erstellung einer Dissertation unter Anleitung von Prof. Dr. J.B. Dressman
12.2006 – 06.2010	Apotheker (nebenberuflich), <i>Adler-Apotheke</i> , Offenbach



Publikationen und Veröffentlichungen

- 2011 "Online monitoring of dissolution tests using dedicated potentiometric sensors in biorelevant media."
Scientific Article, Juenemann D, Bohets H, Ozdemir M, de Maesschalck R, Vanhoutte K, Peeters K, Nagels L, Dressman JB.
Eur J Pharm Biopharm. 2011 May;78(1):158-65.
- 2011 "Biorelevant in vitro dissolution testing of products containing micronized or nanosized fenofibrate with a view to predicting plasma profiles."
Scientific Article, Juenemann D, Jantratid E, Wagner C, Reppas C, Vertzoni M, Dressman JB.
Eur J Pharm Biopharm. 2011 Feb;77(2):257-64.
- 2010 "Can dissolution rate calculations establish the formulation parameters necessary to avoid food effects?"
Poster, AAPS 2010, New Orleans, USA
- 2010 "Comparison of drug analysis using potentiometric sensors and HPLC-UV in dissolution testing"
Poster, APV 2010 Valletta, Malta
- 2009 "Evaluation of different filter pore sizes in the dissolution test of nanosized fenofibrate and their effect on *in silico* modeling of plasma profiles"
Poster, AAPS 2009 Los Angeles, USA
- 2008 "Comparison of the dissolution performance of nanosized and micronized fenofibrate in biorelevant media"
Poster, APV 2008 Barcelona, Spanien





